2012

Non-metallic metamaterials: modelling, design, and fabrication tolerances analysis

Yang Li
Iowa State University

Non-metallic metamaterials: modelling, design, and fabrication tolerances analysis

by

Yang Li

A dissertation submitted to the graduate faculty

in partial fulfillment of the requirements for the degree of

DOCTOR OF PHILOSOPHY

Major: Electrical Engineering

Program of Study Committee:

Nicola Bowler, Major Professor

Rana Biswas

Brian K. Hornbuckle

Ronald Roberts

Jiming Song

Iowa State University

Ames, Iowa

2012

DEDICATION

$$\nabla \times \mathbf{E} = -\mathbf{M}_{\mathrm{i}} - \frac{\partial \mathbf{B}}{\partial t}$$
$$\nabla \times \mathbf{H} = \mathbf{J}_{\mathrm{i}} + \mathbf{J}_{\mathrm{c}} + \frac{\partial \mathbf{D}}{\partial t}$$
$$\nabla \cdot \mathbf{D} = q_{\mathrm{ev}}$$
$$\nabla \cdot \mathbf{B} = q_{\mathrm{mv}}$$

$$\oint_C \mathbf{E} \cdot d\mathbf{l} = -\iint_S \mathbf{M}_{\mathrm{i}} \cdot d\mathbf{s} - \frac{\partial}{\partial t} \iint_S \mathbf{B} \cdot d\mathbf{s}$$
$$\oint_C \mathbf{H} \cdot d\mathbf{l} = \iint_S \mathbf{J}_{\mathrm{i}} \cdot d\mathbf{s} + \iint_S \mathbf{J}_{\mathrm{c}} \cdot d\mathbf{s} + \frac{\partial}{\partial t} \iint_S \mathbf{D} \cdot d\mathbf{s}$$
$$\oiint \mathbf{D} \cdot d\mathbf{s} = Q_{\mathrm{e}}$$
$$\oiint \mathbf{B} \cdot d\mathbf{s} = Q_{\mathrm{m}}$$

—James Clerk Maxwell

"Do not go where the path may lead, go instead where there is no path, and leave a trail."

—Ralph Waldo Emerson

TABLE OF CONTENTS

LIST OF TABLES

LIST OF FIGURES

ACKNOWLEDGEMENTS

My advisor Prof. Nicola Bowler definitely deserves my deepest gratitude. Throughout my PhD study in Iowa State, Prof. Nicola creates a great research atmosphere to me. At the beginning of my second semester, my leg was hurt in a car accident. She took care of me instead of discard me. For every research work we have worked on, Prof. Nicola can always catch the points of my real interests and motivate me to pursue them. Prof. Nicola also gives me many opportunities to attend conferences to practice my presentation and social skills.

My special gratitude to Dr. Robert A. Shore (Air Force Research Laboratory, Hanscom AFB, MA). It is no exaggeration to say that Dr. Shore is my co-advisor outside Iowa State. Dr. Shore always give rapid replies, in great detail, to my questions on metamaterials, LaTex, and balance of life, etc. I believe that my research work on theoretical modeling of metamaterials could not have been done without his guidance and help.

I indeed appreciate Prof. Jiming Song's teaching and guidance throughout my study in Iowa State. He established my fundamental on advanced Electromagnetics through his graduate-level courses: EE512, 513, 516, and 517. Meanwhile, Prof. Song gives me numerous advice on my daily research questions.

I would also like to thank Profs. Rana Biswas, Brian K. Hornbuckle, Ronald Roberts, Costas M. Soukoulis, and Namrata Vaswani for their invaluable comments and suggestions on my thesis work. I am also very grateful to my friends and officemates, who give me a lot of technical support and a joyful life.

Finally, I would like to thank my parents, who always love me and support me to pursue my dream.

The work presented in this thesis is based upon work supported by the Air Force Research Laboratory under Contract FA8650-04-C-5228 at Iowa State University's Center for Nondestructive Evaluation.

ABSTRACT

Metamaterials are artificial materials, consisting of sub-wavelength building blocks, which can show anomalous and exotic electromagnetic responses. Metal-based metamaterials, as the first experimentally implemented metamaterials, have achieved significant progress in theory, fabrication, and characterization over a broad frequency range from microwave to visible. To alleviate the drawbacks of metal-based metamaterials, such as conductive loss and anisotropy, non-metallic metamaterials have been proposed and developed rapidly in the last decade. This thesis focuses on the analytical modeling and fabrication-tolerance analysis of non-metallic metamaterials consisting of an array of magnetodielectric spheres. Here, the term "magnetodielectric" refers, generally, to materials with relative permittivity and permeability both much greater than one, or to purely dielectric or magnetic materials.

The first half of this thesis presents the exact (within the dipole scattering approximation) dispersion equations of traveling waves supported by three-dimensional (3D) periodic arrays of two different magnetodielectric spheres arbitrarily arranged on a simple tetragonal lattice. To improve the calculation efficiency, fast converging expressions and their double summation form are derived for slowly converging summations in the dispersion equations. The presented theory has been tested by comparing its dispersion diagrams with corresponding ones in previous literature, and with those calculated by MIT Photonic-Bands (MPB). The dispersion diagrams of seven different arrangements of the spheres are analyzed for three combination of sphere types: 1) dielectric spheres with equal permittivity but different radius, 2) dielectric spheres with equal radius but different permittivity and 3) one set of spheres is purely dielectric while the other set is magnetic. Compared with results reported in previous literature, analysis of these possible arrangements of the spheres shows similar narrow double negative (DNG) bandwidths for spheres combinations 1) and 2), and wider DNG bandwidths for spheres combination 3). Based on this theory, this thesis also develops a clear design procedure for

DNG metamaterials consisting of 3D periodic arrays of two different magnetodielectric spheres arranged on a simple tetragonal lattice. This procedure can give a design with widest possible DNG bandwidth and prescribed effective constitutive parameters at the operating frequency.

Effects of parameter variations on negative effective constitutive parameters of non-metallic metamaterials are analyzed in the second half of this thesis. These effects are evaluated in terms of the variability in effective constitutive parameters around the DNG or single negative (S-NG) region for given geometric and material parameters and their variations. Based on the Clausius-Mossotti expressions for the effective (bulk) constitutive parameters of non-metallic metamaterials, analytical expressions of variability of effective constitutive parameters depending on geometric and material parameters variations are developed using total differential. In practice, these expressions can be used to estimate the performance of a non-metallic metamaterial with given parameter variations that might exist due to fabrication tolerances. Based on these expressions, effects of parameter variations on effective constitutive parameters are analyzed for three type of metamaterials: a) 3D cubic array of identical magnetodielectric spheres; b) 3D cubic array of two different dielectric spheres with equal radius but different permittivity; c) 3D cubic array of two different dielectric spheres with equal permittivity but different radius. Results show that varying the following parameters impacts negative effective constitutive parameters in the following order from most to least: 1) radius of spheres; 2) constitutive parameters of spheres providing negative effective permittivity and/or permeability; 3) lattice constant of the array and the constitutive parameters of the array medium. For three particular case studies, results show that the DNG behavior may be extinguished if there are 0.78%, 0.0164%, and 0.0158% variations in all parameters of metamaterials a), b), and c), respectively. A complete set of analytical expressions for derivatives of Mie scattering coefficients are also obtained in order to calculate the total differential of variabilities of effective constitutive parameters of non-metallic metamaterials.

CHAPTER 1. GENERAL INTRODUCTION

1.1 Introduction

The work presented in this thesis is within the research area of electromagnetic (EM) metamaterials. Particularly, it is a development of non-metallic metamaterials.

1.1.1 Metamaterials

Every natural material may be regarded as a composite consisting of atoms and molecules. The original purpose in defining permittivity/permeability was to give a homogeneous view of the EM properties of a material in the presence of an applied electric/magnetic field, whose wavelength is much larger than the inclusions. Following this trail, when the atoms and molecules are replaced by large-scale structures, which are still much smaller than the wavelength of the applied field, the entire composite can be treated, in a macroscopic view, as a homogeneous medium with *effective* permittivity, ϵ^{eff}, and permeability, μ^{eff}, as shown in Fig. 1.1. If ϵ^{eff} and μ^{eff} are unavailable in nature, the composite is a so-called "metamaterial". The prefix "meta" means "beyond".

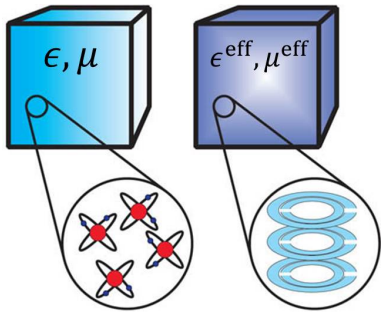

Figure 1.1 Metamaterials concept. Reprinted by permission from Macmillan Publishers Ltd: [NATURE MATERIALS] [1], copyright (2006).

Here, a rigid definition of metamaterials is given: metamaterials are artificially structured composites, composed of sub-wavelength building blocks, with EM properties unavailable in nature [2], [3].

EM metamaterials can be categorized into the following classes [2], [4]: 1) double negative (DNG) metamaterials with both ϵ^{eff} and μ^{eff} negative, occupying the third quadrant in Fig. 1.2; 2) single negative (SNG) metamaterials with either ϵ^{eff} or μ^{eff} negative, the second and fourth quadrants in Fig. 1.2; 3) EM bandgap metamaterials, which can control the propagation of EM waves; 4) bi-isotropic and bi-anisotropic metamaterials, in which backward waves and forward waves can exist simultaneously; and 5) chiral metamaterials, which can support backward wave propagation without SNG or DNG.

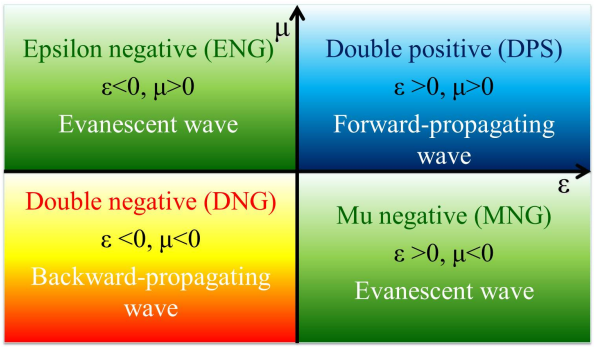

Figure 1.2 Classification of metamaterials [2].

Possible applications of metamaterials include achieving subdiffraction imaging by a superlens [5], Fig. 1.3(a), cloaking of objects from EM fields [6]-[8], Fig. 1.3(b), and improving performance of antennas [9], Fig. 1.3(c). Although metamaterials were first accomplished in electromagnetics, the idea of metamaterials has already been extended into acoustics and seismology, and yielded many interesting outcomes, such as acoustic cloaking [10] and shielding objects from earthquakes [11].

In academia, research in metamaterials is interdisciplinary and includes such areas as electromagnetics, optics, materials science, solid state physics, acoustics, and seismology, etc.

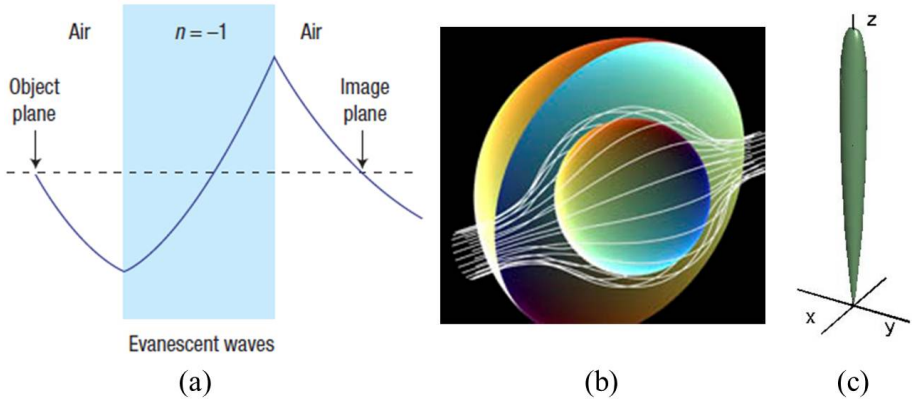

Figure 1.3 Possible applications of metamaterials. (a) Superlens. Reprinted by permission from Macmillan Publishers Ltd: [NATURE MATERIALS] [12], copyright (2008). (b) Cloak. From [6]. Reprinted with permission from AAAS. (c) Improving directivity of antenna [13]. © [2012] IEEE.

1.1.2 Metal-based metamaterials

The first metamaterial achieved experimentally consisted of an array of thin metal wires, which provide negative ϵ^{eff}, and double split-ring resonators (SRR), which provide negative μ^{eff}, at gigahertz frequencies [14], Fig. 1.4. In this structure, the incident EM waves have to propagate parallel to the sample surface [14]. Since the magnetic resonance frequency of SRR is inversely proportional to its size, this scheme was simply scaled down from microwave frequencies to higher frequencies [15]. To increase operation bandwidth and decrease losses, metamaterials consisting of periodically L-C loaded transmission lines at microwave frequencies were proposed [16], [17], Fig. 1.4. However, it's challenging to implement this scheme in higher frequencies due to the fabrication of high frequency capacitors and inductors. For ease of fabrication, double SRR was replaced by single SRR, which works up to about 200 THz [18], Fig. 1.4. Further, metallic cut-wire pairs, providing both negative ϵ^{eff} and μ^{eff}, were achieved in optical regime, for the light propagating normal to the sample surface [19]-[21], Fig. 1.4. In the optical and visible regime, double-fishnet structures were applied widely to achieve an effective negative refractive index for light propagating normal to the layers [22]-[24], Fig. 1.4. To alleviate metallic conduction loss, these structures operating in optical and visible regime are fabricated by low-loss metals, such as silver [24]. In conclusion, drawbacks of metal-based metamaterials include conduction loss and anisotropy [3].

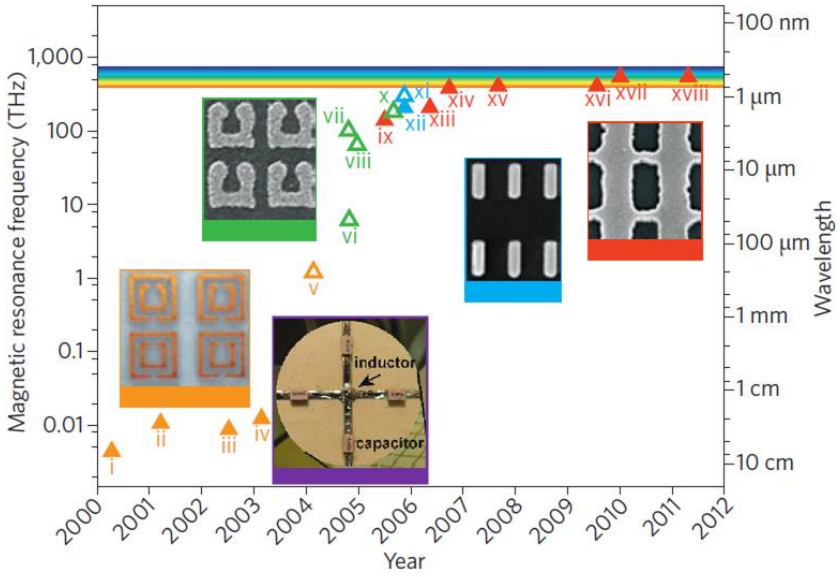

Figure 1.4 Development of metal-based metamaterial as a function of operation frequency and time. Orange: double SRRs; purple: transmission-Line structures [17], copyright (2004) by the American Physical Society; green: U-shaped SRRs; blue: metallic cut-wire pairs; red: double fishnet structures. The five insets show optical or electron micrographs of the five kinds of structure. Reprinted by permission from Macmillan Publishers Ltd: [NATURE PHOTONICS] [3], copyright (2011).

1.1.3 Non-metallic metamaterials

Non-metallic metamaterials are the focus of this thesis. To avoid the drawbacks of metal-based metamaterials, three-dimensional (3D) arrays of non-metallic inclusions have been proposed as an alternative to metal-based metamaterials [25]. In such a scheme, the negative constitutive parameters are designed to appear in a frequency band above the Mie resonances of the inclusions: the negative ϵ^{eff} is designed to appear in a frequency band above the resonance of the Mie electric dipole scattering coefficient whereas negative μ^{eff} is designed to appear in a frequency band above the resonance of the Mie magnetic dipole scattering coefficient, and double negative (DNG) is designed to appear in a frequency band above the overlap of resonances of Mie electric and magnetic dipole scattering coefficients. The particles usually have the following combinations: 1) one set of magnetodielectric particles with values of relative permittivity and permeability much greater than one and close to each other; 2) two different dielectric particles with equal permittivity but different size; 3) and two different dielectric particles with equal size but different permittivity. In theory, the particles analyzed are com-

monly spherical but, in practice, particles are usually fabricated as cubes or cylinders for ease of fabrication. To meet the criteria of homogenization, which may be stated in the form that the lattice constant is much smaller than the operating wavelength, the relative permittivity of the dielectric particles should be much greater than 1, e.g. $\epsilon_r > 200$.

Non-metallic metamaterials can be modeled by both analytical and numerical methods. Analytical methods include mixing formulas [26]-[32] and scattering-matrix based methods [31]-[38]. In these methods, the particle is modeled by either an electric dipole, which is parallel to the applied electric field, or a pair of crossed electric and magnetic dipoles, which are parallel to the electric and magnetic fields, respectively, of the applied EM wave. These dipoles are the leading terms in the multipole series, and the only existing ones for a homogeneous sphere, whose polarisabilities can be easily obtained from the Mie scattering coefficients [39]. In general, this procedure is known as the "point-dipole approximation" [40], which is a good approximation for metamaterials consisting of arrays of electrically small spheres [2]. Such an approximation restricts the application of these methods to arrays of spheres, however. Merits of these methods include low calculation cost and mathematical simplicity.

Many classical numerical methods, such as finite-difference time-domain (FDTD) [41], [42], finite element method (FEM) [43], and method of moments (MOM) [44] have been applied to model non-metallic metamaterials and achieved reasonable accuracy compared with measurement results. Different from analytical methods, numerical methods are able to account for scattering elements (inclusions) with arbitrary geometric shape. Disadvantages of these methods include high computation cost and mathematical complexity.

Although non-metallic metamaterials alleviate the drawbacks of metal-based metamaterials, their practical implementations still meet challenges from the restricted range of naturally-occurring electromagnetic material parameters (permittivity and permeability) at desired frequencies, and fabrication tolerances. For example, magnetodielectric materials with values of relative permittivity and permeability much greater than one are not currently available above 1 GHz. Dielectric materials with relative permittivity much greater than 1 are currently unavailable in the optical regime. To overlap the electric and magnetic Mie resonances, which are very narrow, provided by two different dielectric particles, the permittivities or sizes of the

particles require extremely tight fabrication tolerances, e.g. less than 1%.

The work presented in this thesis focuses on modeling non-metallic metamaterials based on the point-dipole approximation. Using a scattering-matrix based method, two-sphere arrays with arbitrary arrangements have been modeled. Based on these models, effects of fabrication tolerances on the performance of different arrays have been analyzed.

1.2 Thesis Organization

The thesis can be divided into two parts. Chapters 1 and 2 present analytical models for non-metallic metamaterials consisting of two-sphere arrays, while Chapters 3 and 4 present analysis of effects of fabrication tolerances on DNG/SNG performance of non-metallic metamaterials.

Chapter 1 develops the exact (within the dipole scattering approximation) $k-\beta$ (dispersion) equations of traveling waves supported by 3D periodic arrays of two sets of magnetodielectric spheres *arbitrarily* arranged on a simple tetragonal lattice. Based on this theory, Chapter 2 presents a rational design procedure for DNG metamaterials consisting of 3D periodic arrays of two different non-metallic spheres arranged on a simple tetragonal lattice.

In Chapter 3, the analytical expressions are derived for derivatives of Mie scattering coefficients with respect to the sphere size, relative permittivity and permeability of both the sphere and medium, which are utilized in Chapter 4. Analytical expressions of variabilities of effective (bulk) constitutive parameters of non-metallic metamaterials due to geometric and electromagnetic material parameters variations are developed in Chapter 4 by computing the total differential of Clausius-Mossotti expressions for the effective constitutive parameters.

1.3 Literature Review

In 1968, Veselago [45] introduced, for the first time, the concept of DNG metamaterials and their potential application as a superlens with refractive index equal to negative one, which can break the diffraction limit. However, no feasible experimental scheme was proposed to fulfill this concept in the following twenty-eight years. In 1996, Pendry *et al.* [46] proposed to use a 3D array of thin metal wires to decrease their plasma frequency, below which the

permittivity of metal can be negative, into the far infrared or even microwave regime. Such structure can exhibit a negative ϵ^{eff} below a very low plasma frequency, such as somewhere in GHz band [46]. Three years later, Pendry *et al.* [5] proposed to utilize an array of non-magnetic conducting double SRRs to achieve a negative permeability around its resonance frequency. In 2001, Shelby *et al.* [14] experimentally demonstrated the first DNG metamaterial consisting of two-dimensional (2D) periodic arrays of metal wire and double SRRs in the X-band. Since then, the area of metamaterials has received a lot of attention and has progressed rapidly over the last decade.

As mentioned in Section 1.1.2, significant progress has been achieved in theory, fabrication, and characterization of metal-based metamaterials in microwave/millimeter wave, THz, optical, and visible regimes. Since the focus of this thesis is non-metallic metamaterials, the following part of this review concentrates on the topic of non-metallic metamaterials.

1.3.1 Theoretical schemes

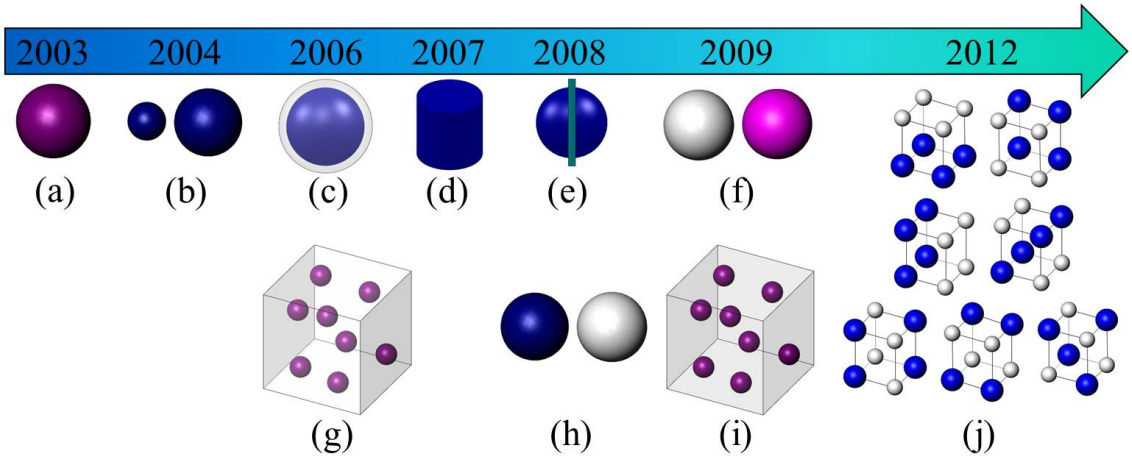

Figure 1.5 Development of theoretical schemes of non-metallic metamaterials. Different colors indicate different materials for inclusions. Purple: magnetodielectric; blue: purely dielectric material with larger permittivity; white: purely dielectric material with smaller permittivity; green: metal; pink: purely magnetic.

Using Lewin's model [47], Holloway *et al.* [25] showed, theoretically, that a DNG metamaterial can be formed by an array of non-metallic, magnetodielectric spheres with relative permittivity and permeability much greater than one and similar to each other, Fig. 1.5(a).

In this scheme, the negative permittivity and permeability are provided by the resonances of Mie electric and magnetic dipole scattering coefficients of the magnetodielectric spheres. Since such magnetodielectric materials are currently not available above 1 GHz, this scheme cannot presently be practically accomplished in microwave and higher frequency ranges. Based on this idea, however, several alternative but more practical approaches have proposed to form non-metallic metamaterials. These are listed as follows:

(1) Based on the generalized Lewin's model and FDTD calculations, Vendik and Gashinova [48] proposed that non-metallic metamaterials can be formed by an array of two different dielectric spheres with equal permittivity but different size, Fig. 1.5(b);

(2) Using FDTD simulation, Ahmadi and Mosallaei [41] showed that non-metallic metamaterials can be formed by an array of two different dielectric spheres with equal size but different permittivity, Fig. 1.5(h);

(3) Based on the dispersion equations developed through scattering-matrix method and point-dipole approximation, as described in Section 1.1.3, Shore and Yaghjian [32] showed that non-metallic metamaterials can be formed by interpenetrating arrays of purely dielectric and purely magnetic spheres, Fig. 1.5(f);

(4) Using a method generalized from that in scheme (3), Chapter 2 of this thesis [38] analyzed the backward wave and DNG bandwidths of seven different arrangements of spheres for three combinations of sphere types, Fig. 1.5(j).

(5) Peng *et al.* [49] theoretically demonstrated that by using displacement currents in dielectric resonators to mimic the conductive currents in thin metal wires and SRRs, a DNG metamaterial can be formed by an array of high dielectric cylindrical resonators, Fig. 1.5(d);

(6) An array of dielectric spheres, which provide negative permeability, combined with metal wires or dielectric rods, which provide negative permittivity below the plasma frequency, were proposed to form DNG metamaterial [50], [51], Fig. 1.5(e);

(7) Using Claussius-Mossotti mixing rules, Seo *et al.* [52] proposed to realize a non-metallic metamaterial by randomly embedding dielectric spheres in a negative permittivity plasmonic host material, Fig. 1.5(g);

(8) Utilizing a method developed from that in scheme (3), Ghadarghadr and Mosallaei [53] showed that a non-metallic metamaterial can be formed by randomly embedding dielectric spheres in a negative permeability host material with Lorentzian behavior, Fig. 1.5(i);

(9) Using an extended Clausius-Mossotti formula, Wheeler [54] demonstrated that a collection of polaritonic spheres coated with a thin layer of Drude material can show DNG behavior at infrared frequencies, Fig. 1.5(c).

Although purely dielectric materials with relative permittivity much greater than one are already available to form metamaterials based on schemes (1) and (2), it still very challenging to fabricate them due to their narrow DNG bandwidths requiring tight fabrication tolerances [38]. Since magnetic materials with relative permeability much greater than one above 1 GHz are currently unavailable for scheme (3), it cannot be practically fulfilled in microwave and higher frequency ranges despite the fact that this scheme gives much wider DNG bandwidths than those of schemes (1) and (2) [38]. Since the negative permittivity of scheme (6) is provided by the metal wires or dielectric rods, at frequencies below their plasma frequency, and only one set of Mie resonances is applied, this scheme has a looser fabrication tolerance. In schemes (5) and (6), due to the use of metal wires or dielectric rods, the incident EM waves have to propagate normal to the wires or rods. Since the negative permittivity and permeability of schemes (7) and (8), respectively, provided by the host material are negative over a wide frequency range and only one set of Mie resonances is utilized, these schemes have a looser fabrication tolerance.

1.3.2 Experiments

Based on the schemes presented in Section 1.3.1, many works have been carried out to experimentally fulfill non-metallic metamaterials. These are listed as follows:

(1) Holloway *et al.* [55] experimentally demonstrated that a metafilm consisting of spherical magnetodielectric (Yttrium Iron Garnet or YIG) particles exhibits negative electric and

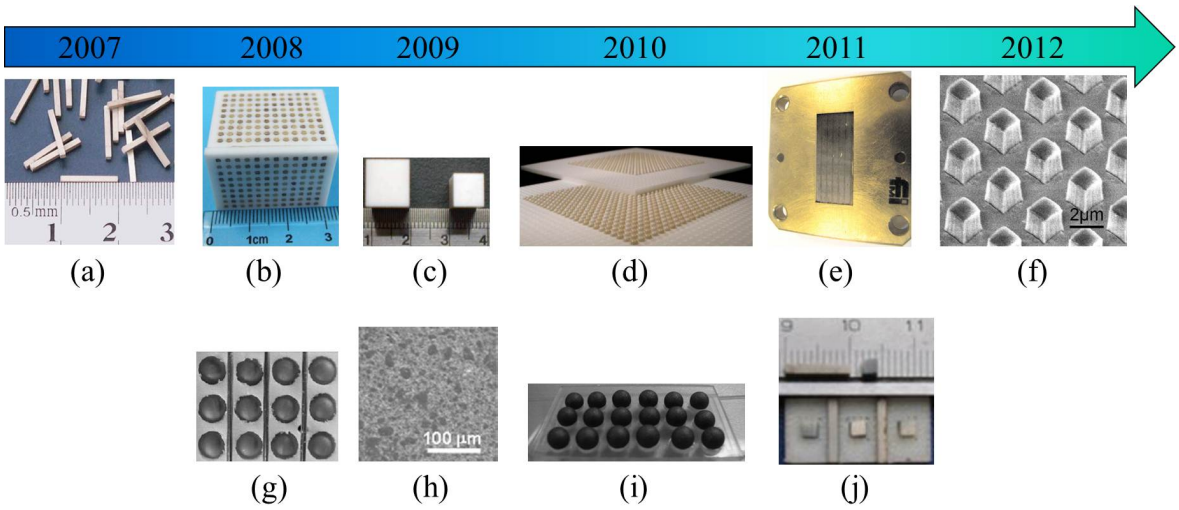

Figure 1.6 Development of experimental works of non-metallic metamaterials. (a) [49]. Copyright (2007) by the American Physical Society. (b) [57]. Copyright (2008) by the American Physical Society. (c) [59]. Copyright (2009) by the Optical Society of America. (d) [60]. Copyright (2010) by Metamorphose-VI. (e) [62]. Reprinted with permission from [62]. Copyright [2011], American Institute of Physics. (f) [58]. Copyright (2012) by the American Physical Society. (g) [50]. Reprinted from [50], Copyright (2008), with permission from Elsevier. (h) [64]. Reprinted with permission from [64]. Copyright [2009], American Institute of Physics. (i) [55]. Copyright (2010) by The Institution of Engineering and Technology. (j) [51]. Reprinted with permission from [51]. Copyright [2011], American Institute of Physics.

magnetic surface susceptibilities, which are equivalent to the effective constitutive parameters of 3D homogenous (bulk) metamaterials, at 2.724 GHz, Fig. 1.6(i). Holloway *et al.* [56] also emphasized that these surface susceptibilities are the most appropriate quantities that can be utilized to characterize a metafilm since its thickness is not well-defined;

(2) Zhao *et al.* [57] experimentally realized a cubic array of $Ba_{0.5}Sr_{0.5}TiO_3$ (BST) cubes with isotropic negative μ^{eff} from 8.53 to 8.85 GHz, Fig. 1.6(b). Ginn *et al.* [58] demonstrated an all-dielectric metamaterial, in the midinfrared, composed of a 2D array of tellurium cubes with magnetic behavior around 9 μm, Fig. 1.6(f);

(3) Lai *et al.* [59] showed that an array of two sets of zirconia cubes with different sizes exhibit negative refractive index around 5.84 GHz, Fig. 1.6(c);

(4) Carroll *et al.* [60] realized DNG around 17 GHz using an array of (Zr, Sn)TiO_4 (ZST) and (Mg, Ca)Ti_3 (MCT) spheres arranged on a ROHACELL® 31HF foam matrix, Fig. 1.6(d);

(5) Lepetit *et al.* [61] showed that an array of two different $Ba_xSr_{1-x}Ti_{1-y}Mn_yO_3$ (BST/Mn) rods exhibit DNG behavior around 10.6 GHz. The same group also demonstrated that an array of identical BST/Mn rods can provide either negative ϵ^{eff} or μ^{eff} [62], Fig. 1.6(e);

(6) Peng *et al.* [49] demonstrated that a collection of randomly or periodically arranged BST rods can show negative refractive index around 7 GHz, Fig. 1.6(a);

(7) Cai *et al.* [50] showed that an array of $BaCO_3$-TiO_2 spheres in combination with a wire frame exhibits DNG behavior around 6 GHz, Fig. 1.6(g). Ma *et al.* [63] demonstrated that an array of rectangular $SrTiO_3$ (STO) resonators and metal wires can show DNG behavior around 9.8 GHz. Wang *et al.* [51] demonstrated that an array of $Ba_{0.6}Sr_{0.4}TiO_3$-$La(Mg_{0.5}$-$Ti_{0.5})O_3$ cubes and square rods can show DNG behavior between 9.97 and 10.4 GHz, Fig. 1.6(j);

(8) Limberopoulos *et al.* [64] fabricated and characterized an isotropic 3D metamaterial composed of silicon carbide (SiC) nanoparticles embedded randomly in the polycrystalline magnesium diboride (MgB_2) host. It exhibits DNG behavior at 632 nm, Fig. 1.6(h).

In (1), Holloway *et al.* experimentally accomplished their original theoretical design of non-metallic metamaterials in the form of a 2D metafilm. Parts of the work listed in (2), (3), and (7) fabricated the scattering unit as a cube instead of a sphere for ease of fabrication, as mentioned in Section 1.1.2. SNG was achieved in (2) since only one set of dielectric cubes were employed. Experimental schemes (3), (4), (6), (7), and (8) are the implementations of theoretical schemes (1), (2), (5), (6), and (7), respectively, discussed in Section 1.3.1. Note that although experimental schemes (5) and (6) both applied dielectric rods to achieve DNG, they are based on different theoretical schemes. Samples in (5) were designed according to Mie theory while those of (6) were designed based on theoretical scheme (5) of Section 1.3.1.

1.4 Conclusion and Outlook

As an alternative scheme to achieve EM metamaterials, non-metallic metamaterials have the advantages of low-loss and isotropy compared with their metal-based counterpart. Over

the last decade, many analytical and numerical methods have been applied to analyze the non-metallic metamaterials while only several reasonable experimental fabrication and characterization works have been achieved at microwave frequencies. The experimental implementations of non-metallic metamaterials at higher frequencies are restricted to the availability of magnetodielectric materials or dielectric materials with high permittivity and low loss. If this restriction is overcome by developments in materials science and engineering, it may become possible to realize low-loss 3D isotropic metamaterials consisting of a random collection of magnetodielectric particles in microwave and higher frequency ranges.

1.5 References

[1] J. Pendry, "Photonics: Metamaterials in the sunshine," *Nat. Mater.*, vol. 5, no. 8, pp. 599–600, Aug. 2006.

[2] N. Engheta and R. W. Ziolkowski, *Electromagnetic Metamaterials: Physics and Engineering Explorations*. Wiley, New York, 2006.

[3] C. M. Soukoulis and M. Wegener, "Past achievements and future challenges in the development of three-dimensional photonic metamaterials," *Nat. Photonics*, vol. 5, no. 9, pp. 523–530, Sep. 2011.

[4] S. Zouhdi, A. Sihvola, and A. P. Vinogradov, *Metamaterials and Plasmonics: Fundamentals, Modelling, Applications*. Springer, New York, 2008.

[5] J. Pendry, "Negative refraction makes a perfect lens," *Phys. Rev. Lett.*, vol. 85, no. 18, pp. 3966–3969, Oct. 2000.

[6] J. Pendry, D. Schurig, and D. Smith, "Controlling electromagnetic fields," *Science*, vol. 312, no. 5781, pp. 1780–1782, Jun. 2006.

[7] D. Schurig, J. J. Mock, B. J. Justice, S. A. Cummer, J. B. Pendry, A. F. Starr, and D. R. Smith, "Metamaterial electromagnetic cloak at microwave frequencies," *Science*, vol. 314, no. 5801, pp. 977–980, Nov. 2006.

[8] J. Valentine, J. Li, T. Zentgraf, G. Bartal, and X. Zhang, "An optical cloak made of dielectrics," *Nat. Mater.*, vol. 8, no. 7, pp. 568–571, Jul. 2009.

[9] R. W. Ziolkowski, P. Jin, and C. C. Lin, "Metamaterial-inspired engineering of antennas," *Proc. IEEE*, vol. 99, no. 10, pp. 1720–1731, Oct. 2011.

[10] S. Zhang, C. Xia, and N. Fang, "Broadband acoustic cloak for ultrasound waves," *Phys. Rev. Lett.*, vol. 106, no. 2, p. 024301, Jan. 2011.

[11] M. Brun, S. Guenneau, and A. B. Movchan, "Achieving control of in-plane elastic waves," *Appl. Phys. Lett.*, vol. 94, no. 6, p. 061903, Feb. 2009.

[12] X. Zhang and Z. Liu, "Superlenses to overcome the diffraction limit," *Nat. Mater.*, vol. 7, no. 6, pp. 435–441, Jun. 2008.

[13] W. Shu and J. Song, "Sommerfeld integral path for layered double negative metamaterials," *IEEE Trans. Antennas Propag.*, vol. 60, no. 3, pp. 1496–1504, Mar. 2012.

[14] R. Shelby, D. Smith, and S. Schultz, "Experimental verification of a negative index of refraction," *Science*, vol. 292, no. 5514, pp. 77–79, Apr. 2001.

[15] C. M. Soukoulis, S. Linden, and M. Wegener, "Negative refractive index at optical wavelengths," *Science*, vol. 315, no. 5808, pp. 47–49, Jan. 2007.

[16] G. Eleftheriades, A. Iyer, and P. Kremer, "Planar negative refractive index media using periodically L-C loaded transmission lines," *IEEE Trans. Microw. Theory Tech.*, vol. 50, no. 12, pp. 2702-2712, Dec. 2002.

[17] A. Grbic and G. Eleftheriades, "Overcoming the diffraction limit with a planar left-handed transmission-line lens," *Phys. Rev. Lett.*, vol. 92, no. 11, Mar. 2004.

[18] T. Yen, W. Padilla, N. Fang, D. Vier, D. Smith, J. Pendry, D. Basov, and X. Zhang, "Terahertz magnetic response from artificial materials," *Science*, vol. 303, no. 5663, pp. 1494–1496, Mar. 2004.

[19] V. Shalaev, W. Cai, U. Chettiar, H. Yuan, A. Sarychev, V. Drachev, and A. Kildishev, "Negative index of refraction in optical metamaterials," *Opt. Lett.*, vol. 30, no. 24, pp. 3356–3358, Dec. 2005.

[20] S. Zhang, W. Fan, N. Panoiu, K. Malloy, R. Osgood, and S. Brueck, "Experimental demonstration of near-infrared negative-index metamaterials," *Phys. Rev. Lett.*, vol. 95, no. 13, p. 137404, Sep. 2005.

[21] G. Dolling, C. Enkrich, M. Wegener, C. Soukoulis, and S. Linden, "Low-loss negative-index metamaterial at telecommunication wavelengths," *Opt. Lett.*, vol. 31, no. 12, pp. 1800–1802, Jun. 2006.

[22] ——, "Simultaneous negative phase and group velocity of light in a metamaterial," *Science*, vol. 312, no. 5775, pp. 892–894, May 2006.

[23] G. Dolling, M. Wegener, C. M. Soukoulis, and S. Linden, "Negative-index metamaterial at 780 nm wavelength," *Opt. Lett.*, vol. 32, no. 1, pp. 53–55, Jan. 2007.

[24] J. Valentine, S. Zhang, T. Zentgraf, E. Ulin-Avila, D. A. Genov, G. Bartal, and X. Zhang, "Three-dimensional optical metamaterial with a negative refractive index," *Nature*, vol. 455, no. 7211, pp. 376–U32, Sep. 2008.

[25] C. Holloway, E. Kuester, J. Baker-Jarvis, and P. Kabos, "A double negative (DNG) composite medium composed of magnetodielectric spherical particles embedded in a matrix," *IEEE Trans. Antennas Propag.*, vol. 51, no. 10, pp. 2596–2603, Oct. 2003.

[26] C. Simovski and S. He, "Frequency range and explicit expressions for negative permittivity and permeability for an isotropic medium formed by a lattice of perfectly conducting Omega particles," *Phys. Lett. A*, vol. 311, no. 2-3, pp. 254–263, May 2003.

[27] P. Belov and C. Simovski, "Homogenization of electromagnetic crystals formed by uniaxial resonant scatterers," *Phys. Rev. E*, vol. 72, no. 2, p. 026615, Aug. 2005.

[28] A. Alu and N. Engheta, "Three-dimensional nanotransmission lines at optical frequencies: A recipe for broadband negative-refraction optical metamaterials," *Phys. Rev. B*, vol. 75, no. 2, p. 024304, Jan. 2007.

[29] C. Simovski, P. Belov, and S. He, "Backward wave region and negative material parameters of a structure formed by lattices of wires and split-ring resonators," *IEEE Trans. Antennas Propag.*, vol. 51, no. 10, pp. 2582–2591, Oct. 2003.

[30] J. Li and J. B. Pendry, "Non-local effective medium of metamaterial," arXiv:cond-mat/0701332v1.

[31] R. A. Shore and A. D. Yaghjian, "Traveling waves on two- and three-dimensional periodic arrays of lossless scatterers," *Radio Sci.*, vol. 42, no. 6, p. RS6S21, Dec. 2007.

[32] ——, "Traveling waves on three-dimensional periodic arrays of two different alternating magnetodielectric spheres," *IEEE Trans. Antennas Propag.*, vol. 57, no. 10, pp. 3077–3091, Oct. 2009.

[33] ——, "Traveling electromagnetic waves on linear periodic arrays of lossless penetrable spheres," *IEICE Trans. Commun.*, vol. E88B, no. 6, pp. 2346–2352, Jun. 2005.

[34] ——, "Travelling electromagnetic waves on linear periodic arrays of lossless spheres," *Electron. Lett.*, vol. 41, no. 10, pp. 578–580, May 2005.

[35] ——, "Electromagnetic waves on partially finite periodic arrays of lossless or lossy penetrable spheres," *IEICE Trans. Commun.*, vol. E91B, no. 6, pp. 1819–1824, Jun. 2008.

[36] ——, "Complex waves on periodic arrays of lossy and lossless permeable spheres: 1. Theory," *Radio Sci.*, vol. 47, p. RS2014, Apr. 2012.

[37] ——, "Complex waves on periodic arrays of lossy and lossless permeable spheres: 2. Numerical results," *Radio Sci.*, vol. 47, p. RS2015, Apr. 2012.

[38] Y. Li and N. Bowler, "Traveling waves on three-dimensional periodic arrays of two different magnetodielectric spheres arbitrarily arranged on a simple tetragonal lattice," *IEEE Trans. Antennas Propag.*, vol. 60, no. 6, pp. 2727–2739, Jun. 2012.

[39] J. A. Stratton, *Electromagnetic Theory*. McGraw-Hill, New York, 1941.

[40] A. Alu, A. D. Yaghjian, R. A. Shore, and M. G. Silveirinha, "Causality relations in the homogenization of metamaterials," *Phys. Rev. B*, vol. 84, no. 5, p. 054305, Aug. 2011.

[41] A. Ahmadi and H. Mosallaei, "Physical configuration and performance modeling of all-dielectric metamaterials," *Phys. Rev. B*, vol. 77, no. 4, p. 045104, Jan. 2008.

[42] A. F. Oskooi, D. Roundy, M. Ibanescu, P. Bermel, J. D. Joannopoulos, and S. G. Johnson, "MEEP: A flexible free-software package for electromagnetic simulations by the FDTD method," *Comput. Phys. Commun.*, vol. 181, no. 3, pp. 687–702, Mar. 2010.

[43] L. Petersson and J. Jin, "A three-dimensional time-domain finite-element formulation for periodic structures," *IEEE Trans. Antennas Propag.*, vol. 54, no. 1, pp. 12–19, Jan. 2006.

[44] M.-F. Wu, X.-X. Liu, A. Alu, and A. E. Yilmaz, "A fast surface integral equation solver for composite structures with metamaterial regions," in *2011 IEEE International Symposium on Antennas and Propagation*. IEEE, 2011, pp. 2688–2691.

[45] V. G. Veselago, "Electrodynamics of substances with simultaneously negative values of sigma and mu," *Soviet Phys. Uspekhi-Ussr*, vol. 10, no. 4, p. 509, 1968.

[46] J. Pendry, A. Holden, W. Stewart, and I. Youngs, "Extremely low frequency plasmons in metallic mesostructures," *Phys. Rev. Lett.*, vol. 76, no. 25, pp. 4773–4776, Jun. 1996.

[47] L. Lewin, "The electrical constants of a material loaded with spherical particles," *Proc. Inst. Elec. Eng.*, vol. 94, no. 27, pp. 65–68, Jan. 1947.

[48] O. Vendik and M. Gashinova, "Artificial double negative (DNG) media composed by two different dielectric sphere lattices embedded in a dielectric matrix," in *34th Eur. Microw. Conf.*, 2004, pp. 1209–1212.

[49] L. Peng, L. Ran, H. Chen, H. Zhang, J. A. Kong, and T. M. Grzegorczyk, "Experimental observation of left-handed behavior in an array of standard dielectric resonators," *Phys. Rev. Lett.*, vol. 98, no. 15, p. 157403, Apr. 2007.

[50] X. Cai, R. Zhu, and G. Hu, "Experimental study for metamaterials based on dielectric resonators and wire frame," *Metamaterials*, vol. 2, no. 4, pp. 220–226, 2008.

[51] J. Wang, Z. Xu, Z. Yu, X. Wei, Y. Yang, J. Wang, and S. Qu, "Experimental realization of all-dielectric composite cubes/rods left-handed metamaterial," *J. Appl. Phys.*, vol. 109, no. 8, p. 084918, Apr. 2011.

[52] B. Seo, T. Ueda, T. Itoh, and H. Fetterman, "Isotropic left handed material at optical frequency with dielectric spheres embedded in negative permittivity medium," *Appl. Phys. Lett.*, vol. 88, no. 16, p. 161122, Apr. 2006.

[53] S. Ghadarghadr and H. Mosallaei, "Dispersion diagram characteristics of periodic array of dielectric and magnetic materials based spheres," *IEEE Trans. Antennas Propag.*, vol. 57, no. 1, pp. 149–160, Jan. 2009.

[54] M. Wheeler, J. Aitchison, and M. Mojahedi, "Coated nonmagnetic spheres with a negative index of refraction at infrared frequencies," *Phys. Rev. B*, vol. 73, no. 4, p. 045105, Jan. 2006.

[55] C. L. Holloway, P. Kabos, M. A. Mohamed, E. F. Kuester, J. A. Gordon, M. D. Janezic, and J. Baker-Jarvis, "Realisation of a controllable metafilm/metasurface composed of resonant magnetodielectric particles: measurements and theory," *IET Microw. Antennas Propag.*, vol. 4, no. 8, pp. 1111–1122, Aug. 2010.

[56] C. L. Holloway, E. F. Kuester, and A. Dienstfrey, "Characterizing metasurfaces/metafilms: the connection between surface susceptibilities and effective material properties," *IEEE Antennas Wirel. Propag. Lett.*, vol. 10, pp. 1507–1511, 2011.

[57] Q. Zhao, L. Kang, B. Du, H. Zhao, Q. Xie, X. Huang, B. Li, J. Zhou, and L. Li, "Experimental demonstration of isotropic negative permeability in a three-dimensional dielectric composite," *Phys. Rev. Lett.*, vol. 101, no. 2, p. 027402, Jul. 2008.

[58] J. C. Ginn, I. Brener, D. W. Peters, J. R. Wendt, J. O. Stevens, P. F. Hines, L. I. Basilio, L. K. Warne, J. F. Ihlefeld, P. G. Clem, and M. B. Sinclair, "Realizing optical magnetism from dielectric metamaterials," *Phys. Rev. Lett.*, vol. 108, no. 9, p. 097402, Feb. 2012.

[59] Y.-J. Lai, C.-K. Chen, and T.-J. Yen, "Creating negative refractive identity via single-dielectric resonators," *Opt. Express*, vol. 17, no. 15, pp. 12 960–12 970, Jul. 2009.

[60] J. F. Carroll III, J. H. Loui, P. G. Clem, and M. B. Sinclair, "Magnetodielectric sphere composites: an all dielectric route for low loss DNG metamaterials," in *Fourth International Congress on Advanced Electromagnetic Materials in Microwaves and Optics*, 2010.

[61] T. Lepetit, E. Akmansoy, and J.-P. Ganne, "Experimental measurement of negative index in an all-dielectric metamaterial," *Appl. Phys. Lett.*, vol. 95, no. 12, p. 121101, Sep. 2009.

[62] T. Lepetit, E. Akmansoy, and J. P. Ganne, "Experimental evidence of resonant effective permittivity in a dielectric metamaterial," *J. Appl. Phys.*, vol. 109, no. 2, p. 023115, Jan. 2011.

[63] Y. G. Ma, L. Zhao, P. Wang, and C. K. Ong, "Fabrication of negative index materials using dielectric and metallic composite route," *Appl. Phys. Lett.*, vol. 93, no. 18, p. 184103, Nov. 2008.

[64] N. Limberopoulos, A. Akyurtlu, K. Higginson, A.-G. Kussow, and C. D. Merritt, "Negative refractive index metamaterials in the visible spectrum based on MgB2/SiC composites," *Appl. Phys. Lett.*, vol. 95, no. 2, p. 023306, Jul. 2009.

CHAPTER 2. TRAVELING WAVES ON THREE-DIMENSIONAL PERIODIC ARRAYS OF TWO DIFFERENT MAGNETODIELECTRIC SPHERES ARBITRARILY ARRANGED ON A SIMPLE TETRAGONAL LATTICE

A paper published in *IEEE Transactions on Antennas and Propagation*

Yang Li, Nicola Bowler

2.1 Abstract

Based on Shore and Yaghjian's work [R. A. Shore and A. D. Yaghjian, *IEEE Trans. Antennas Propag.*, vol. 57, no. 10, pp. 3077-3091, Oct. 2009.], a general theory has been developed to describe traveling waves on three-dimensional (3D) periodic arrays of two sets of magnetodielectric spheres *arbitrarily* arranged on a simple tetragonal lattice. This theory is eventually in the form of $k - \beta$ (dispersion) equations. To improve the computational efficiency, rapidly converging expressions and their double summation form are derived for slowly converging summations in the $k - \beta$ equations. The dispersion diagrams of seven different arrangements of the spheres are analyzed for three combinations of sphere types: i) dielectric spheres with equal permittivity but different radius, ii) dielectric spheres with equal radius but different permittivity and iii) one set of spheres is purely dielectric while the other set is magnetic. Results show that the maximum bandwidths of the DNG region provided by different spheres arrangements for spheres combinations i) to iii) are, respectively, 0.21%, 0.069%, and 7.403%. Compared with results reported in previous literature, analysis of these possible arrangements of the spheres shows similar narrow DNG bandwidths for spheres combinations i) and ii), and wider DNG bandwidths for spheres combination iii). Although purely dielectric materials with

relative permittivity much greater than one are readily available, the usefulness of purely dielectric DNG metamaterials still depends on whether the narrow bandwidths achievable are acceptable for the particular applications. Since purely magnetic materials with relative permeability much greater than one above 1 GHz are not currently available, the practicality of fabricating DNG metamaterials using arrays with spheres combination iii) is questionable for radio frequency (RF) applications, at least at present, despite the fact that this combination yields much wider DNG bandwidths than those of spheres combinations i) and ii).

2.2 Introduction

Since Shelby *et al.* [1] experimentally realized DNG materials—-those with negative real parts of effective permittivity and permeability—-for the first time following Pendry's theoretical scheme [2], [3], significant progress has been achieved both in the theoretical development and practical application of metamaterials [4], such as achieving sub-diffraction imaging by a 'perfect' lens [5], cloaking of objects from electromagnetic fields [6]-[8], and improving performance of antennas [9], [10].

Present realizations of metamaterials often employ sub-wavelength resonant metallic elements, such as metallic split ring resonators combined with wires [1], short wire pairs [11], and fishnet structures [12], etc. The drawbacks of metal-based metamaterials include conduction loss, anisotropy, and fabrication challenge in the infrared and optical frequency range.

In a contrasting approach, Holloway *et al.* [13] demonstrated, theoretically, that a DNG metamaterial can be formed by a 3D periodic array of non-conductive, magnetodielectric spheres with values of relative permittivity and permeability much greater than one and close to each other. Further, several complementary approaches have been proposed to form non-conductive DNG metamaterials. Examples of these, close to the configurations of this work, are 3D periodic arrays of two sets of dielectric spheres either with the same permittivity but different radius [14]-[17] ([17] contains a considerable number of mostly typographical mistakes which have been corrected in [18]), or with the same radius but different permittivity [17]-[19], or with one set of spheres being purely dielectric and the other set being magnetic [17]. Other examples employ dielectric spheres embedded randomly in a negative permittivity plasmonic

host material [20] or embedded inside a ferrite material with negative permeability [21], or employ coated nonmagnetic spheres [22]-[24]. All these works focus on the combination of spheres and host materials or different core-shell combinations rather than the arrangement of spheres.

This paper presents the exact (within the dipole scattering approximation) $k-\beta$ (dispersion) equations of traveling waves supported by 3D periodic arrays of two sets of magnetodielectric spheres arbitrarily arranged on a simple tetragonal lattice. Although the two different magnetodielectric spheres can be arbitrarily arranged on a simple tetragonal lattice, the real concern of this paper is with periodic arrays whose tetragonal unit cells contain four of each of the two different spheres, Fig. 2.1. Here, the term "magnetodielectric" refers to spheres with relative permittivity and permeability both greater than one, or purely dielectric/magnetic spheres, or perfect conducting spheres. The $k-\beta$ equation relates the propagation constant, β, of the wave traveling in the direction of the array axis, to the free-space wavenumber, k. Harmonic time dependence of $\exp(-\mathrm{i}\omega t)$ is assumed in this paper. It is an extension of Shore and Yaghjian's systematic works describing traveling waves on linear, 2D, and 3D periodic arrays of acoustic monopoles, electric dipoles, and magnetodielectric spheres [17], [25]-[33]. The developments of this work include the derivation of $k-\beta$ equations of traveling waves on 3D periodic arrays of two different magnetodielectric spheres *arbitrarily* arranged on a simple tetragonal lattice, Fig. 2.2, which goes beyond previous work in which only arrangements (b) and (g), Fig. 2.1, have been considered [21] and [17], respectively. The analysis is supported by the derivation of rapidly converging expressions and their double summation form for the slowly converging summations in the $k-\beta$ equations using Floquet mode expansions and expressions for the rapid summation of Schlömilch series. The paper is arranged as follows. Section 2.3 gives the

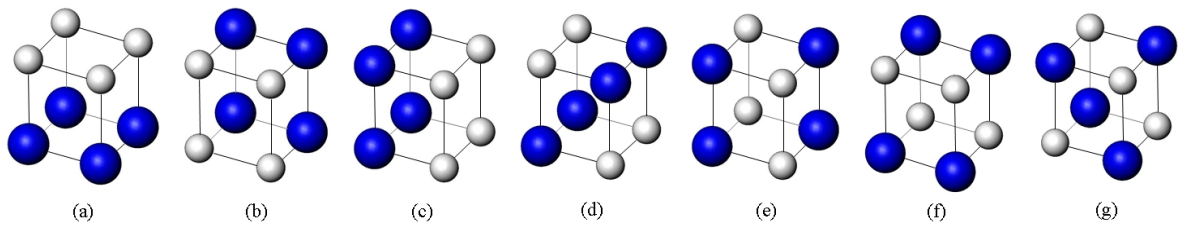

Figure 2.1 Seven different arrangements of four 1-spheres (dark) and four 2-spheres (pale) within the unit cell.

derivation of $k-\beta$ equations. Verification of the presented theory and performance analysis

of arrays with different arrangements of spheres, Fig. 2.1, are given in Section 2.4. Rapidly converging expressions and their double summation form are derived in Appendices 2.6 and 2.7, respectively.

2.3 Theory

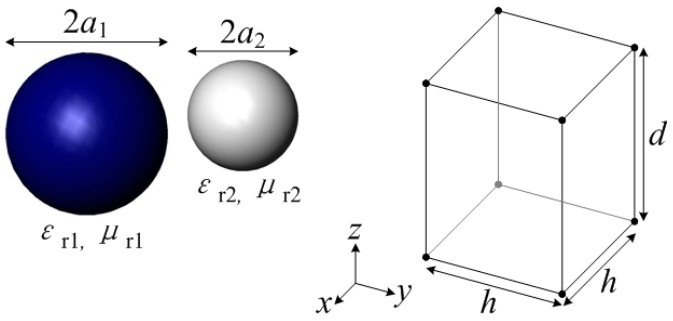

Figure 2.2 Two sets of spheres and unit cell geometry.

In this theory, two sets of magnetodielectric spheres are arbitrarily arranged on each lattice point of the unit tetragon. One set of spheres with relative permittivity ϵ_{r1}, relative permeability μ_{r1}, and radius a_1 will be referred to as "1-spheres" while the other set with relative permittivity ϵ_{r2}, relative permeability μ_{r2}, and radius a_2 will be referred to as "2-spheres". The z axis is chosen as the array axis in which the height of each unit cell lies, as shown in Fig. 2.2. The cross-section of each unit cell is normal to the z axis with equal length and width in the x and y directions, respectively. In the planes $z = 2nd, n = 0, \pm1, \pm2, \cdots$ or $z = (2n-1)\,d, n = 0, \pm1, \pm2, \cdots$, either set of spheres could be centered at $[x = 2mh, y = 2lh]$, $[x = (2m-1)h, y = 2lh]$, $[x = 2mh, y = (2l-1)h]$, or $[x = (2m-1)h, y = (2l-1)h]\,, l, m = 0, \pm1, \pm2, \cdots$. Seven different arrangements of four 1-spheres and four 2-spheres on the vertices of the unit cell are shown in Fig. 2.1. Note that analysis of the arrangements (b) and (g) are given in [21] and [17], respectively, but the other arrangements have not been studied previously. Also note that the $k - \beta$ equation for *any* other arrangement of a total of eight 1-spheres and 2-spheres on the vertices of the unit cell, in addition to those seven, can be easily derived based on the presented theory. Indeed, it is unnecessary to have four of each type of sphere, in the theory presented here.

Following Shore and Yaghjian's [30] approach, each sphere is modeled by a pair of crossed electric and magnetic dipoles, which are oriented in the x and y directions, respectively. It is assumed that the array is excited by a wave traveling in the z direction, with the electric field parallel to the x axis and magnetic field parallel to the y axis, and that all the spheres are excited identically apart from a phase factor. In the presence of the excitation, let $\mathbf{E}_0^0$ and $\mathbf{H}_0^0$ be the electric and magnetic fields, respectively, that are incident on the sphere at position $(x, y, z) = (0, 0, 0)$ from all the other spheres in the array. $\mathbf{E}_0^0$ and $\mathbf{H}_0^0$ are obtained by summing the electric and magnetic fields that are incident on the reference sphere from all the other spheres of the array.

According to [30, Eqs. (9.1) to (9.28)], the x-directed electric dipole field at (0,0,0) from a unit x-directed electric dipole at (mh, lh, nd) multiplied by $(kh)^3$ is [17, Eq. (2.1)]

$$f_1(m,l,n,kh,d/h,0) = \frac{\mathrm{e}^{\mathrm{i}kh\rho}}{\rho}\left[\frac{-2\mathrm{i}}{\rho}\left(kh+\frac{\mathrm{i}}{\rho}\right)\frac{m^2}{\rho^2}2eq1 + \left((kh)^2+\frac{\mathrm{i}kh}{\rho}-\frac{1}{\rho^2}\right)\frac{l^2+(nd/h)^2}{\rho^2}\right] \tag{2.1}$$

where

$$\rho = \sqrt{m^2+l^2+(nd/h)^2}, \tag{2.2}$$

and the x-directed electric dipole field at (0,0,0) from a unit y-directed magnetic dipole at (mh, lh, nd) multiplied by $(kh)^3$ is [17, Eq. (2.3)]

$$f_2(m,l,n,kh,d/h,0) = \frac{\mathrm{e}^{\mathrm{i}kh\rho}}{\rho}\left((kh)^2+\frac{\mathrm{i}kh}{\rho}\right)\frac{nd/h}{\rho}. \tag{2.3}$$

Let

$$\Sigma_{1n}(kh,d/h,0) \overset{n\neq 0}{=} \sum_{m,l=-\infty}^{\infty} f_1(m,l,n,kh,d/h,0), \tag{2.4a}$$

$$\Sigma_{1s}(kh,0) = \sum_{\substack{m,l=-\infty \\ (m,l)\neq(0,0)}}^{\infty} f_1(m,l,0,kh,0,0), \tag{2.4b}$$

$$\Sigma_{2n}(kh,d/h,0) = \sum_{m,l=-\infty}^{\infty} f_2(m,l,n,kh,d/h,0), \tag{2.4c}$$

$$\Sigma_{3n}(kh,d/h,0) \overset{n\neq 0}{=} \sum_{m,l=-\infty}^{\infty} f_1(m-1/2,l-1/2,n,kh,d/h,0), \tag{2.4d}$$

$$\Sigma_{3s}(kh,0) = \sum_{\substack{m,l=-\infty \\ (m,l)\neq(0,0)}}^{\infty} f_1(m-1/2, l-1/2, 0, kh, 0, 0), \tag{2.4e}$$

$$\Sigma_{4n}(kh,d/h,0) = \sum_{m,l=-\infty}^{\infty} f_2(m-1/2, l-1/2, n, kh, d/h, 0), \tag{2.4f}$$

$$\Sigma_{5n}(kh,d/h,0) \overset{n\neq 0}{=} \sum_{m,l=-\infty}^{\infty} f_1(m-1/2, l, n, kh, d/h, 0), \tag{2.4g}$$

$$\Sigma_{5s}(kh,0) = \sum_{\substack{m,l=-\infty \\ (m,l)\neq(0,0)}}^{\infty} f_1(m-1/2, l, 0, kh, 0, 0), \tag{2.4h}$$

$$\Sigma_{6n}(kh,d/h,0) = \sum_{m,l=-\infty}^{\infty} f_2(m-1/2, l, n, kh, d/h, 0), \tag{2.4i}$$

$$\Sigma_{7n}(kh,d/h,0) \overset{n\neq 0}{=} \sum_{m,l=-\infty}^{\infty} f_1(m, l-1/2, n, kh, d/h, 0), \tag{2.4j}$$

$$\Sigma_{7s}(kh,0) = \sum_{\substack{m,l=-\infty \\ (m,l)\neq(0,0)}}^{\infty} f_1(m, l-1/2, 0, kh, 0, 0), \tag{2.4k}$$

and

$$\Sigma_{8n}(kh,d/h,0) = \sum_{m,l=-\infty}^{\infty} f_2(m, l-1/2, n, kh, d/h, 0). \tag{2.4l}$$

Note that (2.4a) to (2.4f) are given in [17, Eq. (2.4)]. Then the total x-directed electric dipole field at (0,0,0) multiplied by $(kh)^3$ is the sum of contributions from all the other spheres of the array. Those contributions will be different for different arrangements of 1-spheres and 2-spheres. Here, those for arrangement (g), Fig. 2.1, are given in (2.5) as an example. Accordingly, similar derivations can be made for other arrangements. It should be noted that, different from [17, Eq. (2.5)], the summations over m even and l odd, as well as m odd and l even are given directly using (2.4g) to (2.4l) here. In [17, Eq. (2.5)], the sum of the summations over m even and l odd, and m odd and l even is treated as the summation over all m and l minus the sum of the summations over m and l both even and over m and l both odd. The approach taken here simplifies the mathematical expressions and improves the computational

efficiency. The contributions of the different subsets of the array spheres to the total x-directed electric dipole field at the origin multiplied by $(kh)^3$ are as follows:

1. x-directed electric dipoles of the 1-spheres in the nth plane, n even, $n \neq 0$

$$b_{e1,n}\frac{1}{8}\left(\Sigma_{1n}(2kh, d/2h, 0) + \Sigma_{3n}(2kh, d/2h, 0)\right); \tag{2.5a}$$

2. x-directed electric dipoles of the 1-spheres in the $n = 0$ plane

$$b_{e1,0}\frac{1}{8}\left(\Sigma_{1s}(2kh, 0) + \Sigma_{3s}(2kh, 0)\right); \tag{2.5b}$$

3. y-directed magnetic dipoles of the 1-spheres in the nth plane, n even, $n \neq 0$

$$b_{m1,n}\frac{1}{8}\left(\Sigma_{2n}(2kh, d/2h, 0) + \Sigma_{4n}(2kh, d/2h, 0)\right); \tag{2.5c}$$

4. y-directed magnetic dipoles of the 1-spheres in the $n = 0$ plane: zero;

5. x-directed electric dipoles of the 2-spheres in the nth plane, n even, $n \neq 0$

$$b_{e2,n}\frac{1}{8}\left(\Sigma_{5n}(2kh, d/2h, 0) + \Sigma_{7n}(2kh, d/2h, 0)\right); \tag{2.5d}$$

6. x-directed electric dipoles of the 2-spheres in the $n = 0$ plane

$$b_{e2,0}\frac{1}{8}\left(\Sigma_{5s}(2kh, 0) + \Sigma_{7s}(2kh, 0)\right); \tag{2.5e}$$

7. y-directed magnetic dipoles of the 2-spheres in the nth plane, n even, $n \neq 0$

$$b_{m2,n}\frac{1}{8}\left(\Sigma_{6n}(2kh, d/2h, 0) + \Sigma_{8n}(2kh, d/2h, 0)\right); \tag{2.5f}$$

8. y-directed magnetic dipoles of the 2-spheres in the $n = 0$ plane: zero;

9. x-directed electric dipoles of the 1-spheres in the nth plane, n odd

$$b_{e1,n}\frac{1}{8}\left(\Sigma_{5n}(2kh, d/2h, 0) + \Sigma_{7n}(2kh, d/2h, 0)\right); \tag{2.5g}$$

10. y-directed magnetic dipoles of the 1-spheres in the nth plane, n odd

$$b_{m1,n}\frac{1}{8}\left(\Sigma_{6n}(2kh, d/2h, 0) + \Sigma_{8n}(2kh, d/2h, 0)\right); \tag{2.5h}$$

11. x-directed electric dipoles of the 2-spheres in the nth plane, n odd

$$b_{e2,n}\frac{1}{8}\left(\Sigma_{1n}(2kh, d/2h, 0) + \Sigma_{3n}(2kh, d/2h, 0)\right); \tag{2.5i}$$

12. y-directed magnetic dipoles of the 2-spheres in the nth plane, n odd

$$b_{m2,n}\frac{1}{8}\left(\Sigma_{2n}(2kh, d/2h, 0) + \Sigma_{4n}(2kh, d/2h, 0)\right). \tag{2.5j}$$

The coefficients $b_{e1,n}$, $b_{e2,n}$ ($b_{m1,n}$, $b_{m2,n}$) in (2.5) are related to the electric (magnetic) field E_{0x}^{0n} (H_{0y}^{0n}/Y_0) incident on the 1-spheres and 2-spheres in the nth plane by the scattering equations [17, Eq. (2.6)]

$$b_{e1,n} = S_{e1}E_{0x}^{0n}, \quad b_{m1,n} = S_{m1}\frac{H_{0y}^{0n}}{Y_0}, \quad b_{e2,n} = S_{e2}E_{0x}^{0n}, \quad b_{m2,n} = S_{m2}\frac{H_{0y}^{0n}}{Y_0} \tag{2.6}$$

where S_{e1}, S_{m1}, S_{e2}, and S_{m2} are the normalized electric and magnetic dipole scattering coefficients of the 1-spheres and 2-spheres, respectively, given by [17, Eq. (2.7)]

$$S_{e1} = -\mathrm{i}\frac{3}{2}b_{11}^{\mathrm{sc}}, \quad S_{m1} = -\mathrm{i}\frac{3}{2}a_{11}^{\mathrm{sc}}, \quad S_{e2} = -\mathrm{i}\frac{3}{2}b_{12}^{\mathrm{sc}}, \quad S_{m2} = -\mathrm{i}\frac{3}{2}a_{12}^{\mathrm{sc}}. \tag{2.7}$$

In (2.7), b_{1i}^{sc} and a_{1i}^{sc} are, respectively, the electric and magnetic Mie dipole scattering coefficients [34, Sec. 9.25, Eqs. (11), (10)] for the i-spheres ($i = 1, 2$). Note that the theory given here is equally applicable to any array elements that can be modeled by a pair of crossed electric and magnetic dipoles perpendicular to the array axis [30]. S_{e1}, S_{m1}, S_{e2}, and S_{m2} must be obtained through other methods if the array elements are not magnetodielectric spheres.

Assuming that the array is excited by a traveling wave in the z direction with real or complex propagation constant β, the coefficients $b_{e1,n}$, $b_{m1,n}$, $b_{e2,n}$, and $b_{m2,n}$ in (2.5) are identical to $b_{e1,0}$, $b_{m1,0}$, $b_{e2,0}$, and $b_{m2,0}$, respectively, other than a phase shift given by [17, Eq. (2.8)]

$$b_{e1,n} = b_{e1,0}\mathrm{e}^{\mathrm{i}n\beta d}, \quad b_{m1,n} = b_{m1,0}\mathrm{e}^{\mathrm{i}n\beta d}, \quad b_{e2,n} = b_{e2,0}\mathrm{e}^{\mathrm{i}n\beta d}, \quad b_{m2,n} = b_{m2,0}\mathrm{e}^{\mathrm{i}n\beta d}. \tag{2.8}$$

Substituting (2.8) into (2.5) and summing over n to obtain the total x-directed electric field incident on the spheres at $(0, 0, 0)$, the homogeneous equation in the four unknowns $b_{e1,0}$, $b_{m1,0}$, $b_{e2,0}$, and $b_{m2,0}$ is obtained [17, Eq. (2.9)]

$$(kh)^3 E_{0x}^{00} = (kh)^3 \frac{b_{e1,0}}{S_{e1}} = A_1 b_{e1,0} - A_2 b_{m1,0} + A_3 b_{e2,0} - A_4 b_{m2,0}. \tag{2.9}$$

In (2.9), A_i $(i = 1, 2, ..., 4)$ are different for different arrangements of 1-spheres and 2-spheres on the vertices of the unit cell. The expressions for A_i of arrangement (g), Fig. 2.1, are given in (2.10). Since expressions of A_i for arrangements (a) to (f) are similar to (2.10), those terms are summarized in Tables 2.1 to 2.4.

$$\begin{aligned} A_1 =& \frac{1}{8}\Bigg[\sum_{\substack{n=-\infty \\ n\neq 0 \\ n \text{ even}}}^{\infty} \mathrm{e}^{\mathrm{i}n\beta d}\left(\Sigma_{1n}(2kh, d/2h, 0) \ +\Sigma_{3n}(2kh, d/2h, 0)\right) + \left(\Sigma_{1s}(2kh, 0) + \Sigma_{3s}(2kh, 0)\right) \\ &+ \sum_{\substack{n=-\infty \\ n \text{ odd}}}^{\infty} \mathrm{e}^{\mathrm{i}n\beta d}\left(\Sigma_{5n}(2kh, d/2h, 0) \ +\Sigma_{7n}(2kh, d/2h, 0)\right)\Bigg], \end{aligned} \tag{2.10a}$$

$$\begin{aligned} A_2 =& \frac{1}{8}\Bigg[\sum_{\substack{n=-\infty \\ n\neq 0 \\ n \text{ even}}}^{\infty} \mathrm{e}^{\mathrm{i}n\beta d}\left(\Sigma_{2n}(2kh, d/2h, 0) \ +\Sigma_{4n}(2kh, d/2h, 0)\right) \\ &+ \sum_{\substack{n=-\infty \\ n \text{ odd}}}^{\infty} \mathrm{e}^{\mathrm{i}n\beta d}\left(\Sigma_{6n}(2kh, d/2h, 0) \ +\Sigma_{8n}(2kh, d/2h, 0)\right)\Bigg], \end{aligned} \tag{2.10b}$$

$$\begin{aligned} A_3 =& \frac{1}{8}\Bigg[\sum_{\substack{n=-\infty \\ n\neq 0 \\ n \text{ even}}}^{\infty} \mathrm{e}^{\mathrm{i}n\beta d}\left(\Sigma_{5n}(2kh, d/2h, 0) \ +\Sigma_{7n}(2kh, d/2h, 0)\right) + \left(\Sigma_{5s}(2kh, 0) \ +\Sigma_{7s}(2kh, 0)\right) \\ &+ \sum_{\substack{n=-\infty \\ n \text{ odd}}}^{\infty} \mathrm{e}^{\mathrm{i}n\beta d}\left(\Sigma_{1n}(2kh, d/2h, 0) \ +\Sigma_{3n}(2kh, d/2h, 0)\right)\Bigg], \end{aligned} \tag{2.10c}$$

$$\begin{aligned} A_4 =& \frac{1}{8}\Bigg[\sum_{\substack{n=-\infty \\ n\neq 0 \\ n \text{ even}}}^{\infty} \mathrm{e}^{\mathrm{i}n\beta d}\left(\Sigma_{6n}(2kh, d/2h, 0) \ +\Sigma_{8n}(2kh, d/2h, 0)\right) \\ &+ \sum_{\substack{n=-\infty \\ n \text{ odd}}}^{\infty} \mathrm{e}^{\mathrm{i}n\beta d}\left(\Sigma_{2n}(2kh, d/2h, 0) \ +\Sigma_{4n}(2kh, d/2h, 0)\right)\Bigg]. \end{aligned} \tag{2.10d}$$

Similar to the derivation of (2.9), when the total y-directed magnetic field incident on the sphere at $(0, 0, 0)$, the total x-directed electric field incident on the sphere at $(0, 0, d)$, and the

total y-directed magnetic field incident on the sphere at $(0,0,d)$ are considered, three more homogeneous equations in the four unknowns $b_{e1,0}$, $b_{m1,0}$, $b_{e2,0}$, and $b_{m2,0}$ are obtained [17, Eqs. (2.11)-(2.13)]

$$(kh)^3 \frac{H_{0y}^{00}}{Y_0} = (kh)^3 \frac{b_{m1,0}}{S_{m1}} = -A_2 b_{e1,0} + A_1 b_{m1,0} - A_4 b_{e2,0} + A_3 b_{m2,0}, \tag{2.11}$$

$$(kh)^3 E_{0x}^{01} = (kh)^3 \frac{b_{e2,0}}{S_{e2}} = A_3 b_{e1,0} - A_4 b_{m1,0} + A_1 b_{e2,0} - A_2 b_{m2,0}, \tag{2.12}$$

and

$$(kh)^3 \frac{H_{0y}^{01}}{Y_0} = (kh)^3 \frac{b_{m2,0}}{S_{m2}} = -A_4 b_{e1,0} + A_3 b_{m1,0} - A_2 b_{e2,0} + A_1 b_{m2,0}. \tag{2.13}$$

Since a solution to the system of four homogeneous equations exists if and only if the determinant of the equation matrix is equal to zero, the $k-\beta$ equation [17, Eq. (2.14)] is obtained and shown in (2.14).

$$\begin{vmatrix} (kh)^3 - S_{e1}A_1 & S_{e1}A_2 & -S_{e1}A_3 & S_{e1}A_4 \\ S_{m1}A_2 & (kh)^3 - S_{m1}A_1 & S_{m1}A_4 & -S_{m1}A_3 \\ -S_{e2}A_3 & S_{e2}A_4 & (kh)^3 - S_{e2}A_1 & S_{e2}A_2 \\ S_{m2}A_4 & -S_{m2}A_3 & S_{m2}A_2 & (kh)^3 - S_{m2}A_1 \end{vmatrix} = 0. \tag{2.14}$$

Rapidly converging expressions and their double summation form for the infinite summations in (2.10) are derived in Appendices 2.6 and 2.7, respectively. The double summations give better accuracy and higher computational efficiency than the triple summations presented in (2.10). For example, (2.35), (2.37), (2.46), and (2.48) in Appendix 2.7 as well as [17, Eqs. (A.4), (A.14)] can be used to give the double summations in (2.10a). Similarly, the other expressions in Appendix 2.7 as well as (2.27), (2.33), (2.22), and (2.24) can be used for (2.10b) to (2.10d).

For an array of lossless scatterers and real βd, using aforementioned double summation form of the rapidly converging expressions, (2.14) can be solved for βd for a given kd by

sweeping βd from 0 to π in suitable increments, noting that a change in sign of the real part of the determinant indicates the position of a root. For the choice of increment, decreasing the increment increases the accuracy, but at the expense of increasing the computation time. Also note that pseudo-roots at $\beta d = kd$ and $\beta d = 2\pi - kd$, due to the factor of $\cos(2\beta d) - \cos(2kd)$ in the denominator of some rapidly converging expressions, e.g. (2.35), should be ignored in this procedure. For an array of lossy scatterers and complex βd, the root finding procedure of (2.14) is more complicated and is discussed in [17] and [33].

2.4 Performance analysis of different arrays

In this section, the performance of 3D periodic arrays with different arrangements of 1-spheres and 2-spheres on the vertices of the unit cell, Figs. 2.1 (a) to (g), is analyzed for three combinations of sphere types. It should be noted that, different from arrangements (b) to (g), Fig. 2.1, whose $k - \beta$ diagrams are mirror-symmetric with respect to $\beta d = \pi$ for $0 < \beta d < 2\pi$ [27], that of arrangement (a) is mirror-symmetric with respect to $\beta d = \pi/2$ for $0 < \beta d < \pi$. The reason is that, in the range $0 < \beta d < \pi$, if $\beta d = (\pi/2 - a)$ is a root of the $k - \beta$ equation of arrangement (a), then so is $\beta d = (\pi/2 + a)$ a root. Thus, only the $k - \beta$ diagrams for $0 < \beta d < \pi$ and $0 < \beta d < 2\pi$ are considered, respectively, for arrangements (a), and (b) to (g). The presented results are obtained by solving (2.14) following the procedure mentioned in the last paragraph of Section 2.3 with an increment of 10^{-4} in βd. Lossless spheres and a cubic lattice ($h = d$) are assumed for all calculations. The tetragonal lattice ($h \neq d$) is not considered here since it can only provide further change, compared with simple cubic lattice, in the volume fraction for the case of two sets of dielectric spheres with equal permittivity but different radius, which has already been investigated in previous work [17], [21] for arrangements (g) and (b), Fig. 2.1, respectively. Except where noted, $\mu_1 = \mu_2 = 1$. The fractional bandwidth of the backward wave or DNG region is defined as the width of the backward wave or DNG kd interval divided by the average value of kd in that interval.

2.4.1 Verification

First, the theory of Section 2.3 is tested for arrangements (a) to (g). The $k-\beta$ diagrams of arrangements (a) to (g), Fig. 2.1, with parameters $\epsilon_{r1} = \epsilon_{r2} = 400$, $a_2/a_1 = 1.4291$, and $(a_1 + a_2)/(2d) = 0.2271$, are obtained by solving (2.14) with Tables 2.1 to 2.4 and compared with those calculated using MIT Photonic-Bands (MPB) [35] and [17, Eq. (2.10)] in Fig. 2.3. Good agreements are achieved. Note that MPB results for arrangements (a), (d), (f), and (g) are only shown in the range of $0 < \beta d < \pi/2$ instead of $0 < \beta d < \pi$. The reason is that, in MPB, the lattice constant in the array axis direction of these arrangements is set two times larger than that of arrangements (b), (c), and (e) to guarantee the translational symmetry in this direction. This means that the size of the corresponding reciprocal lattice in the Brillouin zone of arrangements (a), (d), (f), and (g) is half the size of that of arrangements (b), (c), and (e). This has been discussed in detail in the literature in the context of photonic band structure theory [36], [37]. Also note that MPB gives several pass-bands around $kd = 0.6$ while presented and [17] results show a band-gap in this region, which may due to the fact that MPB accounts for all the possible polarizations in addition to the TEM mode of the electromagnetic waves in 3D inhomogeneous structures [38], [39].

2.4.2 Two sets of dielectric spheres

Next, the performance of different arrangements of two sets of dielectric spheres with equal permittivity but different radius is investigated. The relative permittivity of both spheres is chosen as 214.28, following [17], and the ratio of the radius of the larger sphere to that of the smaller sphere is 1.4294, which is obtained by the division of $ka_2 = 0.3054$, corresponding to the first electric dipole resonance, by $ka_1 = 0.2137$, corresponding to the first magnetic dipole resonance. Since a larger volume fraction will increase the coupling between the electric and magnetic dipoles of the spheres so as to give a wider backward wave bandwidth [21], a large volume fraction, $v_f = 0.3308$ ($a_2/d = 0.49$), is chosen. It should be noted that a larger v_f can be achieved by choosing a tetragonal lattice ($h \neq d$), but this is not investigated in detail here since the focus of this paper is on the relative arrangements of the spheres. Backward

wave and DNG regions and parameters are shown in Table 2.5. To treat two-spheres periodic arrays macroscopically as a homogeneous medium with effective permittivity and permeability, the condition $kd', \beta d' \ll 1$ must be met in which d' is the period of the array. In practice this can be relaxed to the condition that both $\beta d'$ and kd' are less than approximately 1. However, the period of a particular array may be different in different directions. For example, arrangement (a), Fig. 2.1, has a period $d' = d$, which is the separation of adjacent spheres, in x and y directions, and a period $d' = 2d$, which is the separation of two adjacent 1-spheres or two adjacent 2-spheres, in the z direction. Since effective constitutive parameters should be independent of the direction of the traveling wave [40], the homogenization criteria given by the maximum period, which is $2kd, 2\beta d \leq 1$ i.e. $kd, \beta d \leq 0.5$, is chosen for arrangements (a) to (g), Fig. 2.1. Note that only when kd and βd are both less than about 0.5 can the negative slope of the dispersion curve (backward wave) imply DNG behavior of the array. Consequently, and following [33], both the entire backward wave region (the part of the dispersion curve with negative slope) and the DNG region for which $kd, \beta d \leq 0.5$ are reported here. $(kd)_u$ and $(kd)_{l1}$ are the upper and lower values of kd, respectively, for the entire backward wave region, while $(kd)_{l2}$ is the lower value of kd for the portion of DNG region where $\beta d \leq 0.5$. BW_1 and BW_2 are the fractional bandwidths for the entire backward wave region and for the portion of the DNG region where $\beta d \leq 0.5$. As shown in Table 2.5, arrangements (c) and (d) give the widest BW_1 and BW_2, respectively. Note that all the backward wave and DNG regions in Table 2.5 are around $kd = 0.6233$, which corresponds to the first magnetic dipole resonance of the 1-spheres at $ka_1 = 0.2137$ and the first electric dipole resonance of the 2-spheres at $ka_2 = 0.3054$.

Table 2.6 shows the results for different arrangements of two sets of dielectric spheres with equal radius but different permittivity. The relative permittivity of the 1-spheres is chosen to be $\epsilon_{r1} = 214.28$, the value for which the first magnetic dipole resonance is at $ka = 0.2137$, and the relative permittivity of the 2-spheres is chosen to be $\epsilon_{r2} = 440.20$, the value for which the first electric dipole resonance is at $ka = 0.2137$. Similar to the previous example for spheres of different radius, a large volume fraction, $v_f = 0.4928$ $(a/d = 0.49)$, is chosen. It can be seen that arrangement (c) provides both the widest BW_1 and BW_2. Also, all the backward wave and DNG regions in Table 2.6 are around $kd = 0.4360$, which corresponds to the first magnetic

dipole resonance of the 1-spheres and the first electric dipole resonance of the 2-spheres, both at $ka = 0.2137$.

Accounting for different arrangements of two sets of purely dielectric spheres, therefore, it has been shown here that the maximum DNG bandwidth ($BW_2 = 0.21\%$) is not significantly different from that reported in previous literature ($BW_2 = 0.169\%$) [17].

2.4.3 Dielectric and magnetic spheres

Different arrangements of one set of purely dielectric spheres and one of magnetic spheres, with $\epsilon_{r1} = \mu_{r2} = 214.28$, $\epsilon_{r2} = \mu_{r1} = 1$, are now considered. The first magnetic dipole resonance for 1-spheres and first electric dipole resonance for 2-spheres are both at $ka = 0.2137$. Backward wave and DNG regions and parameters are shown in Table 2.7. Here, arrangement (b) yields both the widest BW_1 and BW_2. As in Table 2.6, all the backward wave and DNG regions in Table 2.7 occur at around $kd = 0.4360$, which corresponds to the resonance at $ka = 0.2137$.

In this case of mixed dielectric and magnetic spheres, different arrangements of spheres, Fig. 2.1, yield quite different DNG bandwidths ($3.599\% \leq BW_2 \leq 7.403\%$).

2.5 Conclusion

In this paper, exact (within the dipole scattering approximation) $k-\beta$ (dispersion) equations have been obtained for 3D periodic arrays of two different magnetodielectric spheres arbitrarily arranged on a simple tetragonal lattice. Using Floquet mode expansions and expressions for the rapid summation of Schlömilch series, rapidly converging expressions and their double summation form have been derived to replace the slowly converging summations, in order to improve the computational efficiency. The presented theory has been tested by comparing its $k - \beta$ diagrams with the corresponding one in [17] and those calculated by MPB. The backward wave and DNG bandwidths of 3D periodic arrays with different arrangements of spheres, Fig. 2.1, have been analyzed for various combinations of sphere types. In previous work, only arrangements (b) and (g) have been analyzed [21], [17]. Results show that arrangements (d), (c), and (b), Fig. 2.1, can provide, respectively, the widest DNG bandwidths 0.21%, 0.069%, and 7.403% for spheres combinations i), ii), and iii) (see abstract), respectively. Compared

with these reported in [17] with arrangement (g), 0.169%, 0.075%, and 2.891%, analysis of those available arrangements of the spheres shows similar narrow DNG bandwidths for spheres combinations i) and ii), and wider DNG bandwidths for spheres combination iii). This indicates that 3D periodic arrays with different arrangements of two sets of dielectric spheres on a simple tetragonal lattice yield similar narrow DNG bandwidths. Due at least partially to the fact that the magnetic dipole resonances of the purely dielectric spheres coincide perfectly with the electric dipole resonances of the purely magnetic spheres at all frequencies when $\epsilon_{r1} = \mu_{r2}$ and $\epsilon_{r2} = \mu_{r1} = 1$ [17], the backward wave and DNG bandwidths for this combination of spheres are much wider than those of any of the 3D periodic arrays of two sets of purely dielectric spheres. However, it is still, at least at present, not possible to fabricate non-metallic DNG metamaterials for RF applications with this combination since purely magnetic materials with relative permeability much greater than one are currently unavailable above 1 GHz.

Future developments of the present theory include the following aspects. First, DNG bandwidths for metamaterials composed of 3D periodic arrays of two different magnetodielectric spheres arbitrarily arranged on lattices other than simple tetragonal lattice, such as body-centered, face-centered, and diamond lattices may be analyzed. Second, considering that DNG behavior is extinguished if the constituents exhibit losses above a certain threshold value [13], [41], [42], 3D periodic arrays of two different lossy spheres can be studied by extension of the theory presented here.

2.6 Appendix A
Derivation of rapidly converging expressions

In this Appendix, rapidly converging expressions for the infinite summations in (2.10) corresponding to (2.4g) to (2.4l) are derived. The derivations of those corresponding to (2.4a) to (2.4f) are given in [17, Appendix A]. These derivations are all based on the work in [30] of developing rapidly converging expressions to replace the slowly converging summations.

Referring to the derivation of [30, Eq. (5.64)] (see [30, Eqs. (5.23) to (5.64)]), but now with the z axis, rather than the x axis, of the Cartesian coordinate system as the array axis,

with $(m-1/2)$ substituted for m, and with $(x,y,z)=(h/2,0,|n|d)$ substituted for $(x,y,z)=(|n|d,0,0)$, the following is obtained:

$$\Sigma_{5n}(kh,d/h,0)\overset{n\neq 0}{=}2\pi \mathrm{i}kh\mathrm{e}^{\mathrm{i}|n|kd}-2\pi\sum_{m,l=-\infty}^{\infty}(-1)^m\left[(2\pi l)^2-(kh)^2\right]\times\frac{\mathrm{e}^{-|n|(d/h)\sqrt{(2\pi)^2(m^2+l^2)-(kh)^2}}}{\sqrt{(2\pi)^2(m^2+l^2)-(kh)^2}},\quad 0<kh<2\pi. \tag{2.15}$$

Since from [30, Eq. (5.65)], it follows that, noting that summation over even n is equivalent to doubling d,

$$\begin{aligned}\sum_{\substack{n=-\infty\\ n\neq 0\\ n\text{ even}}}^{\infty}\mathrm{e}^{\mathrm{i}n\beta d}\Sigma_{5n}(2kh,d/2h,0)=&-4\pi\mathrm{i}kh-4\pi kh\frac{\sin(2kd)}{\cos(2\beta d)-\cos(2kd)}\\&-4\pi\sum_{n=1}^{\infty}\cos(2n\beta d)\sum_{\substack{m,l=-\infty\\(m,l)\neq(0,0)}}^{\infty}(-1)^m\left[(2\pi l)^2-(2kh)^2\right]\\&\times\frac{\mathrm{e}^{-n(d/h)\sqrt{(2\pi)^2(m^2+l^2)-(2kh)^2}}}{\sqrt{(2\pi)^2(m^2+l^2)-(2kh)^2}}.\end{aligned} \tag{2.16}$$

Similarly, replacing the factor $(-1)^m$ by $(-1)^l$ gives

$$\begin{aligned}\sum_{\substack{n=-\infty\\ n\neq 0\\ n\text{ even}}}^{\infty}\mathrm{e}^{\mathrm{i}n\beta d}\Sigma_{7n}(2kh,d/2h,0)=&-4\pi\mathrm{i}kh-4\pi kh\frac{\sin(2kd)}{\cos(2\beta d)-\cos(2kd)}\\&-4\pi\sum_{n=1}^{\infty}\cos(2n\beta d)\sum_{\substack{m,l=-\infty\\(m,l)\neq(0,0)}}^{\infty}(-1)^l\left[(2\pi l)^2-(2kh)^2\right]\\&\times\frac{\mathrm{e}^{-n(d/h)\sqrt{(2\pi)^2(m^2+l^2)-(2kh)^2}}}{\sqrt{(2\pi)^2(m^2+l^2)-(2kh)^2}}.\end{aligned} \tag{2.17}$$

Note that $\Sigma_{5s}(kh,0)$ given by (2.4h) represents the contribution from array scatterers in the self-plane ($n=0$) and that its rapidly converging expression for the self-column ($l=0$), $\Sigma_{5ss}(kh,0)$, is different from that for the other column, $\Sigma_{5sn}(kh,0)$. For this reason, they are derived separately. For the non-self-column, from the derivation of [30, Eq. (4.44)] (see [30, Eqs. (4.18) to (4.43)]) with $m-1/2$ substituted for m, with l substituted for nd/h, and with

$(h/2, |l|h)$ substituted for $(0, |n|d)$,

$$\sum_{m=-\infty}^{\infty} f_1(m-1/2, l, 0, kh, 0, 0) = \mathrm{i}\pi(kh)^2 H_0^{(1)}(|l|kh) - 4\sum_{m=-1}^{\infty}(-1)^m\left[(2\pi m)^2-(kh)^2\right]K_0\left(|l|\sqrt{(2\pi m)^2-(kh)^2}\right). \tag{2.18}$$

Next, referring to [30, Eq. (4.45)]

$$\Sigma_{5\mathrm{sn}}(2kh, 0) = 2\pi\mathrm{i}(2kh)^2\sum_{l=1}^{\infty} H_0^{(1)}(2lkh) - 8\sum_{m,l=1}^{\infty}(-1)^m\left[(2\pi m)^2-(2kh)^2\right]K_0\left(l\sqrt{(2\pi m)^2-(2kh)^2}\right). \tag{2.19}$$

For the self-column, from the derivation of [30, Eq. (4.55)] with $m-1/2$ substituted for m,

$$\Sigma_{5\mathrm{ss}}(2kh, 0) = 4\sum_{m=1}^{\infty}\frac{\mathrm{e}^{\mathrm{i}kh(2m-1)}}{m-1/2}\frac{-\mathrm{i}}{m-1/2}\left(2kh+\frac{\mathrm{i}}{m-1/2}\right). \tag{2.20}$$

This sum is evaluated using [43, Eqs. 1.443(5), 1.444(6)] and [30, Eqs. (D8) to (D10)] with the Clausen functions, $\mathrm{Cl}_i(a)$ $(i = 2, 3)$, having the summation over m odd treated as the summation over all m minus the summation over m even. Then

$$\Sigma_{5\mathrm{ss}}(2kh, 0) = 4\pi\mathrm{i}(kh)^2 + 32kh\mathrm{Cl}_2(kh) - 8kh\mathrm{Cl}_2(2kh) + 32\mathrm{Cl}_3(kh) - 4\mathrm{Cl}_3(2kh). \tag{2.21}$$

Combining (2.19) and (2.21) leads to

$$\Sigma_{5\mathrm{s}}(2kh, 0) = 2\mathrm{i}\pi(2kh)^2\sum_{l=1}^{\infty} H_0^{(1)}(2lkh) - 8\sum_{m,l=1}^{\infty}(-1)^m\left[(2\pi m)^2-(2kh)^2\right] \times K_0\left(l\sqrt{(2\pi m)^2-(2kh)^2}\right) + 4\pi\mathrm{i}(kh)^2 + 32kh\mathrm{Cl}_2(kh) - 8kh\mathrm{Cl}_2(2kh) + 32\mathrm{Cl}_3(kh) - 4\mathrm{Cl}_3(2kh) \tag{2.22}$$

with the Clausen functions $\mathrm{Cl}_2(a)$ and $\mathrm{Cl}_3(a)$ approximated by [17, Eq. (B1)]. The Clausen functions $\mathrm{Cl}_2(a)$ and $\mathrm{Cl}_3(a)$ can also be obtained from the dilogarithm and trilogarithm functions, respectively [18, Correction 26]. $\sum_{l=1}^{\infty} H_0^{(1)}(2lkh)$ can be efficiently evaluated by [17, Eqs. (B2), (B3)]. The series including zeroth order modified Bessel function of the second kind, K_0, converges very fast due to the exponential decay of this function.

The term $\Sigma_{7s}(kh,0)$ given by (2.4k) involves summation over l odd which means that its rapidly converging expression includes no self-column term. Following the derivation of [6, Eq. (4.44)] with $l-1/2$ substituted for nd/h, and $(0,|l-1/2|h)$ substituted for $(0,|n|d)$,

$$\sum_{m=-\infty}^{\infty} f_1(m,l-1/2,0,kh,0,0) = \mathrm{i}\pi(kh)^2 H_0^{(1)}\left(|l-1/2|kh\right) - 4\sum_{m=1}^{\infty}\left[(2\pi m)^2-(kh)^2\right] K_0\left(|l-1/2|\sqrt{(2\pi m)^2-(kh)^2}\right). \tag{2.23}$$

Then

$$\Sigma_{7s}(2kh,0) = 2\pi\mathrm{i}(2kh)^2\sum_{l=1}^{\infty} H_0^{(1)}\left[(2l-1)kh\right] - 8\sum_{m,l=1}^{\infty}\left[(2\pi m)^2-(2kh)^2\right] \times K_0\left((2l-1)\sqrt{(\pi m)^2-(kh)^2}\right). \tag{2.24}$$

The sum $\sum_{l=1}^{\infty} H_0^{(1)}\left[(2l-1)kh\right]$ can be efficiently evaluated using [17, Eqs. (A.15), (B.2), and (B.3)].

Considering $\Sigma_{6n}(kh,d/h,0)$ from (2.4i) and the derivation of [30, Eq. (9.74)] (see [30, Eqs. (9.32) to (9.74)]) with $m-1/2$ substituted for m, and $(x,y)=(h/2,0)$ substituted for $(x,y)=(0,0)$,

$$\begin{aligned}\Sigma_{6n}(kh,d/h,0) =& \mathrm{sgn}(n)\Big[2\pi\mathrm{i}(kh)\mathrm{e}^{\mathrm{i}|n|kd} + 2\pi\mathrm{i}(kh) \\ &\times \sum_{\substack{m,l=-\infty \\ (m,l)\neq(0,0)}}^{\infty} (-1)^m \times \mathrm{e}^{-|n|(d/h)\sqrt{(2\pi)^2(m^2+l^2)-(kh)^2}}\Big], \quad n\neq 0; \\ =& 0, \quad n=0.\end{aligned} \tag{2.25}$$

From [30, Eq. (9.76)]

$$\sum_{\substack{n=-\infty \\ n\neq 0 \\ n \text{ even}}}^{\infty} \mathrm{e}^{\mathrm{i}n\beta d}\Sigma_{6n}(2kh,d/2h,0) = 4\pi kh\frac{\sin(2\beta d)}{\cos(2\beta d)-\cos(2kd)} - 8\pi kh\sum_{n=1}^{\infty}\sin(2n\beta d) \times \sum_{\substack{m,l=-\infty \\ (m,l)\neq(0,0)}}^{\infty} (-1)^m \mathrm{e}^{-n(d/h)\sqrt{(2\pi)^2(m^2+l^2)-(2kh)^2}}. \tag{2.26}$$

Similarly, replacing the factor $(-1)^m$ by $(-1)^l$ gives

$$\sum_{\substack{n=-\infty\\ n\neq 0\\ n\text{ even}}}^{\infty} \mathrm{e}^{\mathrm{i}n\beta d}\Sigma_{8n}(2kh,d/2h,0)=\sum_{\substack{n=-\infty\\ n\neq 0\\ n\text{ even}}}^{\infty} \mathrm{e}^{\mathrm{i}n\beta d}\Sigma_{6n}(2kh,d/2h,0). \tag{2.27}$$

For the summation for odd n, $\sum_{n=-\infty}^{\infty}\mathrm{e}^{\mathrm{i}n\beta d}\Sigma_{5n}(2kh,d/2h,0)$, n odd, is accounted for firstly. According to (2.15) and using [17, Eq.(A.16)]

$$2\pi \mathrm{i}kh\sum_{n=-\infty}^{\infty}\mathrm{e}^{\mathrm{i}(n-1/2)\beta d}\mathrm{e}^{\mathrm{i}|n-1/2|kd}=\frac{8\pi kh\mathrm{e}^{\mathrm{i}kd}\cos(\beta d/2)\sin(kd/2)}{1-2\cos(\beta d)\mathrm{e}^{\mathrm{i}kd}+\mathrm{e}^{2\mathrm{i}kd}}, \tag{2.28}$$

then summing over odd n by doubling d leads to

$$\begin{aligned}\sum_{\substack{n=-\infty\\ n\text{ odd}}}^{\infty} \mathrm{e}^{\mathrm{i}n\beta d}\Sigma_{5n}(2kh,d/2h,0)=&\frac{16\pi kh\mathrm{e}^{2\mathrm{i}kd}\cos(\beta d)\sin(kd)}{1-2\cos(2\beta d)\mathrm{e}^{2\mathrm{i}kd}+\mathrm{e}^{4\mathrm{i}kd}}-4\pi\sum_{n=1}^{\infty}\cos(2n-1)\beta d\\ &\times\sum_{\substack{m,l=-\infty\\ (m,l)\neq(0,0)}}^{\infty}(-1)^m\left[(2\pi l)^2-(2kh)^2\right]\\ &\times\frac{\mathrm{e}^{-(2n-1)(d/2h)\sqrt{(2\pi)^2(m^2+l^2)-(2kh)^2}}}{\sqrt{(2\pi)^2(m^2+l^2)-(2kh)^2}}.\end{aligned} \tag{2.29}$$

Similarly, replacing the factor $(-1)^m$ by $(-1)^l$ gives

$$\begin{aligned}\sum_{\substack{n=-\infty\\ n\text{ odd}}}^{\infty} \mathrm{e}^{\mathrm{i}n\beta d}\Sigma_{7n}(2kh,d/2h,0)=&\frac{16\pi kh\mathrm{e}^{2\mathrm{i}kd}\cos(\beta d)\sin(kd)}{1-2\cos(2\beta d)\mathrm{e}^{2\mathrm{i}kd}+\mathrm{e}^{4\mathrm{i}kd}}-4\pi\sum_{n=1}^{\infty}\cos(2n-1)\beta d\\ &\times\sum_{\substack{m,l=-\infty\\ (m,l)\neq(0,0)}}^{\infty}(-1)^l\left[(2\pi l)^2-(2kh)^2\right]\\ &\times\frac{\mathrm{e}^{-(2n-1)(d/2h)\sqrt{(2\pi)^2(m^2+l^2)-(2kh)^2}}}{\sqrt{(2\pi)^2(m^2+l^2)-(2kh)^2}}.\end{aligned} \tag{2.30}$$

For $\sum_{n=-\infty}^{\infty}\mathrm{e}^{\mathrm{i}n\beta d}\Sigma_{6n}(2kh,d/2h,0)$, n odd, beginning with (2.25) and using [17, Eq.(A.18)]

$$2\pi \mathrm{i}kh\sum_{n=-\infty}^{\infty}\mathrm{sgn}(n-1/2)\mathrm{e}^{\mathrm{i}(n-1/2)\beta d}\mathrm{e}^{\mathrm{i}|n-1/2|kd}=-\frac{8\pi kh\mathrm{e}^{\mathrm{i}kd}\sin(\beta d/2)\cos(kd/2)}{1-2\cos(\beta d)\mathrm{e}^{\mathrm{i}kd}+\mathrm{e}^{2\mathrm{i}kd}}, \tag{2.31}$$

then summing over odd n by doubling d leads to

$$\sum_{\substack{n=-\infty\\ n\text{ odd}}}^{\infty} \mathrm{e}^{\mathrm{i}n\beta d}\Sigma_{6n}(2kh, d/2h, 0) = -\frac{16\pi kh\mathrm{e}^{2\mathrm{i}kd}\sin(\beta d)\cos(kd)}{1-2\cos(2\beta d)\mathrm{e}^{2\mathrm{i}kd}+\mathrm{e}^{4\mathrm{i}kd}} - 8\pi kh\sum_{n=1}^{\infty}\sin(2n-1)\beta d \times \sum_{\substack{m,l=-\infty\\ (m,l)\neq(0,0)}}^{\infty}(-1)^m\mathrm{e}^{-(2n-1)(d/2h)\sqrt{(2\pi)^2(m^2+l^2)-(2kh)^2}}. \tag{2.32}$$

Similarly, replacing the factor $(-1)^m$ by $(-1)^l$ gives

$$\sum_{\substack{n=-\infty\\ n\text{ odd}}}^{\infty} \mathrm{e}^{\mathrm{i}n\beta d}\Sigma_{8n}(2kh, d/2h, 0) = \sum_{\substack{n=-\infty\\ n\text{ odd}}}^{\infty} \mathrm{e}^{\mathrm{i}n\beta d}\Sigma_{6n}(2kh, d/2h, 0). \tag{2.33}$$

2.7 Appendix B

Derivation of double summation form of the rapidly converging expressions

To further accelerate the calculation while improving the accuracy, double summation form of the rapidly converging expressions for the infinite summations of (2.4a), (2.4c), (2.4d), (2.4f), (2.4g), (2.4i), (2.4j), and (2.4l) with respect to n for n even ($n \neq 0$), and for n odd in (2.10) are obtained by performing the summation over n from 1 to ∞ in closed form using [30, Eq. (D.4)]

$$\sum_{n=1}^{\infty} z^n = \frac{z}{1-z},\ z = \mathrm{e}^{\mathrm{i}(kd\pm\beta d)}. \tag{2.34}$$

This leads to

$$\sum_{\substack{n=-\infty\\ n\neq 0\\ n\text{ even}}}^{\infty} \mathrm{e}^{\mathrm{i}n\beta d}\Sigma_{1n}(2kh, d/2h, 0) = -4\pi\mathrm{i}kh - 4\pi kh\frac{\sin(2kd)}{\cos(2\beta d)-\cos(2kd)} - 4\pi\sum_{\substack{m,l=-\infty\\ (m,l)\neq(0,0)}}^{\infty}\frac{(2\pi m)^2-(2kh)^2}{r} \times \frac{\cos(2\beta d)\mathrm{e}^{-rd/h}-\mathrm{e}^{-2rd/h}}{1-2\cos(2\beta d)\mathrm{e}^{-rd/h}+\mathrm{e}^{-2rd/h}}, \tag{2.35}$$

$$\sum_{\substack{n=-\infty\\ n\neq 0\\ n \text{ even}}}^{\infty} \mathrm{e}^{\mathrm{i}n\beta d}\Sigma_{2n}(2kh, d/2h, 0) = 4\pi kh\frac{\sin(2\beta d)}{\cos(2\beta d)-\cos(2kd)} - 8\pi kh \sum_{\substack{m,l=-\infty\\ (m,l)\neq(0,0)}}^{\infty} \frac{\sin(2\beta d)\mathrm{e}^{-rd/h}}{1-2\cos(2\beta d)\mathrm{e}^{-rd/h}+\mathrm{e}^{-2rd/h}}, \tag{2.36}$$

$$\sum_{\substack{n=-\infty\\ n\neq 0\\ n \text{ even}}}^{\infty} \mathrm{e}^{\mathrm{i}n\beta d}\Sigma_{3n}(2kh, d/2h, 0) = -4\pi\mathrm{i}kh - 4\pi kh\frac{\sin(2kd)}{\cos(2\beta d)-\cos(2kd)} - 4\pi \sum_{\substack{m,l=-\infty\\ (m,l)\neq(0,0)}}^{\infty} (-1)^{m+l}\frac{(2\pi m)^2-(2kh)^2}{r} \times \frac{\cos(2\beta d)\mathrm{e}^{-rd/h}-\mathrm{e}^{-2rd/h}}{1-2\cos(2\beta d)\mathrm{e}^{-rd/h}+\mathrm{e}^{-2rd/h}}, \tag{2.37}$$

$$\sum_{\substack{n=-\infty\\ n\neq 0\\ n \text{ even}}}^{\infty} \mathrm{e}^{\mathrm{i}n\beta d}\Sigma_{4n}(2kh, d/2h, 0) = 4\pi kh\frac{\sin(2\beta d)}{\cos(2\beta d)-\cos(2kd)} - 8\pi kh \sum_{\substack{m,l=-\infty\\ (m,l)\neq(0,0)}}^{\infty} (-1)^{m+l}\frac{\sin(2\beta d)\mathrm{e}^{-rd/h}}{1-2\cos(2\beta d)\mathrm{e}^{-rd/h}+\mathrm{e}^{-2rd/h}}, \tag{2.38}$$

$$\sum_{\substack{n=-\infty\\ n\neq 0\\ n \text{ even}}}^{\infty} \mathrm{e}^{\mathrm{i}n\beta d}\Sigma_{5n}(2kh, d/2h, 0) = -4\pi\mathrm{i}kh - 4\pi kh\frac{\sin(2kd)}{\cos(2\beta d)-\cos(2kd)} - 4\pi \sum_{\substack{m,l=-\infty\\ (m,l)\neq(0,0)}}^{\infty} (-1)^{m}\frac{(2\pi l)^2-(2kh)^2}{r} \times \frac{\cos(2\beta d)\mathrm{e}^{-rd/h}-\mathrm{e}^{-2rd/h}}{1-2\cos(2\beta d)\mathrm{e}^{-rd/h}+\mathrm{e}^{-2rd/h}}, \tag{2.39}$$

$$\sum_{\substack{n=-\infty\\ n\neq 0\\ n\text{ even}}}^{\infty} \mathrm{e}^{\mathrm{i}n\beta d}\Sigma_{6n}(2kh,d/2h,0) = 4\pi kh\frac{\sin(2\beta d)}{\cos(2\beta d)-\cos(2kd)} - 8\pi kh\sum_{\substack{m,l=-\infty\\ (m,l)\neq(0,0)}}^{\infty}(-1)^m\frac{\sin(2\beta d)\mathrm{e}^{-rd/h}}{1-2\cos(2\beta d)\mathrm{e}^{-rd/h}+\mathrm{e}^{-2rd/h}}, \tag{2.40}$$

$$\sum_{\substack{n=-\infty\\ n\neq 0\\ n\text{ even}}}^{\infty} \mathrm{e}^{\mathrm{i}n\beta d}\Sigma_{7n}(2kh,d/2h,0) = -4\pi\mathrm{i}kh - 4\pi kh\frac{\sin(2kd)}{\cos(2\beta d)-\cos(2kd)} - 4\pi\sum_{\substack{m,l=-\infty\\ (m,l)\neq(0,0)}}^{\infty}(-1)^l\frac{(2\pi l)^2-(2kh)^2}{r} \times\frac{\cos(2\beta d)\mathrm{e}^{-rd/h}-\mathrm{e}^{-2rd/h}}{1-2\cos(2\beta d)\mathrm{e}^{-rd/h}+\mathrm{e}^{-2rd/h}}, \tag{2.41}$$

$$\sum_{\substack{n=-\infty\\ n\text{ odd}}}^{\infty} \mathrm{e}^{\mathrm{i}n\beta d}\Sigma_{1n}(2kh,d/2h,0) = \frac{16\pi kh\mathrm{e}^{2\mathrm{i}kd}\cos(\beta d)\sin(kd)}{1-2\cos(2\beta d)\mathrm{e}^{2\mathrm{i}kd}+\mathrm{e}^{4\mathrm{i}kd}} - 8\pi\mathrm{e}^{-\mathrm{i}\beta d}\sum_{\substack{m,l=-\infty\\ (m,l)\neq(0,0)}}^{\infty}\frac{\mathrm{e}^{rd/2h}}{r}\left[(\pi m)^2-(kh)^2\right] \times\frac{(1+\mathrm{e}^{2\mathrm{i}\beta d})(\mathrm{e}^{-rd/h}-\mathrm{e}^{-2rd/h})}{1-2\cos(2\beta d)\mathrm{e}^{-rd/h}+\mathrm{e}^{-2rd/h}}, \tag{2.42}$$

$$\sum_{\substack{n=-\infty\\ n\text{ odd}}}^{\infty} \mathrm{e}^{\mathrm{i}n\beta d}\Sigma_{2n}(2kh,d/2h,0) = -\frac{16\pi kh\mathrm{e}^{2\mathrm{i}kd}\sin(\beta d)\cos(kd)}{1-2\cos(2\beta d)\mathrm{e}^{2\mathrm{i}kd}+\mathrm{e}^{4\mathrm{i}kd}} + 4\mathrm{i}\pi kh\mathrm{e}^{-\mathrm{i}\beta d}\sum_{\substack{m,l=-\infty\\ (m,l)\neq(0,0)}}^{\infty}\mathrm{e}^{rd/2h}\frac{(\mathrm{e}^{2\mathrm{i}\beta d}-1)(\mathrm{e}^{-rd/h}+\mathrm{e}^{-2rd/h})}{1-2\cos(2\beta d)\mathrm{e}^{-rd/h}+\mathrm{e}^{-2rd/h}}, \tag{2.43}$$

$$\sum_{\substack{n=-\infty\\ n\text{ odd}}}^{\infty} \mathrm{e}^{\mathrm{i}n\beta d}\Sigma_{3n}(2kh,d/2h,0) = \frac{16\pi kh\mathrm{e}^{2\mathrm{i}kd}\cos(\beta d)\sin(kd)}{1-2\cos(2\beta d)\mathrm{e}^{2\mathrm{i}kd}+\mathrm{e}^{4\mathrm{i}kd}} - 8\pi\mathrm{e}^{-\mathrm{i}\beta d}\sum_{\substack{m,l=-\infty\\ (m,l)\neq(0,0)}}^{\infty}(-1)^{m+l}\frac{\mathrm{e}^{rd/2h}}{r}\left[(\pi m)^2-(kh)^2\right] \times\frac{(1+\mathrm{e}^{2\mathrm{i}\beta d})(\mathrm{e}^{-rd/h}-\mathrm{e}^{-2rd/h})}{1-2\cos(2\beta d)\mathrm{e}^{-rd/h}+\mathrm{e}^{-2rd/h}}, \tag{2.44}$$

$$\sum_{\substack{n=-\infty\\ n\text{ odd}}}^{\infty} \mathrm{e}^{\mathrm{i}n\beta d}\Sigma_{4n}(2kh,d/2h,0) = -\frac{16\pi kh\mathrm{e}^{2\mathrm{i}kd}\sin(\beta d)\cos(kd)}{1-2\cos(2\beta d)\mathrm{e}^{2\mathrm{i}kd}+\mathrm{e}^{4\mathrm{i}kd}} + 4\mathrm{i}\pi kh\mathrm{e}^{-\mathrm{i}\beta d}\sum_{\substack{m,l=-\infty\\ (m,l)\neq(0,0)}}^{\infty}(-1)^{m+l}\mathrm{e}^{rd/2h} \times\frac{(\mathrm{e}^{2\mathrm{i}\beta d}-1)(\mathrm{e}^{-rd/h}+\mathrm{e}^{-2rd/h})}{1-2\cos(2\beta d)\mathrm{e}^{-rd/h}+\mathrm{e}^{-2rd/h}}, \tag{2.45}$$

$$\sum_{\substack{n=-\infty\\ n\text{ odd}}}^{\infty} \mathrm{e}^{\mathrm{i}n\beta d}\Sigma_{5n}(2kh,d/2h,0) =\frac{16\pi kh\mathrm{e}^{2\mathrm{i}kd}\cos(\beta d)\sin(kd)}{1-2\cos(2\beta d)\mathrm{e}^{2\mathrm{i}kd}+\mathrm{e}^{4\mathrm{i}kd}} - 8\pi\mathrm{e}^{-\mathrm{i}\beta d}\sum_{\substack{m,l=-\infty\\ (m,l)\neq(0,0)}}^{\infty}(-1)^{m}\frac{\mathrm{e}^{rd/2h}}{r}\left[(\pi l)^2-(kh)^2\right] \times\frac{(1+\mathrm{e}^{2\mathrm{i}\beta d})(\mathrm{e}^{-rd/h}-\mathrm{e}^{-2rd/h})}{1-2\cos(2\beta d)\mathrm{e}^{-rd/h}+\mathrm{e}^{-2rd/h}}, \tag{2.46}$$

$$\sum_{\substack{n=-\infty\\ n\text{ odd}}}^{\infty} \mathrm{e}^{\mathrm{i}n\beta d}\Sigma_{6n}(2kh,d/2h,0) = -\frac{16\pi kh\mathrm{e}^{2\mathrm{i}kd}\sin(\beta d)\cos(kd)}{1-2\cos(2\beta d)\mathrm{e}^{2\mathrm{i}kd}+\mathrm{e}^{4\mathrm{i}kd}} + 4\mathrm{i}\pi kh\mathrm{e}^{-\mathrm{i}\beta d}\sum_{\substack{m,l=-\infty\\ (m,l)\neq(0,0)}}^{\infty}(-1)^{m}\mathrm{e}^{rd/2h} \times\frac{(\mathrm{e}^{2\mathrm{i}\beta d}-1)(\mathrm{e}^{-rd/h}+\mathrm{e}^{-2rd/h})}{1-2\cos(2\beta d)\mathrm{e}^{-rd/h}+\mathrm{e}^{-2rd/h}}, \tag{2.47}$$

$$\sum_{\substack{n=-\infty\\ n\text{ odd}}}^{\infty} \mathrm{e}^{\mathrm{i}n\beta d}\Sigma_{7n}(2kh,d/2h,0) =\frac{16\pi kh\mathrm{e}^{2\mathrm{i}kd}\cos(\beta d)\sin(kd)}{1-2\cos(2\beta d)\mathrm{e}^{2\mathrm{i}kd}+\mathrm{e}^{4\mathrm{i}kd}} - 8\pi\mathrm{e}^{-\mathrm{i}\beta d}\sum_{\substack{m,l=-\infty\\ (m,l)\neq(0,0)}}^{\infty}(-1)^{l}\frac{\mathrm{e}^{rd/2h}}{r}\left[(\pi l)^2-(kh)^2\right] \times\frac{(1+\mathrm{e}^{2\mathrm{i}\beta d})(\mathrm{e}^{-rd/h}-\mathrm{e}^{-2rd/h})}{1-2\cos(2\beta d)\mathrm{e}^{-rd/h}+\mathrm{e}^{-2rd/h}}, \tag{2.48}$$

where $r=2\sqrt{\pi^2(m^2+l^2)-(kh)^2}$. According to (2.27) and (2.33), $\sum_{n=-\infty}^{\infty}\mathrm{e}^{\mathrm{i}n\beta d}\Sigma_{8n}(2kh,d/2h,0)$, $n\neq 0$, n even, as well as $\sum_{n=-\infty}^{\infty}\mathrm{e}^{\mathrm{i}n\beta d}\Sigma_{8n}(2kh,d/2h,0)$, n odd, are equal to (2.40) and (2.47), respectively.

2.8 Acknowledgment

This material is based upon work supported by the Air Force Research Laboratory under Contract FA8650-04-C-5228 at Iowa State University's Center for NDE. The authors wish to express their deep gratitude to Dr. Robert A. Shore (Air Force Research Laboratory, Hanscom AFB, MA), Prof. Andrea Alù (The University of Texas at Austin), Prof. Rana Biswas (Iowa State University), and Mr. Sidharath Jain (Iowa State University) for very helpful discussions and communications. The authors also thank the reviewers for their insightful comments which significantly improved the paper.

Table 2.1 Terms used to construct A_1 of arrangements (a) to (g), Fig. 2.1

Arrangement	$(1/8)\sum_{n=-\infty}^{\infty} e^{in\beta d}$, $n \neq 0$, n even	$1/8$	$(1/8)\sum_{n=-\infty}^{\infty} e^{in\beta d}$, n odd
a	$\Sigma_{1n}(2kh, d/2h, 0) + \Sigma_{3n}(2kh, d/2h, 0)$ $+\Sigma_{5n}(2kh, d/2h, 0) + \Sigma_{7n}(2kh, d/2h, 0)$	$\Sigma_{1s}(2kh, 0) + \Sigma_{3s}(2kh, 0)$ $+\Sigma_{5s}(2kh, 0) + \Sigma_{7s}(2kh, 0)$	-
b	$\Sigma_{1n}(2kh, d/2h, 0) + \Sigma_{7n}(2kh, d/2h, 0)$	$\Sigma_{1s}(2kh, 0) + \Sigma_{7s}(2kh, 0)$	$\Sigma_{1n}(2kh, d/2h, 0) + \Sigma_{7n}(2kh, d/2h, 0)$
c	$\Sigma_{1n}(2kh, d/2h, 0) + \Sigma_{5n}(2kh, d/2h, 0)$	$\Sigma_{1s}(2kh, 0) + \Sigma_{5s}(2kh, 0)$	$\Sigma_{1n}(2kh, d/2h, 0) + \Sigma_{5n}(2kh, d/2h, 0)$
d	$\Sigma_{1n}(2kh, d/2h, 0) + \Sigma_{5n}(2kh, d/2h, 0)$	$\Sigma_{1s}(2kh, 0) + \Sigma_{5s}(2kh, 0)$	$\Sigma_{3n}(2kh, d/2h, 0) + \Sigma_{7n}(2kh, d/2h, 0)$
e	$\Sigma_{1n}(2kh, d/2h, 0) + \Sigma_{3n}(2kh, d/2h, 0)$	$\Sigma_{1s}(2kh, 0) + \Sigma_{3s}(2kh, 0)$	$\Sigma_{1n}(2kh, d/2h, 0) + \Sigma_{3n}(2kh, d/2h, 0)$
f	$\Sigma_{1n}(2kh, d/2h, 0) + \Sigma_{7n}(2kh, d/2h, 0)$	$\Sigma_{1s}(2kh, 0) + \Sigma_{7s}(2kh, 0)$	$\Sigma_{3n}(2kh, d/2h, 0) + \Sigma_{5n}(2kh, d/2h, 0)$
g	$\Sigma_{1n}(2kh, d/2h, 0) + \Sigma_{3n}(2kh, d/2h, 0)$	$\Sigma_{1s}(2kh, 0) + \Sigma_{3s}(2kh, 0)$	$\Sigma_{5n}(2kh, d/2h, 0) + \Sigma_{7n}(2kh, d/2h, 0)$

Table 2.2 Terms used to construct A_2 of arrangements (a) to (g), Fig. 2.1

Arrangement	$(1/8)\sum_{n=-\infty}^{\infty} e^{in\beta d}$, $n \neq 0$, n even	$(1/8)\sum_{n=-\infty}^{\infty} e^{in\beta d}$, n odd
a	$\Sigma_{2n}(2kh, d/2h, 0) + \Sigma_{4n}(2kh, d/2h, 0) + \Sigma_{6n}(2kh, d/2h, 0) + \Sigma_{8n}(2kh, d/2h, 0)$	-
b	$\Sigma_{2n}(2kh, d/2h, 0) + \Sigma_{8n}(2kh, d/2h, 0)$	$\Sigma_{2n}(2kh, d/2h, 0) + \Sigma_{8n}(2kh, d/2h, 0)$
c	$\Sigma_{2n}(2kh, d/2h, 0) + \Sigma_{6n}(2kh, d/2h, 0)$	$\Sigma_{2n}(2kh, d/2h, 0) + \Sigma_{6n}(2kh, d/2h, 0)$
d	$\Sigma_{2n}(2kh, d/2h, 0) + \Sigma_{6n}(2kh, d/2h, 0)$	$\Sigma_{4n}(2kh, d/2h, 0) + \Sigma_{8n}(2kh, d/2h, 0)$
e	$\Sigma_{2n}(2kh, d/2h, 0) + \Sigma_{4n}(2kh, d/2h, 0)$	$\Sigma_{2n}(2kh, d/2h, 0) + \Sigma_{4n}(2kh, d/2h, 0)$
f	$\Sigma_{2n}(2kh, d/2h, 0) + \Sigma_{8n}(2kh, d/2h, 0)$	$\Sigma_{4n}(2kh, d/2h, 0) + \Sigma_{6n}(2kh, d/2h, 0)$
g	$\Sigma_{2n}(2kh, d/2h, 0) + \Sigma_{4n}(2kh, d/2h, 0)$	$\Sigma_{6n}(2kh, d/2h, 0) + \Sigma_{8n}(2kh, d/2h, 0)$

Table 2.3 Terms used to construct A_3 of arrangements (a) to (g), Fig. 2.1

Arrangement	$(1/8)\sum_{n=-\infty}^{\infty} e^{in\beta d}$, $n \neq 0$, n even	$1/8$	$(1/8)\sum_{n=-\infty}^{\infty} e^{in\beta d}$, n odd
a	-	-	$\Sigma_{1n}(2kh, d/2h, 0) + \Sigma_{3n}(2kh, d/2h, 0)$ $+\Sigma_{5n}(2kh, d/2h, 0) + \Sigma_{7n}(2kh, d/2h, 0)$
b	$\Sigma_{3n}(2kh, d/2h, 0) + \Sigma_{5n}(2kh, d/2h, 0)$	$\Sigma_{3s}(2kh, 0) + \Sigma_{5s}(2kh, 0)$	$\Sigma_{3n}(2kh, d/2h, 0) + \Sigma_{5n}(2kh, d/2h, 0)$
c	$\Sigma_{3n}(2kh, d/2h, 0) + \Sigma_{7n}(2kh, d/2h, 0)$	$\Sigma_{3s}(2kh, 0) + \Sigma_{7s}(2kh, 0)$	$\Sigma_{3n}(2kh, d/2h, 0) + \Sigma_{7n}(2kh, d/2h, 0)$
d	$\Sigma_{3n}(2kh, d/2h, 0) + \Sigma_{7n}(2kh, d/2h, 0)$	$\Sigma_{3s}(2kh, 0) + \Sigma_{7s}(2kh, 0)$	$\Sigma_{1n}(2kh, d/2h, 0) + \Sigma_{5n}(2kh, d/2h, 0)$
e	$\Sigma_{5n}(2kh, d/2h, 0) + \Sigma_{7n}(2kh, d/2h, 0)$	$\Sigma_{5s}(2kh, 0) + \Sigma_{7s}(2kh, 0)$	$\Sigma_{5n}(2kh, d/2h, 0) + \Sigma_{7n}(2kh, d/2h, 0)$
f	$\Sigma_{3n}(2kh, d/2h, 0) + \Sigma_{5n}(2kh, d/2h, 0)$	$\Sigma_{3s}(2kh, 0) + \Sigma_{5s}(2kh, 0)$	$\Sigma_{1n}(2kh, d/2h, 0) + \Sigma_{7n}(2kh, d/2h, 0)$
g	$\Sigma_{5n}(2kh, d/2h, 0) + \Sigma_{7n}(2kh, d/2h, 0)$	$\Sigma_{5s}(2kh, 0) + \Sigma_{7s}(2kh, 0)$	$\Sigma_{1n}(2kh, d/2h, 0) + \Sigma_{3n}(2kh, d/2h, 0)$

Table 2.4 Terms used to construct A_4 of arrangements (a) to (g), Fig. 2.1

Arrangement	$(1/8)\sum_{n=-\infty}^{\infty} e^{in\beta d}$, $n \neq 0$, n even	$(1/8)\sum_{n=-\infty}^{\infty} e^{in\beta d}$, n odd
a	-	$\Sigma_{2n}(2kh, d/2h, 0) + \Sigma_{4n}(2kh, d/2h, 0) + \Sigma_{6n}(2kh, d/2h, 0) + \Sigma_{8n}(2kh, d/2h, 0)$
b	$\Sigma_{4n}(2kh, d/2h, 0) + \Sigma_{6n}(2kh, d/2h, 0)$	$\Sigma_{4n}(2kh, d/2h, 0) + \Sigma_{6n}(2kh, d/2h, 0)$
c	$\Sigma_{4n}(2kh, d/2h, 0) + \Sigma_{8n}(2kh, d/2h, 0)$	$\Sigma_{4n}(2kh, d/2h, 0) + \Sigma_{8n}(2kh, d/2h, 0)$
d	$\Sigma_{4n}(2kh, d/2h, 0) + \Sigma_{8n}(2kh, d/2h, 0)$	$\Sigma_{2n}(2kh, d/2h, 0) + \Sigma_{6n}(2kh, d/2h, 0)$
e	$\Sigma_{6n}(2kh, d/2h, 0) + \Sigma_{8n}(2kh, d/2h, 0)$	$\Sigma_{6n}(2kh, d/2h, 0) + \Sigma_{8n}(2kh, d/2h, 0)$
f	$\Sigma_{4n}(2kh, d/2h, 0) + \Sigma_{6n}(2kh, d/2h, 0)$	$\Sigma_{2n}(2kh, d/2h, 0) + \Sigma_{8n}(2kh, d/2h, 0)$
g	$\Sigma_{6n}(2kh, d/2h, 0) + \Sigma_{8n}(2kh, d/2h, 0)$	$\Sigma_{2n}(2kh, d/2h, 0) + \Sigma_{4n}(2kh, d/2h, 0)$

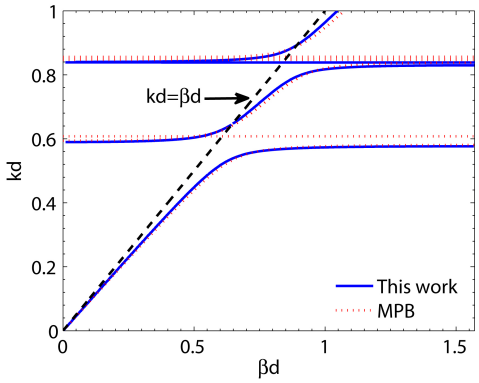

(a) Arrangement (a).

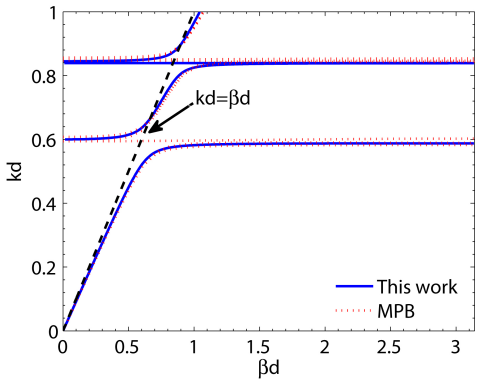

(b) Arrangement (b).

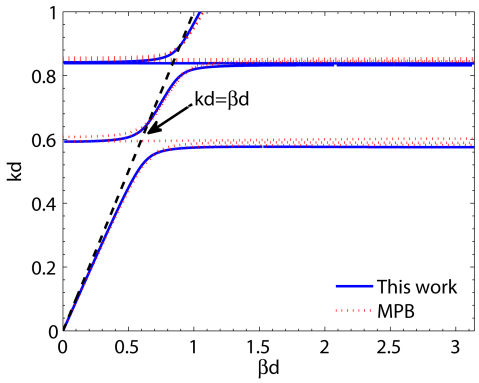

(c) Arrangement (c).

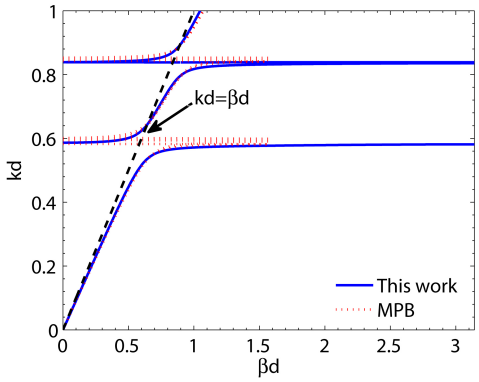

(d) Arrangement (d).

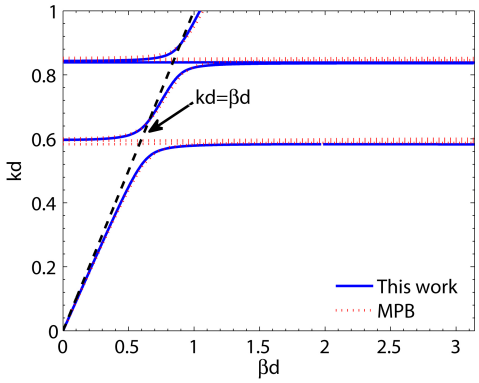

(e) Arrangement (e).

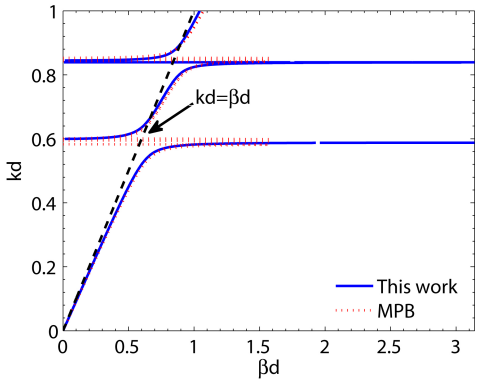

(f) Arrangement (f).

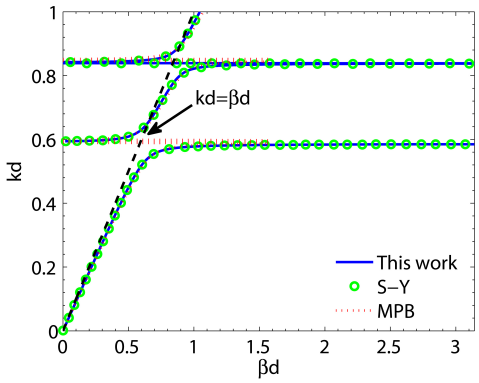

(g) Arrangement (g).

Figure 2.3 Comparisons of $k-\beta$ diagrams for a 3D periodic array with arrangements (a) to (g), Fig. 2.1, obtained by presented formulas in Tables 2.1 to 2.4 with these calculated by MPB [35] and [17, Eq. (2.10)] (for arrangement (g) only). The 20, 30, and 60 lowest bands of arrangements (a) to (c), (d) to (f), and (g), respectively, computed by MPB are shown. In these calculations, $\epsilon_{r1} = \epsilon_{r2} = 400$, $a_2/a_1 = 1.4291$, and $(a_1 + a_2)/(2d) = 0.2271$.

Table 2.5 Backward wave and DNG regions and parameters of different arrangements of two sets of dielectric spheres with equal permittivity but different radius

Arrangement*	$(kd)_u$	$(kd)_{l1}$	$(kd)_{l2}$	$BW_1\%$	$BW_2\%$
a	0.6233	0.6218	0.6227	0.241	0.096
b**	-	-	-	-	-
c	0.6244	0.6006	0.6236	3.886	0.128
d	0.6207	0.6185	0.6194	0.355	0.210
e	0.6251	0.6211	0.6250	0.642	0.016
f**	-	-	-	-	-
g	0.6248	0.6231	0.6245	0.272	0.048

$\epsilon_{r1} = \epsilon_{r2} = 214.28$, $a_2/a_1 = 1.4294$, $a_2/d = 0.49$

*See Fig. 2.1.

**The root finding procedure shows no backward wave in this case.

Table 2.6 Backward wave and DNG regions and parameters of different arrangements of two sets of dielectric spheres with equal radius but different permittivity

Arrangement*	$(kd)_u$	$(kd)_{l1}$	$(kd)_{l2}$	$BW_1\%$	$BW_2\%$
a	0.4353	0.4350	0.4352	0.069	0.023
b**	-	-	-	-	-
c	0.4362	0.3930	0.4359	10.420	0.069
d**	-	-	-	-	-
e	0.4366	0.4349	0.4365	0.390	0.023
f**	-	-	-	-	-
g	0.4364	0.4351	0.4363	0.298	0.023

$\epsilon_{r1} = 214.28$, $\epsilon_{r2} = 440.20$, $a_1 = a_2 = a$, $a/d = 0.49$

*See Fig. 2.1.

**The root finding procedure shows no backward wave in these case.

Table 2.7 Backward wave and DNG regions and parameters of different arrangements of magnetic and dielectric spheres

Arrangement*	$(kd)_u$	$(kd)_{l1}$	$(kd)_{l2}$	$BW_1\%$	$BW_2\%$
a**	-	-	-	-	-
b	0.5029	0.4163	0.4670	18.842	7.403
c	0.4484	0.3817	0.4311	16.070	3.934
d***	-	-	-	-	-
e	0.4810	0.4120	0.4540	15.454	5.775
f	0.5030	0.4165	0.4678	18.815	7.252
g	0.4610	0.4141	0.4447	10.719	3.599

$\epsilon_{r1} = \mu_{r2} = 214.28$, $\epsilon_{r2} = \mu_{r1} = 1$, $a_1 = a_2 = a$, $a/d = 0.49$

*See Fig. 2.1.

**The root finding procedure shows no backward wave in this case.

***For this case, the effective constitutive parameters derived from the solution to the $k - \beta$ equation is not reasonable.

2.9 References

[1] R. A. Shelby, D. R. Smith, and S. Schultz, "Experimental verification of a negative index of refraction," *Science*, vol. 292, no. 5514, pp. 77-79, 2001.

[2] J. B. Pendry, A. J. Holden, W. J. Stewart, and I. Youngs, "Extremely low frequency plasmons in metallic mesostructures," *Phys. Rev. Lett.*, vol. 76, no. 25, pp. 4773-4776, Jun. 1996.

[3] J. B. Pendry, A. J. Holden, D. J. Robbins, and W. J. Stewart, "Magnetism from conductors and enhanced nonlinear phenomena," *IEEE Trans. Microw. Theory Tech.*, vol. 47, no. 11, pp. 2075-2084, Nov. 1999.

[4] N. Engheta and R. W. Ziolkowski, *Metamaterials: Physics and Engineering Explorations.* New York: Wiley, 2006.

[5] J. B. Pendry, "Negative refraction makes a perfect lens," *Phys. Rev. Lett.*, vol. 85, no. 18, pp. 3966-3969, 2000.

[6] J. B. Pendry, D. Schurig, and D. R. Smith, "Controlling electromagnetic fields," *Science*, vol. 312, no. 5781, pp. 1780-1782, 2006.

[7] D. Schurig, J. J. Mock, B. J. Justice, S. A. Cummer, J. B. Pendry, A. F. Starr, and D. R. Smith, "Metamaterial electromagnetic cloak at microwave frequencies," *Science*, vol. 314, no. 5801, pp. 977-980, Nov. 2006.

[8] J. Valentine, J. Li, T. Zentgraf, G. Bartal, and X. Zhang, "An optical cloak made of dielectrics," *Nature Mater.*, vol. 8, no. 7, pp. 568-571, Jul. 2009.

[9] R. W. Ziolkowski and A. Erentok, "Metamaterial-based efficient electrically small antennas," *IEEE Trans. Antennas Propag.*, vol. 54, no. 7, pp. 2113-2130, Jul. 2006.

[10] W. W. Shu and J. M. Song, "Sommerfeld integral path for layered double negative metamaterials," *IEEE Trans. Antennas Propag.*, vol. 60, no. 3, pp. 1496–1504, Mar. 2012.

[11] J. Zhou, L. Zhang, G. Tuttle, T. Koschny, and C. M. Soukoulis, "Negative index materials using simple short wire pairs," *Phys. Rev. B*, vol. 73, no. 4, pp. 041101-1–041101-4, Jan. 2006.

[12] G. Dolling, C. Enkrich, M. Wegener, C. M. Soukoulis, and S. Linden, "Low-loss negative-index metamaterial at telecommunication wavelengths," *Opt. Lett.*, vol. 31, no. 12, pp. 1800-1802, 2006.

[13] C. L. Holloway, E. F. Kuester, J. Baker-Jarvis, and P. Kabos, "A doubly negative (DNG) composite medium composed of magneto-dielectric spherical particles embedded in a matrix," *IEEE Trans. Antennas Propag.*, vol. 51, no. 10, pp. 2596-2603, Oct. 2003.

[14] I. Vendik, O. Vendik, and M. Odit, "Isotropic artificial media with simultaneously negative permittivity and permeability," *Microw. Opt. Technol. Lett.*, vol. 48, no. 12, pp. 2553-2556, Dec. 2006.

[15] I. Vendik, O. Vendik, J. Kolmakov, and M. Odit, "Modelling of isotropic double negative media for microwave applications," *Opto-Electron. Rev.*, vol. 14, no. 3, pp. 179-186, 2006.

[16] L. Jylhä, I. Kolmakov, S. Maslovski, and S. Tretyakov, "Modeling of isotropic backward-wave materials composed of resonant spheres," *J. Appl. Phys.*, vol. 99, no. 4, pp. 043102-1–043102-7, Feb. 2006.

[17] R. A. Shore and A. D. Yaghjian, "Traveling waves on three-dimensional periodic arrays of two different alternating magnetodielectric spheres," *IEEE Trans. Antennas Propag.*, vol. 57, no. 10, pp. 3077-3091, Oct. 2009.

[18] Y. Li and R. A. Shore, "Corrections to "Traveling waves on three-dimensional periodic arrays of two different alternating magnetodielectric spheres (vol 57, pg 3077, 2009)"," *IEEE Trans. Antennas Propag.*, vol. 59, no. 7, Jul. 2011.

[19] A. Ahmadi and H. Mosallaei, "Physical configuration and performance modeling of all-dielectric metamaterials," *Phys. Rev. B*, vol. 77, no. 4, pp. 045104-1–045104-11, Jan. 2008.

[20] B. J. Seo, T. Ueda, T. Itoh, and H. Fetterman, "Isotropic left handed material at optical frequency with dielectric spheres embedded in negative permittivity medium," *Applied Phys. Lett.*, vol. 88, no. 16, pp. 161122-1–161122-3, Apr. 2006.

[21] S. Ghadarghadr and H. Mosallaei, "Dispersion diagram characteristics of periodic array of dielectric and magnetic materials based spheres," *IEEE Trans. Antennas Propag.*, vol. 57, no. 1, pp. 149-160, Jan. 2009.

[22] M. S. Wheeler, J. S. Aitchison, and M. Mojahedi, "Three-dimensional array of dielectric spheres with an isotropic negative permeability at infrared frequencies," *Phys. Rev. B*, vol. 72, no. 19, pp. 193103-1-193103-4, Nov. 2005.

[23] M. S. Wheeler, J. S. Aitchison, and M. Mojahedi, "Coated nonmagnetic spheres with a negative index of refraction at infrared frequencies," *Phys. Rev. B*, vol. 73, no. 4, pp. 045105-1-045105-7, Jan. 2006.

[24] C. W. Qiu and L. Gao, "Resonant light scattering by small coated nonmagnetic spheres: magnetic resonances, negative refraction, and prediction," *J. Opt. Soc. Amer. B, Opt. Phys.*, vol. 25, no. 10, pp. 1728-1737, Oct. 2008.

[25] A. D. Yaghjian, "Scattering-matrix analysis of linear periodic arrays," *IEEE Trans. Antennas Propag.*, vol. 50, no. 8, pp. 1050-1064, Aug. 2002.

[26] R. A. Shore and A. D. Yaghjian, "Scattering-matrix analysis of linear periodic arrays of short electric dipoles," Air Force Res. Lab. In-House Rep., AFRL-SN-HS-TR-2004-045, 2004.

[27] R. A. Shore and A. D. Yaghjian, "Traveling electromagnetic waves on linear periodic arrays of small lossless penetrable spheres," Air Force Res. Lab. In-House Rep., AFRL-SN-HS-TR-2004-044, 2004.

[28] R. A. Shore and A. D. Yaghjian, "Travelling electromagnetic waves on linear periodic arrays of lossless spheres," *Electron. Lett.*, vol. 41, no. 10, pp. 578-580, May 2005.

[29] R. A. Shore and A. D. Yaghjian, "Traveling electromagnetic waves on linear periodic arrays of lossless penetrable spheres," *IEICE Trans. Commun.*, vol. E88-B, no. 6, pp. 2346-2352, Jun. 2005.

[30] R. A. Shore and A. D. Yaghjian, "Traveling electromagnetic waves on two- and three-dimensional periodic arrays of lossless acoustic monopoles, electric dipoles, and magnetodielectric spheres," Air Force Res. Lab. In-House Rep., AFRL-SN-HS-TR-2006-0039, 2006.

[31] R. A. Shore and A. D. Yaghjian, "Traveling waves on two- and three-dimensional periodic arrays of lossless scatterers," *Radio Sci.*, vol. 42, no. RS6S21, Dec. 2007.

[32] R. A. Shore and A. D. Yaghjian, "Electromagnetic waves on partially finite periodic arrays of lossless or lossy penetrable spheres," *IEICE Trans. Commun.*, vol. E91-B, no. 6, pp. 1819-1824, Jun. 2008.

[33] R. A. Shore and A. D. Yaghjian, "Complex waves on 1D, 2D, and 3D periodic arrays of lossy and lossless magnetodielectric spheres," Air Force Res. Lab. In-House Rep., AFRL-RY-HS-TR-2010-0019, May 2010, revised Jun. 2011.

[34] J. A. Stratton, *Electromagnetic Theory.* New York: McGraw-Hill, 1941.

[35] S. Johnson and J. Joannopoulos, "Block-iterative frequency-domain methods for Maxwell's equations in a planewave basis," *Opt. Express*, vol. 8, no. 3, pp. 173-190, Jan. 2001.

[36] R. Biswas, M. M. Sigalas, C. M. Soukoulis, and K. M. Ho, "Photonic band structure," in Topics in Computational Materials Science. C. Y. Fong, Ed. Singapore: World Scientific Publishing Co., 1998.

[37] R. Biswas, M. M. Sigalas, K. M. Ho, and S. Y. Lin, "Three-dimensional photonic band gaps in modified simple cubic lattices," *Phys. Rev. B*, vol. 65, no. 20, pp. 205121-1–205121-5, May 2002.

[38] A. Alù, private communication.

[39] S. Johnson, private communication.

[40] C. R. Simovski, "On electromagnetic characterization and homogenization of nanostructured metamaterials," *J. Opt.*, vol. 13, no. 1, p. 013001, Jan. 2011.

[41] D. R. Smith, D. Schurig, M. Rosenbluth, S. Schultz, S. A. Ramakrishna, and J. B. Pendry, "Limitations on subdiffraction imaging with a negative refractive index slab," *App. Phys. Lett.*, vol. 82, no. 10, pp. 1506-1508, Mar. 2003.

[42] J. Liu and N. Bowler, "Analysis of losses in a double-negative (DNG) metamaterial composed of magnetodielectric spheres embedded in a matrix," *Microw. Opt. Technol. Lett.*, vol. 53, no. 7, pp. 1649-1652, 2011.

[43] I. S. Gradshteyn and I. M. Ryzhik, *Table of Integrals, Series, and Products; 6th Edition.* Boston, MA: Academic Press, 1994.

CHAPTER 3. RATIONAL DESIGN OF DOUBLE-NEGATIVE METAMATERIALS CONSISTING OF 3D ARRAYS OF TWO DIFFERENT NON-METALLIC SPHERES ARRANGED ON A SIMPLE TETRAGONAL LATTICE

A paper published in *2011 IEEE International Symposium on Antennas and Propagation (APSURSI)*

Yang Li, Nicola Bowler

3.1 Abstract

Non-metallic, low-loss double-negative (DNG) metamaterials can be formed by three-dimensional (3D) arrays of two different non-metallic spheres arranged on a simple tetragonal lattice. Such DNG metamaterials have recently been found to provide DNG bandwidths of 10% through 3D arrays of two different dielectric spheres, and of 18% through 3D arrays of dielectric and magnetic spheres. However, a method of rational design of these DNG metamaterials has not yet been presented. This paper develops a design procedure based on the theoretical description of traveling waves supported by the 3D arrays. Analytical calculations of $k - \beta$ (dispersion) diagram and effective constitutive parameters of several DNG metamaterials designed using this rule are presented.

3.2 Introduction

During the last decade, significant progress has been achieved both in the theoretical development and practical application of metamaterials [1]. Present realizations of metamaterials often employ sub-wavelength resonant metallic elements, such as metallic split ring resonators

Table 3.1 Three combinations of sphere types

Combination	Electrical parameters	Radius
I	$\epsilon_{r1} = \epsilon_{r2}, \mu_{r1} = \mu_{r2} = 1$	$a_1 \neq a_2$
II	$\epsilon_{r1} \neq \epsilon_{r2}, \mu_{r1} = \mu_{r2} = 1$	$a_1 = a_2$
III	$\epsilon_{r1} = \mu_{r2}, \mu_{r1} = \epsilon_{r2} = 1$	$a_1 = a_2$

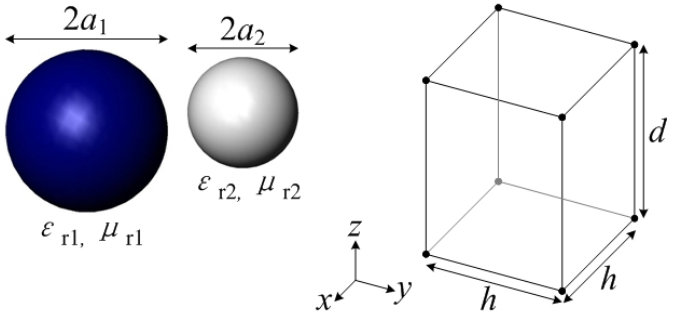

Figure 3.1 Two sets of spheres and unit cell geometry.

combined with wires [2]. The drawbacks of metal-based metamaterials include conduction loss, anisotropy, and fabrication challenge in the infrared and optical frequency range.

In a contrasting approach, Holloway *et al.* [3] demonstrated, theoretically, that a DNG metamaterial can be formed by a 3D array of non-conductive, magnetodielectric spheres with values of relative permittivity and permeability much greater than one and close to each other. However, the practicality of fabricating DNG metamaterials by this approach is questionable, at least at present, because such magnetodielectric materials are currently not available above 1 GHz [4]. Alternatively, several authors proposed using 3D arrays of two different non-metallic spheres to form DNG metamaterials [4]-[6]. The two sets of spheres can have three different combinations, Table 3.1.

Several theoretical and experimental works have been conducted for this type of DNG metamaterials, e.g. [7]-[9], but none of these works provide a rational design method that permits a priori design of a non-metallic DNG metamaterial with prescribed characteristics. This paper presents a clear design procedure for DNG metamaterials consisting of 3D arrays of two different non-metallic spheres arranged on a simple tetragonal lattice. This procedure can give an easy-to-fabricate design with wide DNG bandwidth and desired effective constitutive

parameters at the operating frequency. A brief introduction of the theoretical scheme applied in this design procedure is provided in Section 3.3. Section 3.4 outlines the design procedure, which can yield the array parameters needed to achieve the prescribed bulk parameters. Two examples are provided in Section 3.5 to illustrate the use of the design procedure for achieving the prescribed characteristics.

3.3 Theory

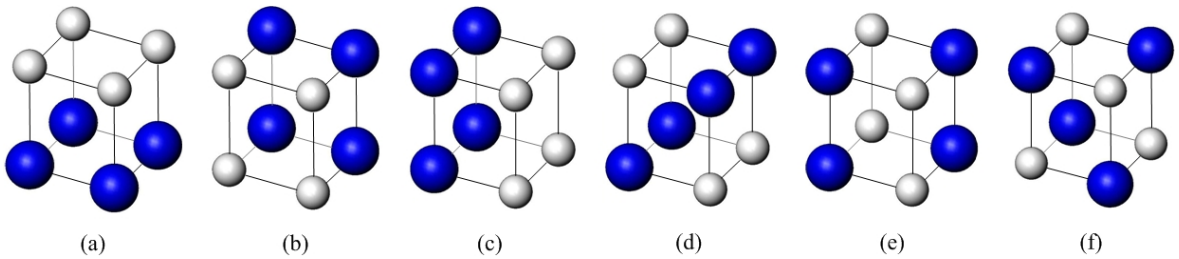

Figure 3.2 Six different arrangements of four 1-spheres and four 2-spheres within the unit cell.

Two sets of non-metallic spheres are arbitrarily arranged on each lattice point of the unit tetragon. One set of spheres with relative permittivity ϵ_{r1}, relative permeability μ_{r1}, and radius a_1 will be referred to as "1-spheres" while the other set with relative permittivity ϵ_{r2}, etc., will be referred to as "2-spheres". The z axis is chosen as the array axis in which the height, d, of each unit cell lies, as shown in Fig. 3.1. The cross-section of each unit cell is normal to the z axis with equal length and width, h, in the x and y directions, respectively. In the planes $z = 2nd, n = 0, \pm1, \pm2, \cdots$ or $z = (2n-1)\,d, n = 0, \pm1, \pm2, \cdots$, either set of spheres could be centered at $[x = 2mh, y = 2lh]$, $[x = (2m-1)h, y = 2lh]$, $[x = 2mh, y = (2l-1)h]$, or $[x = (2m-1)h, y = (2l-1)h]\,, l, m = 0, \pm1, \pm2, \cdots$. Six different arrangements of four 1-spheres and four 2-spheres on the vertices of the unit cell are shown in Fig. 3.2.

Each sphere is modeled by a pair of crossed electric and magnetic dipoles, which are oriented in the x and y direction, respectively. It is assumed that the array is excited by a traveling wave in the array axis direction, with real propagation constant β, and that all the spheres are excited identically. In the presence of the excitation, the electric and magnetic fields that are incident on the sphere at position $(x, y, z) = (0, 0, 0)$ are obtained by summing the contributions from

all the other spheres of the array. This traveling wave is characterized by the $k-\beta$ (dispersion) equation [9, Eq. (9)], which is obtained by a spherical-wave source scattering-matrix approach. The $k-\beta$ equation relates the propagation constant, β, of the traveling wave, to the free-space wavenumber, k. For a given kd and an array of lossless scatters, the $k-\beta$ equation can be solved for real βd by a search procedure [9]. For a 3D array whose sphere elements are sufficiently close to each other, $kd, \beta d < 0.5$, the array can be treated macroscopically as a homogeneous medium with effective permittivity $\epsilon_{\mathrm{r}}^{\mathrm{eff}}$ and permeability $\mu_{\mathrm{r}}^{\mathrm{eff}}$, which can be obtained based on the solution to the $k-\beta$ equation.

3.4 Design procedure

The goal of the procedure is to achieve, by rational design, a wide DNG bandwidth around a selected operating frequency, f, constrained by the conditions $kd, \beta d < 0.5$. Design steps are as follows.

1) Specify operating frequency f of the desired DNG metamaterial.

2) Based on the particular application and achievable fabrication tolerance of the geometric and electrical parameters of the spheres, select a combination of sphere types from those given in Table 3.1.

3) For the selected combination of sphere types, choose an arrangement from the six different ones, Fig. 3.2, based on the results in Table 3.2 [9] to achieve a wider DNG bandwidth. Here, the fractional bandwidth of the DNG region is defined as the width of the DNG kd interval divided by the average value of kd in that interval. BW_1 and BW_2 are the fractional bandwidths for the entire DNG region and for the portion of the DNG region where $\beta d \leq 0.5$, respectively.

4) Assuming $a_2 \geq a_1$ and considering the chosen spheres arrangement, select proper a_2/d and d/h to achieve a large volume fraction v_f since a larger v_f will increase the coupling between the electric and magnetic dipoles of the spheres so as to give a wider DNG bandwidth [8].

5) Considering that decreasing kd improves the homogenization approximation of the array, but at the expense of decreasing the DNG bandwidth, select a proper kd in the range $kd < 0.5$. Calculate ka_2 based on the selected a_2/d.

6) This step is different for spheres combinations I and II or III. For spheres combination I,

Table 3.2 The widest DNG bandwidths provided by different arrangements of spheres, Fig. 3.2, for each spheres combination

Combination*	Widest BW_1**	Widest BW_2**
I	(c)	(d)
II	(c)	(c)
III	(b)	(b)

*See Table 3.1.
**Arrangement of spheres, Fig. 3.2.

adjust $\epsilon_{\mathrm{r}1}$ until the first electric dipole resonance is located at the ka_2 calculated in step 5. In addition, set ka_1 equal to the value of ka corresponding to the first magnetic dipole resonance. Compute a_1/d through $(a_2/d)/(ka_2/ka_1)$. Note that ka_1 and ka_2 require high accuracy to correspond with, respectively, the first magnetic and electric resonances well. For spheres combinations II or III, select $\epsilon_{\mathrm{r}i}$ and $\mu_{\mathrm{r}i}$ $(i = 1, 2)$ properly to make the first magnetic dipole resonance of 1-spheres and the first electric dipole resonance of 2-spheres coincide with each other at the ka_2 calculated in step 5. Similarly, $\epsilon_{\mathrm{r}i}$ and $\mu_{\mathrm{r}i}$ $(i = 1, 2)$ require high accuracy to achieve a good coincidence between the first magnetic and electric resonances. In this step, the magnetic and electric Mie dipole scattering coefficients, $a_1^{\mathrm{sc}}(ka)$ and $b_1^{\mathrm{sc}}(ka)$, for the i-spheres $(i = 1, 2)$ are calculated by [10, Sec. 9.25, Eqs. (10), (11)], which are shown in (3.1). Here, $m_i = \sqrt{\epsilon_{\mathrm{r}i}\mu_{\mathrm{r}i}}$, $i = 1, 2$.

$$a_1^{\mathrm{sc}}(ka) = -\frac{\mu_{\mathrm{r}i} j_1(m_i ka)\left[(ka) j_1(ka)\right]' - j_1(ka)\left[(m_i ka) j_1(m_i ka)\right]'}{\mu_{\mathrm{r}i} j_1(m_i ka)\left[(ka) h_1^{(1)}(ka)\right]' - h_1^{(1)}(ka)\left[(m_i ka) j_1(m_i ka)\right]'}, \tag{3.1a}$$

$$b_1^{\mathrm{sc}}(ka) = -\frac{\mu_{\mathrm{r}i} j_1(ka)\left[(m_i ka) j_1(m_i ka)\right]' - m_i^2 j_1(m_i ka)\left[(ka) j_1(ka)\right]'}{\mu_{\mathrm{r}i} h_1^{(1)}(ka)\left[(m_i ka) j_1(m_i ka)\right]' - m_i^2 j_1(m_i ka)\left[(ka) h_1^{(1)}(ka)\right]'}. \tag{3.1b}$$

7) Obtain the $k - \beta$ (dispersion) diagram with selected parameters by solving the $k - \beta$ equation [9, Eq. (9)] and obtain $\epsilon_{\mathrm{r}}^{\mathrm{eff}}$ and $\mu_{\mathrm{r}}^{\mathrm{eff}}$ based on the solution to the $k - \beta$ equation [4, Eq. (2.36)]. Then, select a proper value of kd based on the particular application in the DNG region and calculate the corresponding d based on f. Finally, compute a_1, a_2, and h according

to the value of d and selected a_1/d, a_2/d, and d/h.

3.5 Examples

This section provides two metamaterial designs to illustrate the capabilities of the procedure outlined in Section 3.4.

3.5.1 $\epsilon_{\mathrm{r}}^{\mathrm{eff}} = -1$ metamaterial superlens

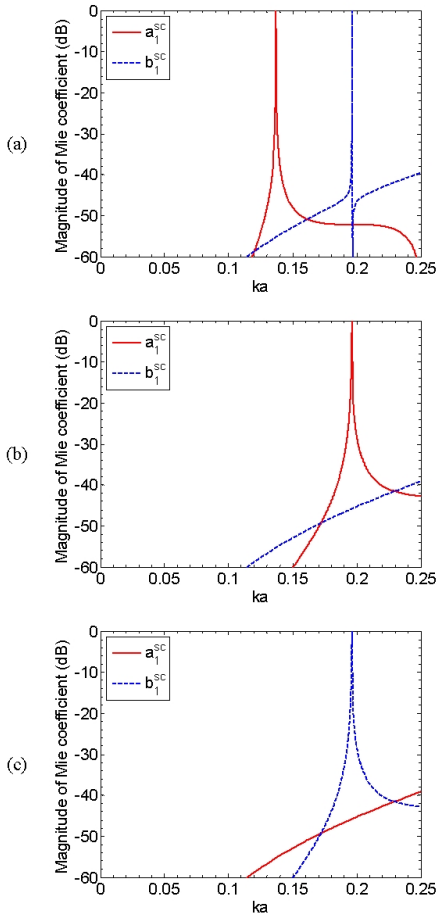

Figure 3.3 Magnetic and electric Mie dipole scattering coefficients for a sphere with (a) $\epsilon_{\mathrm{r}} = 523.5$ and $\mu_{\mathrm{r}} = 1$, (b) $\epsilon_{\mathrm{r}} = 254.98$ and $\mu_{\mathrm{r}} = 1$ and (c) $\epsilon_{\mathrm{r}} = 1$ and $\mu_{\mathrm{r}} = 254.98$.

This first example is intended to achieve a superlens for transverse magnetic (TM) mode of electromagnetic wave with $\epsilon_{\mathrm{r}}^{\mathrm{eff}} = -1$ within the X-band (8-12 GHz). 1) 10 GHz is specified as f. 2) The spheres combination I is selected due to its advantage over spheres combination III:

Table 3.3 Geometric and electrical parameters of examples discussed in Sections 3.5.1 and 3.5.2

Example	ϵ_{r1}	ϵ_{r2}	μ_{r1}	μ_{r2}	a_1 (mm)	a_2 (mm)	d (mm)	h (mm)
1	523.5	523.5	1	1	0.649	0.936	1.910	1.910
2	254.98	1	1	254.98	1.006	1.006	2.053	2.053

the availability of purely dielectric materials with large relative permittivity is better than that of purely magnetic materials with large relative permeability, and its advantage over spheres combination II: the achievable fabrication toleration of spheres radius is tighter than that of spheres permittivity. 3) Arrangement (c) is chosen since it provides the widest BW_1 for spheres combination I, Table 3.2. 4) $a_2/d = 0.49$ and $d/h = 1$ are chosen to give a large $v_f = 0.3287$. 5) To yield a wide DNG bandwidth in the range $kd < 0.5$ and considering the electrostatic limit $d \ll \lambda$ of the $\epsilon_r^{\text{eff}} = -1$ metamaterial superlens [11], $kd = 0.4$ ($d = 0.064\lambda$) is selected and $ka_2 = 0.196$ is obtained. 6) Selecting $\epsilon_{r1} = 523.5$, the first electric dipole resonance is located at $ka_2 = 0.196$, Fig. 3.3 (a). Next, ka_1 is set equal to 0.137 to coincide with the first magnetic resonance as shown in Fig. 3.3 (a). Then, $a_1/d = 0.34$ is obtained. 7) The $k - \beta$ diagram, ϵ_r^{eff} and μ_r^{eff} are calculated and shown in Fig. 3.4. Then, $kd = 0.4$, corresponding to $\epsilon_r^{\text{eff}} = -1$, is selected so as to yield the geometric and electrical parameters given in Table 3.3.

3.5.2 DNG superlens

The second example provides guidance for designing a DNG superlens with $\epsilon_r^{\text{eff}} = \mu_r^{\text{eff}} = -1$ [11] within the X-band (8-12 GHz). 1) As for example 1, 10 GHz is specified as f. 2) To achieve $\epsilon_r^{\text{eff}} = \mu_r^{\text{eff}}$ at all frequencies, the spheres combination III is selected. 3) Arrangement (b) is chosen since it yields the widest BW_1 and BW_2 for spheres combination III, Table 3.2. Then, as for example 1, $a/d = 0.49$ ($a_1 = a_2 = a$), $d/h = 1$, $kd = 0.4$, and $ka = 0.196$ are selected in steps 4 and 5 to give a wide DNG bandwidth. 6) $\epsilon_{r1} = \mu_{r2} = 254.98$ and $\epsilon_{r2} = \mu_{r1} = 1$ are selected and the first magnetic dipole resonance of 1-spheres and first electric dipole resonance of 2-spheres coincide with each other at $ka = 0.196$, Figs. 3.3 (b) and (c). 7) The $k - \beta$ diagram, ϵ_r^{eff} and μ_r^{eff} are computed and shown in Fig. 3.5. Then, $kd = 0.43$, corresponding to

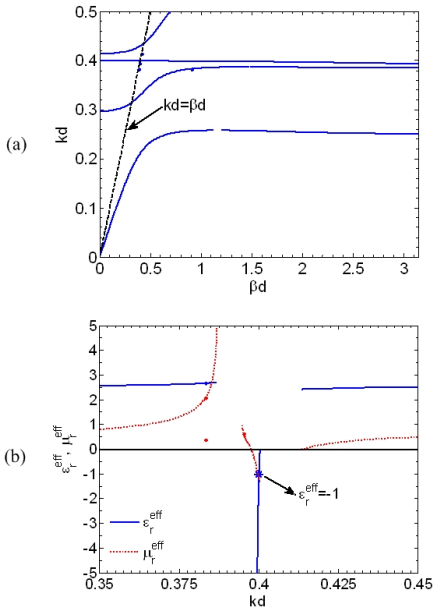

Figure 3.4 (a) $k-\beta$ diagram and (b) effective relative permittivity and permeability of example 1, Section 3.5.1.

$\epsilon_{\mathrm{r}}^{\mathrm{eff}} = \mu_{\mathrm{r}}^{\mathrm{eff}} = -1$, is selected so as to yield the geometric and electrical parameters in Table 3.3.

3.6 Conclusion

This paper presents a design procedure for the DNG metamaterials composed of 3D arrays of two different non-metallic spheres arranged on a simple tetragonal lattice. Future developments of the present design procedure include the following aspects. First, since in practice it may be easier to fabricate the array elements as cubes or cylinders than spheres [7], a design procedure for metamaterials composed of 3D arrays of two sets of cubes or cylinders might be outlined. Second, considering that DNG behavior is extinguished if the constituents exhibit losses above a certain threshold value [3], losses can be considered in the presented design procedure.

3.7 Acknowledgment

This material is based upon work supported by the Air Force Research Laboratory under Contract FA8650-04-C-5228 at Iowa State University's Center for NDE.

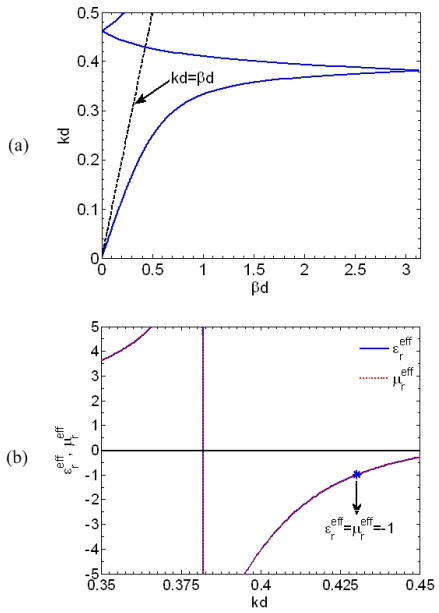

Figure 3.5 (a) $k-\beta$ diagram and (b) effective relative permittivity and permeability of example 2, Section 3.5.2.

3.8 References

[1] N. Engheta and R. W. Ziolkowski, *Metamaterials: Physics and Engineering Explorations.* New York: Wiley, 2006.

[2] R. A. Shelby, D. R. Smith, and S. Schultz, "Experimental verification of a negative index of refraction," *Science*, vol. 292, no. 5514, pp. 77-79, 2001.

[3] C. L. Holloway, E. F. Kuester, J. Baker-Jarvis, and P. Kabos, "A doubly negative (DNG) composite medium composed of magneto-dielectric spherical particles embedded in a matrix," *IEEE Trans. Antennas Propag.*, vol. 51, no. 10, pp. 2596-2603, Oct. 2003.

[4] R. A. Shore and A. D. Yaghjian, "Traveling waves on three-dimensional periodic arrays of two different alternating magnetodielectric spheres," *IEEE Trans. Antennas Propag.*, vol. 57, no. 10, pp. 3077-3091, Oct. 2009.

[5] L. Jylhä, I. Kolmakov, S. Maslovski, and S. Tretyakov, "Modeling of isotropic backward-wave materials composed of resonant spheres," *J. Appl. Phys.*, vol. 99, no. 4, pp. 043102-1–043102-7, Feb. 2006.

[6] A. Ahmadi and H. Mosallaei, "Physical configuration and performance modeling of all-dielectric metamaterials," *Phys. Rev. B*, vol. 77, no. 4, pp. 045104-1–045104-11, Jan. 2008.

[7] Q. Zhao, J. Zhou, F. L. Zhang, and D. Lippens, "Mie resonance-based dielectric metamaterials," *Mater. Today*, vol. 12, no. 12, pp. 60-69, Dec. 2009.

[8] S. Ghadarghadr and H. Mosallaei, "Dispersion diagram characteristics of periodic array of dielectric and magnetic materials based spheres," *IEEE Trans. Antennas Propag.*, vol. 57, no. 1, pp. 149-160, Jan. 2009.

[9] Y. Li and N. Bowler, "Traveling waves on three-dimensional periodic arrays of two different magnetodielectric spheres arbitrarily arranged on a simple tetragonal lattice," *IEEE Trans. Antennas Propag.*, vol. 60, no. 6, pp. 2727–2739, Jun. 2012.

[10] J. A. Stratton, *Electromagnetic Theory.* New York: McGraw-Hill, 1941.

[11] J. B. Pendry, "Negative refraction makes a perfect lens," *Phys. Rev. Lett.*, vol. 85, no. 18, pp. 3966-3969, 2000.

CHAPTER 4. ANALYTICAL EXPRESSIONS FOR MIE DERIVATIVES

A paper to be submitted to *Applied Optics*

Yang Li, Nicola Bowler

4.1 Abstract

Analytical expressions are obtained for the derivatives of Mie scattering coefficients with respect to the size of the spherical scattering particle, and to the relative permittivity and permeability of both the particle and the surrounding medium. These expressions have been verified by comparing their results with those calculated by analytical expressions developed by Mathematica.

4.2 Introduction

Recently, the first all-dielectric metamaterial with magnetic activity was demonstrated at optical frequencies [1]. It follows the general idea of achieving a non-metallic metamaterial based on Mie resonances with electric and magnetic resonances of the inclusions providing the negative effective permittivity and permeability, respectively, of the composite [2]. Design of non-metallic metamaterials of this kind needs not only the Mie scattering coefficients but also their derivatives with respect to the size of the spherical scattering particle, and to the relative permittivity and permeability of both the particle and the surrounding medium, for the purpose of analyzing the effect of parameter variations on the effective constitutive parameters of the proposed metamaterials [3]. Previous work, however, gives derivatives only with respect to particle size and complex refractive index [4]. In this letter, analytical expressions are presented for derivatives with respect to the size of the spherical scattering particle, and to the

relative permittivity and permeability of both the particle and the surrounding medium.

4.3 Theory

Based on the Mie theory, the light scattered from a sphere is represented as partial waves radiated by multipoles located at the center of the sphere. The first partial wave is radiated by a dipole, the second by a quadrupole, and so on. Magnitudes of these partial waves are given by the Mie scattering coefficients a_n and b_n. The magnitude of the nth electric partial wave is a_n while that of the nth magnetic partial wave is b_n [5]:

$$a_n = -\frac{\mu_{\mathrm{r}1}\psi_n(m_1x)\psi_n'(m_2x) - \mu_{\mathrm{r}2}m\psi_n'(m_1x)\psi_n(m_2x)}{\mu_{\mathrm{r}1}\psi_n(m_1x)\xi_n'(m_2x) - \mu_{\mathrm{r}2}m\psi_n'(m_1x)\xi_n(m_2x)}, \tag{4.1}$$

$$b_n = -\frac{\mu_{\mathrm{r}1}\psi_n'(m_1x)\psi_n(m_2x) - \mu_{\mathrm{r}2}m\psi_n(m_1x)\psi_n'(m_2x)}{\mu_{\mathrm{r}1}\psi_n'(m_1x)\xi_n(m_2x) - \mu_{\mathrm{r}2}m\psi_n(m_1x)\xi_n'(m_2x)}, \tag{4.2}$$

where $m_1 = \sqrt{\epsilon_{\mathrm{r}1}\mu_{\mathrm{r}1}}$ and $m_2 = \sqrt{\epsilon_{\mathrm{r}2}\mu_{\mathrm{r}2}}$ are the real refractive indices of the sphere and medium, respectively, in which $\epsilon_{\mathrm{r}i}$ and $\mu_{\mathrm{r}i}$ $(i = 1, 2)$ are the real relative permittivity and permeability of the sphere $(i = 1)$ and medium $(i = 2)$; $m = m_1/m_2$ is the refractive index of the sphere relative to the medium; $x = k_0r = \omega\sqrt{\epsilon_0\mu_0}\, r$ is the electrical radius of the sphere, given that ϵ_0 and μ_0 are the permittivity and permeability of the free space, r is the radius of the sphere; and the prime denotes differentiation with respect to the argument of the function. Further,

$$\psi_n(z) \equiv z j_n(z) \text{ and } \xi_n(z) \equiv z h_n^{(1)}(z), \tag{4.3}$$

where $\psi_n(z)$ and $\xi_n(z)$ are Riccati-Bessel functions defined in terms of the spherical Bessel function of the first kind, $j_n(z)$, and the spherical Hankel function of the first kind, $h_n^{(1)}(z)$ [6, Chap. 4].

The Mie scattering coefficients given in Eqs. (4.1) and (4.2) differ from the classical ones given in [5, Sec. 9.25, Eqs. (10) and (11)] because the classical Mie scattering coefficients use $x = k_2r = \omega\sqrt{\epsilon_2\mu_2}\, r$ instead of $x = k_0r = \omega\sqrt{\epsilon_0\mu_0}\, r$. This small mathematical change from $x = k_2r$ to $x = k_0r$ makes the relative permittivity $(\epsilon_{\mathrm{r}2})$ and relative permeability $(\mu_{\mathrm{r}2})$ of the medium in which the sphere is embedded explicit. In this way, it becomes straightforward to differentiate Eqs. (4.1) and (4.2) with respect to $\epsilon_{\mathrm{r}2}$ and $\mu_{\mathrm{r}2}$.

To obtain the analytical expressions for the derivatives of a_n and b_n, the following identities are used [4], [7]:

$$\psi_n'(z)\xi_n(z) - \psi_n(z)\xi_n'(z) = -i, \tag{4.4}$$

$$\psi_n''(z)\xi_n(z) - \psi_n(z)\xi_n''(z) = 0, \tag{4.5}$$

$$\psi_n''(z)\xi_n'(z) - \psi_n'(z)\xi_n''(z) = -i\left[1 - \frac{n(n+1)}{z^2}\right], \tag{4.6}$$

where i is the imaginary unit $\sqrt{-1}$. Note that there should be an extra minus sign on the right hand side of Eqs. (14) and (17) in [4], which have been remedied in Eqs. (4.4) and (4.6). Based on these expressions, the Mie derivatives are obtained and shown in Eqs. (4.7)-(4.16).

$$\begin{aligned}\frac{\partial a_n}{\partial x} =& i\left\{\mu_{\mathrm{r}2}(\mu_{\mathrm{r}2} - \mu_{\mathrm{r}1})\frac{m_1^2}{m_2}\left[\psi_n'(m_1x)\right]^2 + \mu_{\mathrm{r}1}\mu_{\mathrm{r}2}\frac{m_1^2}{m_2}\psi_n(m_1x)\psi_n''(m_1x)\right.\\ &\left.+\mu_{\mathrm{r}1}^2 m_2\left[\psi_n(m_1x)\right]^2\left[1 - \frac{n(n+1)}{(m_2x)^2}\right]\right\}\\ &\div\left[\mu_{\mathrm{r}1}\psi_n(m_1x)\xi_n'(m_2x) - \mu_{\mathrm{r}2}m\psi_n'(m_1x)\xi_n(m_2x)\right]^2,\end{aligned} \tag{4.7}$$

$$\begin{aligned}\frac{\partial b_n}{\partial x} =& i\left\{\mu_{\mathrm{r}1}(\mu_{\mathrm{r}1}m_2 - \mu_{\mathrm{r}2}\frac{m_1^2}{m_2})\left[\psi_n'(m_1x)\right]^2 + \mu_{\mathrm{r}1}\mu_{\mathrm{r}2}\frac{m_1^2}{m_2}\psi_n(m_1x)\psi_n''(m_1x)\right.\\ &\left.+\mu_{\mathrm{r}2}^2\frac{m_1^2}{m_2}\left[\psi_n(m_1x)\right]^2\left[1 - \frac{n(n+1)}{(m_2x)^2}\right]\right\}\\ &\div\left[\mu_{\mathrm{r}1}\psi_n'(m_1x)\xi_n(m_2x) - \mu_{\mathrm{r}2}m\psi_n(m_1x)\xi_n'(m_2x)\right]^2,\end{aligned} \tag{4.8}$$

$$\begin{aligned}\frac{\partial a_n}{\partial \epsilon_{\mathrm{r}1}} =& 0.5i\left\{\mu_{\mathrm{r}1}^2\sqrt{\frac{\mu_{\mathrm{r}2}}{\epsilon_{\mathrm{r}2}}}x\left\{\psi_n(m_1x)\psi_n''(m_1x) - \left[\psi_n'(m_1x)\right]^2\right\}\right.\\ &\left.+\mu_{\mathrm{r}1}^{1.5}\sqrt{\frac{\mu_{\mathrm{r}2}}{\epsilon_{\mathrm{r}1}\epsilon_{\mathrm{r}2}}}\psi_n(m_1x)\psi_n'(m_1x)\right\}\\ &\div\left[\mu_{\mathrm{r}1}\psi_n(m_1x)\xi_n'(m_2x) - \mu_{\mathrm{r}2}m\psi_n'(m_1x)\xi_n(m_2x)\right]^2,\end{aligned} \tag{4.9}$$

$$\begin{aligned}\frac{\partial b_n}{\partial \epsilon_{\mathrm{r}1}} =& 0.5i\left\{\mu_{\mathrm{r}1}^2\sqrt{\frac{\mu_{\mathrm{r}2}}{\epsilon_{\mathrm{r}2}}}x\left\{\psi_n(m_1x)\psi_n''(m_1x) - \left[\psi_n'(m_1x)\right]^2\right\}\right.\\ &\left.-\mu_{\mathrm{r}1}^{1.5}\sqrt{\frac{\mu_{\mathrm{r}2}}{\epsilon_{\mathrm{r}1}\epsilon_{\mathrm{r}2}}}\psi_n(m_1x)\psi_n'(m_1x)\right\}\\ &\div\left[\mu_{\mathrm{r}1}\psi_n'(m_1x)\xi_n(m_2x) - \mu_{\mathrm{r}2}m\psi_n(m_1x)\xi_n'(m_2x)\right]^2,\end{aligned} \tag{4.10}$$

$$\frac{\partial a_n}{\partial \mu_{r1}} =0.5i \left\{ \epsilon_{r1}\mu_{r1}\sqrt{\frac{\mu_{r2}}{\epsilon_{r2}}}x \left\{ \psi_n(m_1x)\psi_n''(m_1x) - \left[\psi_n'(m_1x)\right]^2 \right\} - \sqrt{\frac{\epsilon_{r1}\mu_{r1}\mu_{r2}}{\epsilon_{r2}}}\psi_n(m_1x)\psi_n'(m_1x) \right\} \div \left[\mu_{r1}\psi_n(m_1x)\xi_n'(m_2x) - \mu_{r2}m\psi_n'(m_1x)\xi_n(m_2x)\right]^2, \tag{4.11}$$

$$\frac{\partial b_n}{\partial \mu_{r1}} =0.5i \left\{ \epsilon_{r1}\mu_{r1}\sqrt{\frac{\mu_{r2}}{\epsilon_{r2}}}x \left\{ \psi_n(m_1x)\psi_n''(m_1x) - \left[\psi_n'(m_1x)\right]^2 \right\} + \sqrt{\frac{\epsilon_{r1}\mu_{r1}\mu_{r2}}{\epsilon_{r2}}}\psi_n(m_1x)\psi_n'(m_1x) \right\} \div \left[\mu_{r1}\psi_n'(m_1x)\xi_n(m_2x) - \mu_{r2}m\psi_n(m_1x)\xi_n'(m_2x)\right]^2, \tag{4.12}$$

$$\frac{\partial a_n}{\partial \epsilon_{r2}} =0.5i \left\{ \epsilon_{r1}\mu_{r1}\left(\frac{\mu_{r2}}{\epsilon_{r2}}\right)^{1.5} x\left[\psi_n'(m_1x)\right]^2 + \mu_{r1}^2\sqrt{\frac{\mu_{r2}}{\epsilon_{r2}}}x\left[\psi_n(m_1x)\right]^2\left[1-\frac{n(n+1)}{(m_2x)^2}\right] - \sqrt{\epsilon_{r1}\mu_{r2}}\left(\frac{\mu_{r1}}{\epsilon_{r2}}\right)^{1.5}\psi_n(m_1x)\psi_n'(m_1x) \right\} \div \left[\mu_{r1}\psi_n(m_1x)\xi_n'(m_2x) - \mu_{r2}m\psi_n'(m_1x)\xi_n(m_2x)\right]^2, \tag{4.13}$$

$$\frac{\partial b_n}{\partial \epsilon_{r2}} =0.5i \left\{ \mu_{r1}^2\sqrt{\frac{\mu_{r2}}{\epsilon_{r2}}}x\left[\psi_n'(m_1x)\right]^2 + \epsilon_{r1}\mu_{r1}\left(\frac{\mu_{r2}}{\epsilon_{r2}}\right)^{1.5} x\left[\psi_n(m_1x)\right]^2\left[1-\frac{n(n+1)}{(m_2x)^2}\right] + \sqrt{\epsilon_{r1}\mu_{r2}}\left(\frac{\mu_{r1}}{\epsilon_{r2}}\right)^{1.5}\psi_n(m_1x)\psi_n'(m_1x) \right\} \div \left[\mu_{r1}\psi_n'(m_1x)\xi_n(m_2x) - \mu_{r2}m\psi_n(m_1x)\xi_n'(m_2x)\right]^2, \tag{4.14}$$

$$\frac{\partial a_n}{\partial \mu_{r2}} =0.5i \left\{ \epsilon_{r1}\mu_{r1}\sqrt{\frac{\mu_{r2}}{\epsilon_{r2}}}x\left[\psi_n'(m_1x)\right]^2 + \mu_{r1}^2\sqrt{\frac{\epsilon_{r2}}{\mu_{r2}}}x\left[\psi_n(m_1x)\right]^2\left[1-\frac{n(n+1)}{(m_2x)^2}\right] + \mu_{r1}^{1.5}\sqrt{\frac{\epsilon_{r1}}{\epsilon_{r2}\mu_{r2}}}\psi_n(m_1x)\psi_n'(m_1x) \right\} \div \left[\mu_{r1}\psi_n(m_1x)\xi_n'(m_2x) - \mu_{r2}m\psi_n'(m_1x)\xi_n(m_2x)\right]^2, \tag{4.15}$$

$$\frac{\partial b_n}{\partial \mu_{\mathrm{r}2}} = 0.5i \left\{ \mu_{\mathrm{r}1}^2 \sqrt{\frac{\epsilon_{\mathrm{r}2}}{\mu_{\mathrm{r}2}}} x \left[\psi_n'(m_1 x)\right]^2 + \epsilon_{\mathrm{r}1}\mu_{\mathrm{r}1} \sqrt{\frac{\mu_{\mathrm{r}2}}{\epsilon_{\mathrm{r}2}}} x \left[\psi_n(m_1 x)\right]^2 \left[1 - \frac{n(n+1)}{(m_2 x)^2}\right] - \mu_{\mathrm{r}1}^{1.5} \sqrt{\frac{\epsilon_{\mathrm{r}1}}{\epsilon_{\mathrm{r}2}\mu_{\mathrm{r}2}}} \psi_n(m_1 x)\psi_n'(m_1 x) \right\} \div \left[\mu_{\mathrm{r}1}\psi_n'(m_1 x)\xi_n(m_2 x) - \mu_{\mathrm{r}2} m \psi_n(m_1 x)\xi_n'(m_2 x)\right]^2. \tag{4.16}$$

In Eqs. (4.7)-(4.16), the Riccati-Bessel functions and their derivatives are evaluated as follows. Because the Riccati-Bessel functions are solutions of the Riccati differential equation [8],

$$z^2 w''(z) + \left[z^2 - n(n+1)\right] w(z) = 0, \tag{4.17}$$

where $n = 0, \pm 1, \pm 2...$, the second order derivative of the Riccati-Bessel functions can be expressed as [4, Eq. (38)]

$$\psi_n''(z) = \psi_n(z) \left[\frac{n(n+1)}{z^2} - 1\right]. \tag{4.18}$$

Note that there should be an extra minus sign on the right hand side of Eq. (38) in [4], which has been remedied in Eq. (4.18).

The first order derivative of Riccati-Bessel functions can be expressed by utilizing the recurrence relation [9]

$$\psi_n'(z) = \psi_{n-1}(z) - \frac{n}{z}\psi_n(z). \tag{4.19}$$

In addition, the recurrence relation for the Riccati-Bessel functions is

$$\psi_n(z) = \frac{2n-1}{z}\psi_{n-1}(z) - \psi_{n-2}(z), \tag{4.20}$$

where $\psi_{-1}(z) = \cos z$, $\psi_0(z) = \sin z$, $\xi_{-1}(z) = \cos z + i \sin z$, and $\xi_0(z) = \sin z - i \cos z$ [4]. Note that Eqs. (4.18)-(4.20) also hold for $\xi_n(z)$.

4.4 Verification

To test the analytical expressions for the derivatives of a_n and b_n, Eqs. (4.7)-(4.16), at least for $n = 1$, the derivatives of Mie dipole scattering coefficients (a_1 and b_1) with parameters for a

DNG metamaterial presented in [10]: $\epsilon_{r1} = 40$, $\mu_{r1} = 200$, $\epsilon_{r2} = 1$, and $\mu_{r2} = 1$, are obtained by Eqs. (4.7)-(4.16) with Eqs. (4.18)-(4.20) and compared with those calculated by the analytical expressions for the derivatives developed by Mathematica. Excellent agreement is achieved, as shown in Fig. 4.1. Using Mathematica, the analytical expressions for the derivatives of Mie dipole scattering coefficients are obtained by differentiating Eqs. (4.1) and (4.2), with Eqs. (4.18)-(4.20) substituted, with respect to x, ϵ_{r1}, μ_{r1}, ϵ_{r2}, and μ_{r2}. Note that the expressions developed by Mathematica are much more cumbersome than the presented ones. Eqs. (4.7)-(4.16) have also been tested for $n = 6$ and excellent agreement is achieved in this case as well, as shown in Fig. 4.2.

4.5 Conclusion

This letter presented and tested analytical expressions for the derivatives of Mie scattering coefficients with respect to the size of the spherical scattering particle, and to the relative permittivity and permeability of both the particle and the surrounding medium.

4.6 Acknowledgement

This material is based upon work supported by the Air Force Research Laboratory under Contract FA8650-04-C-5228 at Iowa State University's Center for Nondestructive Evaluation.

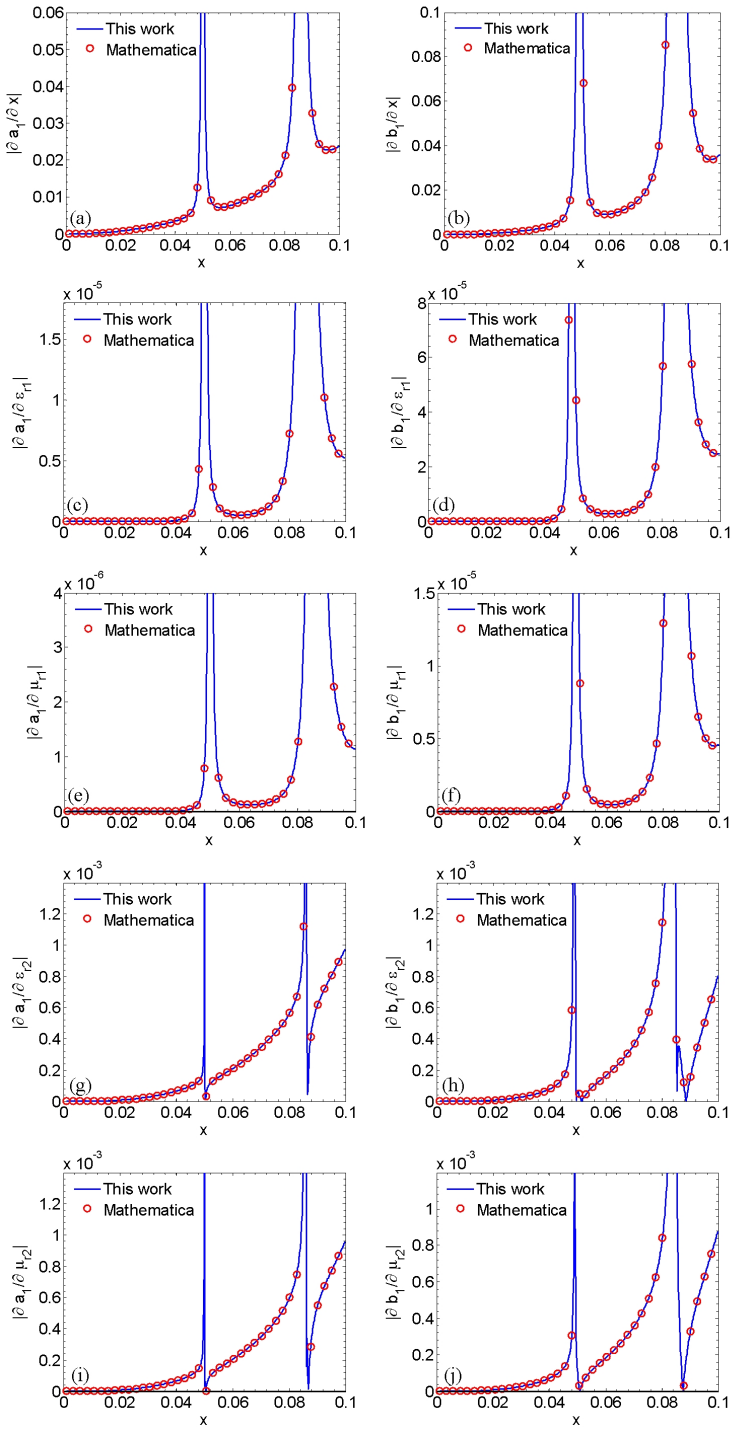

Figure 4.1 Comparisons of magnitudes of derivatives of a_1 and b_1 with respect to x [(a)-(b)], ϵ_{r1} [(c)-(d)], μ_{r1} [(e)-(f)], ϵ_{r2} [(g)-(h)], and μ_{r2} [(i)-(j)], obtained by presented formulas Eqs. (4.7)-(4.16), and (4.18)-(4.20), with these calculated by expressions developed by Mathematica.

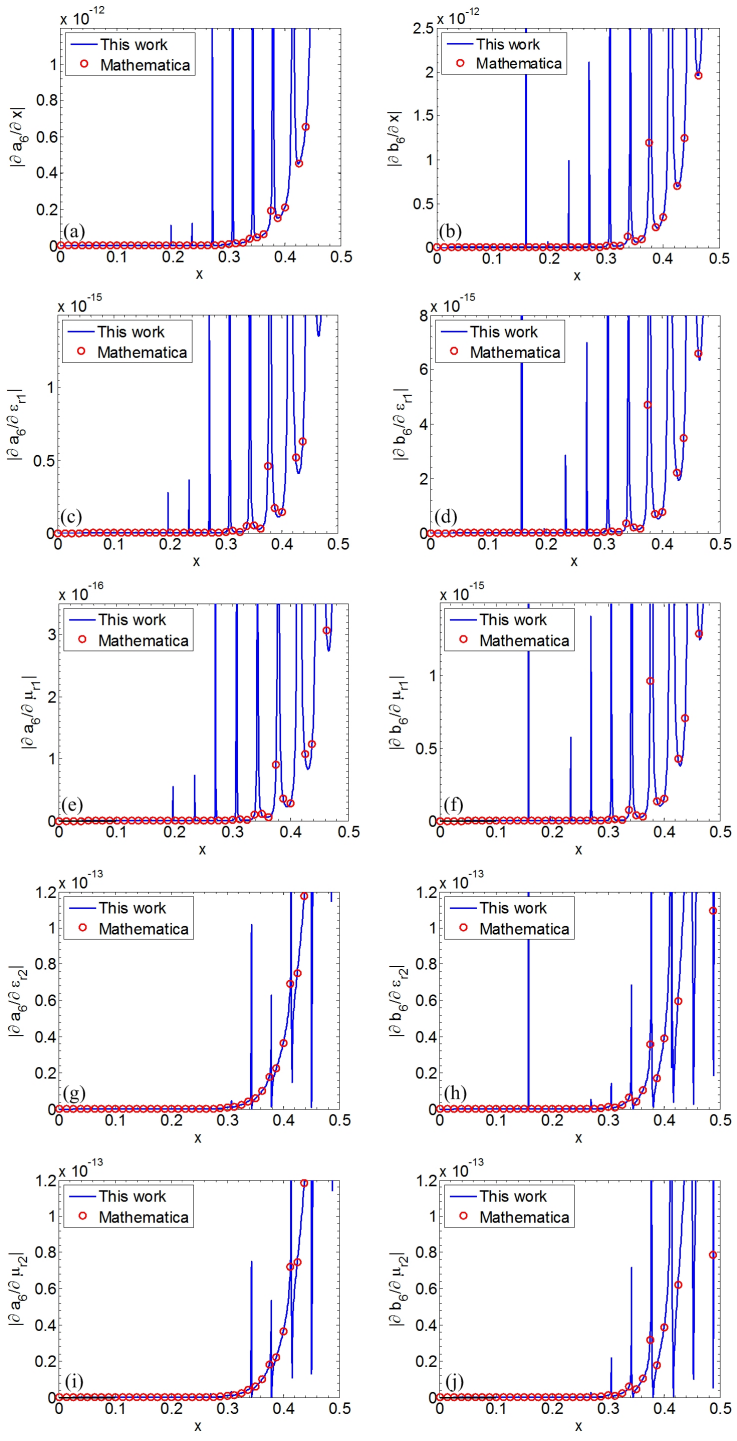

Figure 4.2 Comparisons of magnitudes of derivatives of a_6 and b_6 with respect to x [(a)-(b)], ϵ_{r1} [(c)-(d)], μ_{r1} [(e)-(f)], ϵ_{r2} [(g)-(h)], and μ_{r2} [(i)-(j)], obtained by presented formulas Eqs. (4.7)-(4.16), and (4.18)-(4.20), with these calculated by expressions developed by Mathematica.

4.7 References

[1] J. C. Ginn, I. Brener, D. W. Peters, J. R. Wendt, J. O. Stevens, P. F. Hines, L. I. Basilio, L. K. Warne, J. F. Ihlefeld, P. G. Clem, and M. B. Sinclair, "Realizing optical magnetism from dielectric metamaterials," *Phys. Rev. Lett.*, vol. 108, no. 9, p. 097402, Feb. 2012.

[2] Q. Zhao, J. Zhou, F. Zhang, and D. Lippens, "Mie resonance-based dielectric metamaterials," *Mater. Today*, vol. 12, no. 12, pp. 60–69, Dec. 2009.

[3] R. A. Shore and A. D. Yaghjian, "Traveling waves on two- and three-dimensional periodic arrays of lossless scatterers," *Radio Sci.*, vol. 42, no. 6, p. RS6S21, Dec. 2007.

[4] R. Grainger, J. Lucas, G. Thomas, and G. Ewen, "Calculation of Mie derivatives," *Appl. Optics*, vol. 43, no. 28, pp. 5386–5393, Oct. 2004.

[5] J. A. Stratton, *Electromagnetic Theory*. McGraw-Hill, New York, 1941.

[6] C. F. Bohren and D. R. Huffman, *Absorption and Scattering of Light by Small Particles*. Willey-VCH, Weinheim, 2004.

[7] H. C. van de Hulst, *Light Scattering by Small Particles*. Willey, New York, 1957.

[8] M. Abramowitz and I. A. Stegun, *Handbook of Mathematical Functions with Formulas, Graphs and Mathematical Tables*. Dover, New York, 1972.

[9] B. Verner, "Note on the recurrence between mie's coefficients," *J. Opt. Soc. Am.*, vol. 66, no. 12, pp. 1424–1425, 1976.

[10] C. Holloway, E. Kuester, J. Baker-Jarvis, and P. Kabos, "A double negative (DNG) composite medium composed of magnetodielectric spherical particles embedded in a matrix," *IEEE Trans. Antennas Propag.*, vol. 51, no. 10, pp. 2596–2603, Oct. 2003.

CHAPTER 5. EFFECTS OF PARAMETER VARIATIONS ON NEGATIVE EFFECTIVE CONSTITUTIVE PARAMETERS OF NON-METALLIC METAMATERIALS

A paper submitted to *Journal of Applied Physics*

Yang Li, Nicola Bowler

5.1 Abstract

Analytical expressions describing the variability of effective constitutive parameters of non-metallic metamaterials, as a function of the constituent geometric and material parameters and their variations, have been developed from the total differential of Clausius-Mossotti expressions for the effective (bulk) constitutive parameters of the metamaterial. In practice, these expressions are important for estimating the performance of a metamaterial with particular variations in the parameters of its constituents that arise during the fabrication process, and can be used to guard against extinction of desired double negative (DNG) behavior. With the derived expressions, the effects of parameter variations on effective constitutive parameters of non-metallic metamaterials have been analyzed for three types of metamaterials: i) cubic arrays of identical magnetodielectric spheres; ii) cubic arrays of dielectric spheres with equal radius but two different permittivities; and iii) cubic arrays of dielectric spheres with equal permittivity but two different radii. These effects are evaluated in terms of the calculated variations in values of the effective constitutive parameters of the metamaterial in the vicinity of the DNG or single negative (SNG) band for particular geometric and material parameters and their variations. Results show that variation in the following parameters impacts DNG bandwidth. Listed in order from greatest to least influence: i) sphere radius; ii) sphere permittivity

and permeability; iii) lattice constant of the array and iv) the constitutive parameters of the array medium, all impact the width of the achievable DNG band. For particular cases studied here, results also show that the DNG behavior may be extinguished if there are 0.78%, 0.016%, and 0.016% variations in all parameters of metamaterial types i), ii), and iii), respectively, as defined above. For the design of non-metallic metamaterials with inclusions, having arbitrary shapes and material parameters, in either periodic or random arrangement, the presented results can give a qualitative guide on the level of fabrication tolerances that should be achieved in order to observe the predicted SNG or DNG behavior experimentally.

5.2 Introduction

Metamaterials are artificial composite materials, consisting of sub-wavelength building blocks, which can show anomalous and exotic electromagnetic responses.[1], [2] When the lattice constant is much smaller than the operating wavelength, the composite can be treated macroscopically as a homogeneous medium with effective relative permittivity and permeability, $\epsilon_{\mathrm{r}}^{\mathrm{eff}}$ and $\mu_{\mathrm{r}}^{\mathrm{eff}}$. As the first metamaterials implemented experimentally, metal-based metamaterials have achieved rapid development from microwave to visible frequencies in the last decade.[1], [2] To avoid the drawbacks of metal-based metamaterials, such as conduction loss and anisotropy, composites consisting of non-metallic scatterers embedded in a low permittivity matrix have been proposed to achieve metamaterials.[3]-[6] This scheme usually achieves negative effective permittivity at the resonance(s) of the Mie electric dipole scattering coefficient, negative effective permeability at the resonance(s) of the Mie magnetic dipole scattering coefficient, and DNG behavior by overlapping resonances of Mie electric and magnetic dipole scattering coefficients. [5], [7]-[18] In theory, metamaterials are designed with geometric and electric parameters of the building blocks identical to ideal values. In practice, however, these parameters exhibit variations due to non-ideal, achievable fabrication tolerances, which may extinguish DNG behavior. The purpose of this paper is to present an analytical approach to assessing the effects of those parameter variations on DNG behavior of non-metallic metamaterials.

For metal-based metamaterials, the effect of variation in spacing between the electric ring resonator and the cut wire on the absorbance of an absorbing metamaterial was analyzed using

a statistics-based method in Ref. [19]. The effects of variations of the geometrical parameters and changes in the background on the invisibility properties of the metamaterial cloak were investigated in Ref. [20]. The resonant behaviors of metamaterials with elements disordered from their initially periodic arrangement were studied in Refs. [21], [22]. As for non-metallic metamaterials, the influence of size and permittivity distributions of spherical particles on the DNG characteristics of metamaterial was analyzed in Refs. [23], [24]. Further, the effects of scatterer size variations on the reflection and transmission properties of a metafilm were investigated in Ref. [25]. None of these works, however, give explicit analytical expressions for the variability of effective constitutive parameters of the metamaterial as a function of the constituent geometric and material parameters and their variations.

This paper develops the Clausius-Mossotti relations for effective constitutive parameters of two types of non-metallic metamaterials: a cubic array of identical magnetodielectric spheres and a cubic array of two different magnetodielectric spheres. Explicit analytical expressions for the variability of effective constitutive parameters as a function of the geometric and material parameters of the spheres, the matrix and their variations are developed from the total differential of the Clausius-Mossotti relations. According to these expressions, the effects of parameter variations on the effective constitutive parameters are analyzed for three types of non-metallic metamaterials: i) cubic arrays of identical magnetodielectric spheres; ii) cubic arrays of dielectric spheres with equal radius but two different permittivities; and iii) cubic arrays of dielectric spheres with equal permittivity but two different radii. Here, the term "magnetodielectric" refers to spheres with relative permittivity and permeability both greater than one, or purely dielectric/magnetic spheres.[13], [26] (Ref. [13] contains a considerable number of mostly typographical mistakes which have been corrected in Ref. [27].)

The paper is arranged as follows. Sec. 5.3 gives the expressions for variability of effective constitutive parameters of non-metallic metamaterials. The presented expressions are tested in Sec. 5.4 for particular cases. Comparisons of the effects of different parameters and of different combinations of parameter variations are presented in Sec. 5.5.

5.3 Theory

5.3.1 Cubic arrays of identical magnetodielectric spheres

Magnetodielectric spheres with relative permittivity ϵ_{r1}, relative permeability μ_{r1}, and radius a are arranged on a cubic lattice with lattice constant d, Fig. 5.1. The matrix medium

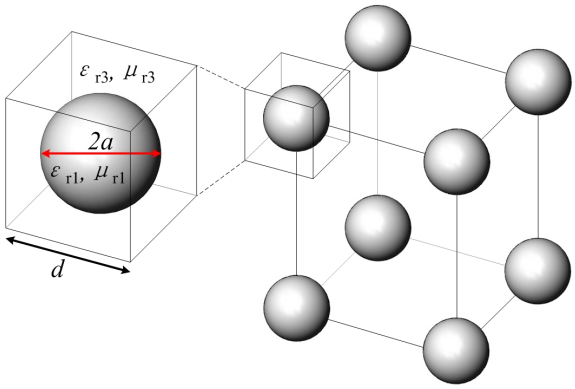

Figure 5.1 An array of identical spheres and unit cell geometry.

has relative permittivity ϵ_{r3} and relative permeability μ_{r3} (the subscript '3' is chosen so that '2' is reserved for a second type of sphere mentioned later, see Fig. 5.2 in Sec. 5.3.2). When the lattice constant is much smaller than the operating wavelength, $kd \leq 1$,[11] the array can be treated macroscopically as a homogeneous medium with effective relative permittivity ϵ_r^{eff} and effective relative permeability μ_r^{eff}. ϵ_r^{eff} can be expressed in the form of Clausius-Mossotti formula (Eq. (3.24) in Ref. [28])

$$\frac{\epsilon_r^{\text{eff}} - \epsilon_{r3}}{\epsilon_r^{\text{eff}} + 2\epsilon_{r3}} = \frac{n\alpha}{3\epsilon_{r3}\epsilon_0} \tag{5.1}$$

where ϵ_{r3} is the relative permittivity of the matrix medium, n is the number density of the dipoles, α is the polarisability of each inclusion (sphere), and ϵ_0 is the vacuum permittivity. Multiply $\mathbf{E_0}$, which is the local, uniform, electric field exciting a single sphere, on both sides of Eq. (5.1). Then, replacing the vector quantities by their corresponding scalar ones gives

$$\frac{\epsilon_r^{\text{eff}} - \epsilon_{r3}}{\epsilon_r^{\text{eff}} + 2\epsilon_{r3}} E_0 = \frac{np}{3\epsilon_{r3}\epsilon_0} \tag{5.2}$$

where p is the moment of each electric dipole. Solving Eq. (5.2) for $\epsilon_{\mathrm{r}}^{\mathrm{eff}}$ gives

$$\epsilon_{\mathrm{r}}^{\mathrm{eff}} = \epsilon_{\mathrm{r3}} \frac{2B_j + 3}{3 - B_j} \tag{5.3}$$

with

$$B_1 = \frac{np}{\epsilon_{\mathrm{r3}} \epsilon_0 E_0}, \tag{5.4}$$

where $j = 1, 2$ depending on the number of types of magnetodielectric spheres composing the array.

Eq. (5.4) can be expressed as [11]

$$B_1 = -\frac{6\pi \mathrm{i} b_1^{\mathrm{sc}}}{(k_0 d)^3 (\epsilon_{\mathrm{r3}} \mu_{\mathrm{r3}})^{1.5}}, \tag{5.5}$$

where b_1^{sc} is the Mie electric dipole scattering coefficient given by Eq. (4.2), $k_0 d = \omega \sqrt{\epsilon_0 \mu_0}\, d$ is the electrical lattice constant. Note that, in contrast with Eq. (76) in Ref. [11], $\epsilon_{\mathrm{r}}^{\mathrm{eff}}$ in Eq. (5.3) is relative to the vacuum permittivity ϵ_0 instead of the matrix medium permittivity ϵ_3. Also note that kd in Eq. (5.5) is expressed as $k_0 \sqrt{\epsilon_{\mathrm{r3}} \mu_{\mathrm{r3}}}\, d$ in order to make ϵ_{r3} and μ_{r3} explicit in Eq. (5.3). By doing so, it becomes easier to study the effects of the variations of ϵ_{r3} and μ_{r3} on $\epsilon_{\mathrm{r}}^{\mathrm{eff}}$ and $\mu_{\mathrm{r}}^{\mathrm{eff}}$.

Expressions for the effective relative permeability $\mu_{\mathrm{r}}^{\mathrm{eff}}$ can be obtained by replacing ϵ_{r3} and b_1^{sc} in Eqs. (5.3) and (5.5), respectively, by μ_{r3} and a_1^{sc}. a_1^{sc} is the Mie magnetic dipole scattering coefficient given by Eq. (4.1).

When a metamaterial of the type shown in Fig. 5.1 is fabricated, departure of $\epsilon_{\mathrm{r}}^{\mathrm{eff}}$ and $\mu_{\mathrm{r}}^{\mathrm{eff}}$ from their designed values may arise due to variation in any of the following parameters: $k_0 a$, ϵ_{r1}, μ_{r1}, ϵ_{r3}, μ_{r3}, and $k_0 d$. The electrical dimensions $k_0 a$ and $k_0 d$ are regarded as parameters here instead of their corresponding physical dimensions to simplify the differentiations. Based on the definition of the total differential,[29] the variability in $\epsilon_{\mathrm{r}}^{\mathrm{eff}}$ due to its dependent parameters and their variations is given by

$$\Delta \epsilon_{\mathrm{r}}^{\mathrm{eff}} = \sum_m \frac{\partial \epsilon_{\mathrm{r}}^{\mathrm{eff}}}{\partial m} \Delta m \tag{5.6}$$

where $m = k_0 a, \epsilon_{\mathrm{r1}}, \mu_{\mathrm{r1}}, \epsilon_{\mathrm{r3}}, \mu_{\mathrm{r3}}$, and $k_0 d$. Similarly, the expression for $\Delta \mu_{\mathrm{r}}^{\mathrm{eff}}$ can be obtained. Since the derivative may have a negative sign after simple computation, the absolute value

of each component variability, $\left|(\partial\epsilon_{\rm r}^{\rm eff}/\partial m)\Delta m\right|$, is used to describe the worst-case scenario. Note that the definition of the total differential requires that all of the dependent parameters are independent. This requirement is met, for the following reasons: i) k_0a and k_0d are the geometric parameters so that they have no correlation with the other four material parameters; ii) due to the fact that spheres and matrix are fabricated independently, k_0a and k_0d are independent of one another, and $\epsilon_{\rm r1}$ and $\mu_{\rm r1}$ are independent from $\epsilon_{\rm r3}$ and $\mu_{\rm r3}$; iii) since there is no functional relation between $\epsilon_{\rm r1}$ ($\epsilon_{\rm r3}$) and $\mu_{\rm r1}$ ($\mu_{\rm r3}$), their variations are basically due to some random effects, such as a small change in temperature, in the synthesis process. So, $\epsilon_{\rm r1}$ ($\epsilon_{\rm r3}$) and $\mu_{\rm r1}$ ($\mu_{\rm r3}$) have no correlation with each other. Also note that, according to the definition of the total differential, it is not required that $|\Delta(k_0a)|$, $|\Delta\epsilon_{\rm r1}|$, $|\Delta\mu_{\rm r1}|$, $|\Delta\epsilon_{\rm r3}|$, $|\Delta\mu_{\rm r3}|$, and $|\Delta(k_0d)|$ be small.

In Eq. (5.6), the derivatives of $\epsilon_{\rm r}^{\rm eff}$ with respect to different parameters are calculated as follows. For $m = k_0a$, $\epsilon_{\rm r1}$, $\mu_{\rm r1}$, $\mu_{\rm r3}$, and k_0d,

$$\frac{\partial\epsilon_{\rm r}^{\rm eff}}{\partial m} = \frac{9\epsilon_{\rm r3}}{(3-B_j)^2}\frac{\partial B_j}{\partial m} \tag{5.7}$$

with

$$\frac{\partial B_1}{\partial m} = -\frac{6\pi{\rm i}}{(k_0d)^3(\epsilon_{\rm r3}\mu_{\rm r3})^{1.5}}\frac{\partial b_1^{\rm sc}}{\partial m} \tag{5.8}$$

for $m = k_0a$, $\epsilon_{\rm r1}$, and $\mu_{\rm r1}$; further

$$\frac{\partial B_1}{\partial \mu_{\rm r3}} = -\frac{6\pi{\rm i}}{(k_0d)^3(\epsilon_{\rm r3}\mu_{\rm r3})^{1.5}}\left[\frac{\partial b_1^{\rm sc}}{\partial \mu_{\rm r3}} - 1.5(\mu_{\rm r3})^{-1}b_1^{\rm sc}\right]; \tag{5.9}$$

$$\frac{\partial B_1}{\partial (k_0d)} = \frac{18\pi{\rm i}b_1^{\rm sc}}{(k_0d)^4(\epsilon_{\rm r3}\mu_{\rm r3})^{1.5}}. \tag{5.10}$$

And

$$\frac{\partial\epsilon_{\rm r}^{\rm eff}}{\partial\epsilon_{\rm r3}} = \frac{2B_j+3}{3-B_j} + \frac{9\epsilon_{\rm r3}}{(3-B_j)^2}\frac{\partial B_j}{\partial\epsilon_{\rm r3}} \tag{5.11}$$

with

$$\frac{\partial B_1}{\partial \epsilon_{\rm r3}} = -\frac{6\pi{\rm i}}{(k_0d)^3(\epsilon_{\rm r3}\mu_{\rm r3})^{1.5}}\left[\frac{\partial b_1^{\rm sc}}{\partial \epsilon_{\rm r3}} - 1.5(\epsilon_{\rm r3})^{-1}b_1^{\rm sc}\right]. \tag{5.12}$$

To compute $\Delta\mu_{\rm r}^{\rm eff}$, the derivatives of $\mu_{\rm r}^{\rm eff}$ with respect to different parameters are calculated as follows. For $m = k_0 a$, $\epsilon_{\rm r1}$, $\mu_{\rm r1}$, $\epsilon_{\rm r3}$, and $k_0 d$,

$$\frac{\partial \mu_{\rm r}^{\rm eff}}{\partial m} = \frac{9\mu_{\rm r3}}{(3-B_j)^2}\frac{\partial B_j}{\partial m} \tag{5.13}$$

with

$$\frac{\partial B_1}{\partial m} = -\frac{6\pi {\rm i}}{(k_0 d)^3(\epsilon_{\rm r3}\mu_{\rm r3})^{1.5}}\frac{\partial a_1^{\rm sc}}{\partial m} \tag{5.14}$$

for $m = k_0 a$, $\epsilon_{\rm r1}$, and $\mu_{\rm r1}$; further

$$\frac{\partial B_1}{\partial \epsilon_{\rm r3}} = -\frac{6\pi {\rm i}}{(k_0 d)^3(\epsilon_{\rm r3}\mu_{\rm r3})^{1.5}}\left[\frac{\partial a_1^{\rm sc}}{\partial \epsilon_{\rm r3}} - 1.5(\epsilon_{\rm r3})^{-1}a_1^{\rm sc}\right]; \tag{5.15}$$

$$\frac{\partial B_1}{\partial (k_0 d)} = \frac{18\pi {\rm i} a_1^{\rm sc}}{(k_0 d)^4(\epsilon_{\rm r3}\mu_{\rm r3})^{1.5}}. \tag{5.16}$$

And

$$\frac{\partial \mu_{\rm r}^{\rm eff}}{\partial \mu_{\rm r3}} = \frac{2B_j+3}{3-B_j} + \frac{9\mu_{\rm r3}}{(3-B_j)^2}\frac{\partial B_j}{\partial \mu_{\rm r3}} \tag{5.17}$$

with

$$\frac{\partial B_1}{\partial \mu_{\rm r3}} = -\frac{6\pi {\rm i}}{(k_0 d)^3(\epsilon_{\rm r3}\mu_{\rm r3})^{1.5}}\left[\frac{\partial a_1^{\rm sc}}{\partial \mu_{\rm r3}} - 1.5(\mu_{\rm r3})^{-1}a_1^{\rm sc}\right]. \tag{5.18}$$

In Eqs. (5.7)-(5.18), the derivatives of Mie dipole scattering coefficients, $a_1^{\rm sc}$ and $b_1^{\rm sc}$, with respect to different parameters are given in Chapter 4.

5.3.2 Cubic arrays of two different magnetodielectric spheres

Two different magnetodielectric spheres are arranged on a cubic lattice with lattice constant $2d$ and matrix medium having relative permittivity $\epsilon_{\rm r3}$, and relative permeability $\mu_{\rm r3}$, Fig. 5.2. One set of spheres with radius a_1, and relative permittivity $\epsilon_{\rm r1}$, and relative permeability $\mu_{\rm r1}$ will be referred to as the "1-spheres", and the other set of spheres with radius a_2, relative permittivity $\epsilon_{\rm r2}$, and relative permeability $\mu_{\rm r2}$ will be referred to as the "2-spheres". Note that the arrangement of the two-sphere array shown in Fig. 5.2 is one of the seven different

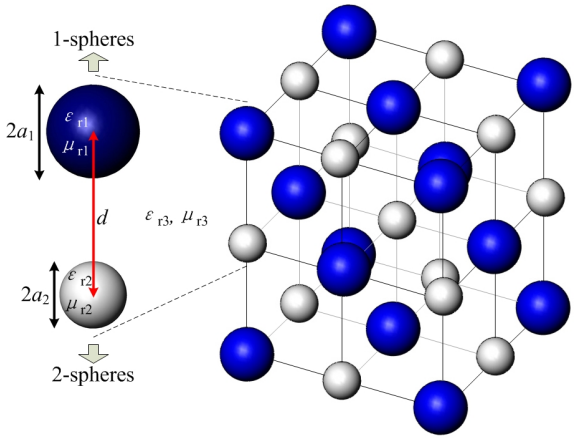

Figure 5.2 Two-sphere array and unit cell geometry.

arrangements analyzed in Refs. [26], [30]. The Clausius-Mossotti formula gives identical result for different arrangements because it accounts for the number of the electric dipoles of the 1-spheres and 2-spheres per unit cell volume, but not for their relative arrangement. Hence, different arrangements of two-sphere arrays are not taken into account here.

Similar to the case of the cubic arrays of identical magnetodielectric spheres treated in Sec. 5.3.1, the two-sphere array can also be treated macroscopically as a homogeneous medium with effective relative permittivity $\epsilon_{\rm r}^{\rm eff}$ and effective relative permeability $\mu_{\rm r}^{\rm eff}$ when the lattice constant is much smaller than the operating wavelength, $kd \leq 0.5$.[13], [26] The expression for $\epsilon_{\rm r}^{\rm eff}$ in the case of the two-sphere arrays is given by Eq. (5.3) with $j = 2$ and

$$B_2 = -\frac{3\pi {\rm i}(b_{11}^{\rm sc} + b_{12}^{\rm sc})}{(k_0 d)^3 (\epsilon_{\rm r3}\mu_{\rm r3})^{1.5}}, \tag{5.19}$$

where $b_{11}^{\rm sc}$ and $b_{12}^{\rm sc}$ are the Mie electric dipole scattering coefficients of the 1-spheres and 2-spheres, respectively, given by Eq. (4.2). A similar expression for $\mu_{\rm r}^{\rm eff}$ of two-sphere arrays can be obtained by replacing $\epsilon_{\rm r3}$ and $b_{1i}^{\rm sc}$ ($i = 1, 2$) in Eqs. (5.3) and (5.19) by $\mu_{\rm r3}$ and $a_{1i}^{\rm sc}$ ($i = 1, 2$), respectively. $a_{1i}^{\rm sc}$ is the Mie magnetic dipole scattering coefficient given by Eq. (4.1).

The variability of $\epsilon_{\rm r}^{\rm eff}$ and $\mu_{\rm r}^{\rm eff}$ is a function of the following parameters and their variations: $k_0 a_1$, $k_0 a_2$, $\epsilon_{\rm r1}$, $\mu_{\rm r1}$, $\epsilon_{\rm r2}$, $\mu_{\rm r2}$, $\epsilon_{\rm r3}$, $\mu_{\rm r3}$, and $k_0 d$. Similarly to the case of the arrays of identical spheres, these parameters are independent. Due to the increased complexity of the system, the expression for $\Delta\epsilon_{\rm r}^{\rm eff}$ in the case of the two-sphere arrays, obtained by total differential of the

Clausius-Mossotti relations as described above, contains more terms than in the case of arrays of identical spheres. Referring to Eq. (5.6), now $m = k_0a_1$, k_0a_2, ϵ_{r1}, μ_{r1}, ϵ_{r2}, μ_{r2}, ϵ_{r3}, μ_{r3}, and k_0d. The expression for $\Delta\mu_r^{\text{eff}}$ in the case of the two-sphere arrays can be obtained in a similar way.

The derivatives of ϵ_r^{eff} with respect to different parameters are computed as follows. For $m = k_0a_1$, k_0a_2, ϵ_{r1}, μ_{r1}, ϵ_{r2}, μ_{r2}, μ_{r3}, and k_0d, $\partial\epsilon_r^{\text{eff}}/\partial m$ can be obtained by Eq. (5.7) with

$$\frac{\partial B_2}{\partial m} = -\frac{3\pi \mathrm{i}}{(k_0d)^3(\epsilon_{r3}\mu_{r3})^{1.5}}\frac{\partial b_{11}^{\text{sc}}}{\partial m} \tag{5.20}$$

for $m = k_0a_1$, ϵ_{r1}, μ_{r1};

$$\frac{\partial B_2}{\partial m} = -\frac{3\pi \mathrm{i}}{(k_0d)^3(\epsilon_{r3}\mu_{r3})^{1.5}}\frac{\partial b_{12}^{\text{sc}}}{\partial m} \tag{5.21}$$

for $m = k_0a_2$, ϵ_{r2}, μ_{r2}; further

$$\frac{\partial B_2}{\partial \mu_{r3}} = -\frac{3\pi \mathrm{i}}{(k_0d)^3(\epsilon_{r3}\mu_{r3})^{1.5}}\left[\left(\frac{\partial b_{11}^{\text{sc}}}{\partial \mu_{r3}} + \frac{\partial b_{12}^{\text{sc}}}{\partial \mu_{r3}}\right) - 1.5(\mu_{r3})^{-1}(b_{11}^{\text{sc}} + b_{12}^{\text{sc}})\right]; \tag{5.22}$$

$$\frac{\partial B_2}{\partial (k_0d)} = \frac{9\pi \mathrm{i}(b_{11}^{\text{sc}} + b_{12}^{\text{sc}})}{(k_0d)^4(\epsilon_{r3}\mu_{r3})^{1.5}}. \tag{5.23}$$

$\partial\epsilon_r^{\text{eff}}/\partial\epsilon_{r3}$ can be expressed as Eq. (5.11) with

$$\frac{\partial B_2}{\partial \epsilon_{r3}} = -\frac{3\pi \mathrm{i}}{(k_0d)^3(\epsilon_{r3}\mu_{r3})^{1.5}}\left[\left(\frac{\partial b_{11}^{\text{sc}}}{\partial \epsilon_{r3}} + \frac{\partial b_{12}^{\text{sc}}}{\partial \epsilon_{r3}}\right) - 1.5(\epsilon_{r3})^{-1}(b_{11}^{\text{sc}} + b_{12}^{\text{sc}})\right]. \tag{5.24}$$

The derivatives of μ_r^{eff} with respect to different parameters are calculated as follows. For $m = k_0a_1$, k_0a_2, ϵ_{r1}, μ_{r1}, ϵ_{r2}, μ_{r2}, ϵ_{r3}, and k_0d, $\partial\mu_r^{\text{eff}}/\partial m$ can be obtained by Eq. (5.13) with

$$\frac{\partial B_2}{\partial m} = -\frac{3\pi \mathrm{i}}{(k_0d)^3(\epsilon_{r3}\mu_{r3})^{1.5}}\frac{\partial a_{11}^{\text{sc}}}{\partial m} \tag{5.25}$$

for $m = k_0a_1$, ϵ_{r1}, and μ_{r1};

$$\frac{\partial B_2}{\partial m} = -\frac{3\pi \mathrm{i}}{(k_0d)^3(\epsilon_{r3}\mu_{r3})^{1.5}}\frac{\partial a_{12}^{\text{sc}}}{\partial m} \tag{5.26}$$

for $m = k_0a_2$, ϵ_{r2}, and μ_{r2}; further

$$\frac{\partial B_2}{\partial \epsilon_{r3}} = -\frac{3\pi \mathrm{i}}{(k_0d)^3(\epsilon_{r3}\mu_{r3})^{1.5}}\left[\left(\frac{\partial a_{11}^{\text{sc}}}{\partial \epsilon_{r3}} + \frac{\partial a_{12}^{\text{sc}}}{\partial \epsilon_{r3}}\right) - 1.5(\epsilon_{r3})^{-1}(a_{11}^{\text{sc}} + a_{12}^{\text{sc}})\right]; \tag{5.27}$$

$$\frac{\partial B_2}{\partial(k_0 d)} = \frac{9\pi \mathrm{i}(a_{11}^{\mathrm{sc}} + a_{12}^{\mathrm{sc}})}{(k_0 d)^4(\epsilon_{\mathrm{r}3}\mu_{\mathrm{r}3})^{1.5}}. \tag{5.28}$$

$\partial\mu_{\mathrm{r}}^{\mathrm{eff}}/\partial\mu_{\mathrm{r}3}$ can be expressed as Eq. (5.17) with

$$\frac{\partial B_2}{\partial \mu_{\mathrm{r}3}} = -\frac{3\pi \mathrm{i}}{(k_0 d)^3(\epsilon_{\mathrm{r}3}\mu_{\mathrm{r}3})^{1.5}} \left[\left(\frac{\partial a_{11}^{\mathrm{sc}}}{\partial \mu_{\mathrm{r}3}} + \frac{\partial a_{12}^{\mathrm{sc}}}{\partial \mu_{\mathrm{r}3}} \right) - 1.5(\mu_{\mathrm{r}3})^{-1}(a_{11}^{\mathrm{sc}} + a_{12}^{\mathrm{sc}}) \right]. \tag{5.29}$$

The derivatives of Mie dipole scattering coefficients a_{11}^{sc}, a_{12}^{sc}, b_{11}^{sc}, and b_{12}^{sc} with respect to various parameters are given in Chapter 4.

5.4 Verification

In this section and Sec. 5.5, magnetodielectric spheres in all the cases considered are lossless. Although the effective constitutive parameters of a lossless array are real, the Clausius-Mossotti expressions, Eq. (5.3), give complex effective constitutive parameters for such an array.[11], [13] Away from the resonance regions, the imaginary parts of the effective constitutive parameters calculated by Clausius-Mossotti expressions are in general small.[11] In the region of homogenization, $kd \leq 1$ and $\beta d \leq 1$ ($kd \leq 0.5$ and $\beta d \leq 0.5$) for arrays of identical spheres (two-sphere arrays), the real parts of the effective constitutive parameters calculated by Clausius-Mossotti expressions are in good consistent with those, which are real values, computed by Shore-Yaghjian formulas.[11] Hence, in all the cases under study, only the real parts of the effective constitutive parameters calculated by the Clausius-Mossotti expressions are taken into account. Further, only the real part of each partial derivative of an effective constitutive parameter with respect to a parameter in Eq. (5.6) is considered so as to give a real variability of effective constitutive parameters, eventually.

5.4.1 Clausius-Mossotti formulas

First, the Clausius-Mossotti expressions for the effective constitutive parameters of non-metallic metamaterials consisting of an array of identical spheres, Eqs. (5.3) and (5.5), and an array of two types of spheres, Eqs. (5.3) and (5.19), are tested by comparing the dispersion

diagrams obtained by the following relation,[11]

$$\frac{\beta d}{k_0 d} = \sqrt{\epsilon_{\rm r}^{\rm eff}\mu_{\rm r}^{\rm eff}}, \tag{5.30}$$

with those calculated by MIT Photonic-Bands (MPB).[31] MPB computes fully-vectorial eigenmodes of Maxwell's equations with periodic boundary conditions by preconditioned conjugate-gradient minimization of the block Rayleigh quotient in a plane-wave basis.[31] Since MPB can only treat dielectric periodic structures, arrays considered in this section are all of dielectric spheres. Fig. 5.3 shows the dispersion diagram for an array of identical dielectric spheres

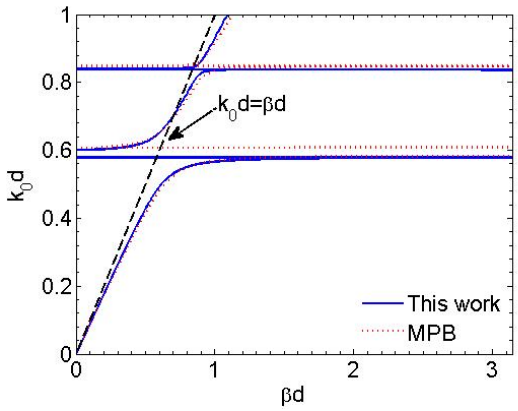

Figure 5.3 Comparison of dispersion diagrams for an array of identical spheres, Fig. 5.1, obtained by formulas presented here, Eqs. (5.3), (5.5), and (5.30), with that calculated by MPB.[31] The 25 lowest bands computed by MPB are shown. In this calculation, $\epsilon_{\rm r1} = 400$, $\mu_{\rm r1} = \epsilon_{\rm r3} = \mu_{\rm r3} = 1$, and $a/d = 0.2672$.

whose parameters are chosen to match those of the larger sphere considered in a design example given in Refs. [23], [32]. The parameter values are provided in the figure caption. This array does not support backward wave propagation but, nonetheless, it can be used to test the effectiveness of the presented Clausius-Mossotti formula. The two-sphere array of Fig. 5.4 is a design example in Refs. [23], [32], which shows backward wave propagation in the vicinity of $k_0 d = 0.8386$. As shown in Figs. 5.3 and 5.4, good agreement is achieved between the calculations of MPB and the formulae presented herein, for these cases. Note that the MPB result for the two-sphere array, Fig. 5.4, is shown only in the range $0 < \beta d < \pi/2$, instead of $0 < \beta d < \pi$, because, in MPB, the lattice constant of this two-sphere array is set to be twice the separation of adjacent spheres, i.e. $d' = 2d$, to guarantee the translational symmetry in the

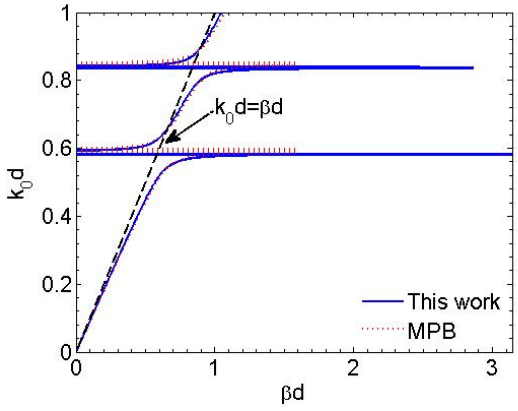

Figure 5.4 Comparison of dispersion diagrams for a two-sphere array, Fig. 5.2, obtained by formulas presented here, Eqs. (5.3), (5.19), and (5.30), with that calculated by MPB.[31] The 60 lowest bands computed by MPB are shown. In this calculation, $\epsilon_{r1} = \epsilon_{r2} = 400$, $\mu_{r1} = \mu_{r2} = \epsilon_{r3} = \mu_{r3} = 1$, $a_1/d = 0.187$, and $a_2/d = 0.2672$.

x, y, and z directions. This means that the size of the corresponding reciprocal lattice in the Brillouin zone is halved.[33]

5.4.2 Expressions for the variabilities of effective constitutive parameters

Next, the variabilities of effective constitutive parameters of non-metallic metamaterials consisting of an array of identical spheres and of a two-sphere array, Eq. (5.6), are tested. In this section, the non-metallic metamaterials are designed following the design procedure in Ref. [34] to achieve a DNG behavior in the vicinity of $k_0 d = 0.4$, which meets the homogenization criteria of metamaterials consisting of an array of identical spheres, $k_0 d \leq 1$, and of a two-sphere array, $k_0 d \leq 0.5$. $\Delta\epsilon_r^{\text{eff}}$ and $\Delta\mu_r^{\text{eff}}$ of an array of identical spheres, Fig. 5.5, are computed by Eq. (5.6) and compared with those calculated by expressions developed by Mathematica. Good agreement is achieved. Using Mathematica, the derivatives of ϵ_r^{eff} and μ_r^{eff} in Eq. (5.6) are obtained by differentiating Eq. (5.3) with respect to $k_0 a$, ϵ_{r1}, μ_{r1}, ϵ_{r3}, μ_{r3}, and $k_0 d$. Note that the expressions developed by Mathematica are much more cumbersome than the presented ones. Further, $\Delta\epsilon_r^{\text{eff}}$ and $\Delta\mu_r^{\text{eff}}$ of a two-sphere array, Fig. 5.6, are computed by Eq. (5.6) and compared with those calculated by expressions developed by Mathematica. Again, good agreement is achieved.

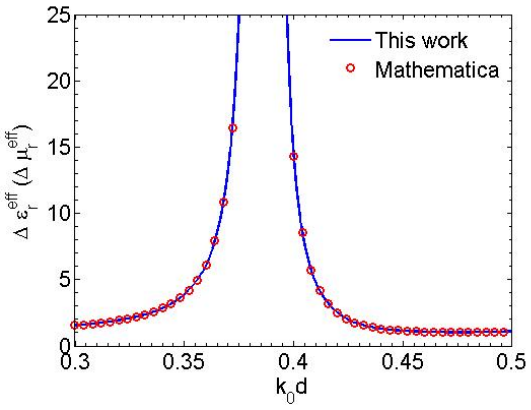

Figure 5.5 Comparison of variabilities of effective constitutive parameters in the vicinity of the DNG band ($k_0 d = 0.4$) of a metamaterial consisting of an array of identical spheres, Fig. 5.1, computed by the formula presented herein Eq. (5.6), with those calculated by expressions developed by Mathematica. In this calculation, $\epsilon_{r1} = \mu_{r1} = 23.9$, $\epsilon_{r3} = \mu_{r3} = 1$, and $a/d = 0.45$; $\Delta m/m = 5\%$ with $m = k_0 a$, ϵ_{r1}, μ_{r1}, ϵ_{r3}, μ_{r3}, and $k_0 d$.

5.5 Results

In this section, the effects of parameter variations on the effective constitutive parameters are analyzed for three types of non-metallic metamaterials: i) a cubic array of identical magnetodielectric spheres; ii) a cubic array of two types of dielectric spheres with equal radius but different permittivities; and iii) a similar array of two types of dielectric spheres with equal permittivity but different radii. For each of these, the effect of variation in individual parameters is first compared. Then, the effects of different combinations of parameter variations are analyzed. The two metamaterials studied in Sec. 5.4.2 are used as the reference cases in Secs. 5.5.1 and 5.5.2, respectively.

5.5.1 Cubic arrays of identical magnetodielectric spheres

Utilizing Eq. (5.6), $\Delta\epsilon_r^{\text{eff}}$ is calculated as one of $k_0 a$, ϵ_{r1}, μ_{r1}, ϵ_{r3}, μ_{r3}, and $k_0 d$ varies by 5% from its nominal value, Table 5.1. As shown in Fig. 5.7, variation of $k_0 a$ has the most significant effect on $\Delta\epsilon_r^{\text{eff}}$; variation of $k_0 d$ has the second most significant effect on $\Delta\epsilon_r^{\text{eff}}$ over the lower part of the DNG band studied ($k_0 d \leq 0.4$) and the fourth most significant effect over

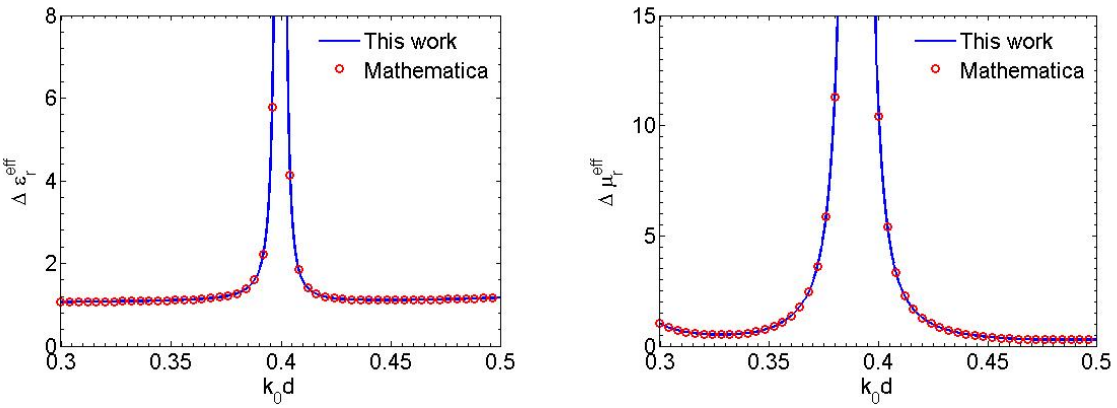

(a) (b)

Figure 5.6 Comparisons of variabilities of effective relative permittivity (a), and permeability (b), in the vicinity of the DNG band ($k_0d = 0.4$) of a metamaterial consisting of a two-sphere array, Fig. 5.2, computed by the formula presented herein Eq. (5.6), with those calculated by expressions developed by Mathematica. In this calculation, $\epsilon_{r1} = 621.1$, $\epsilon_{r2} = 302.7$, $\mu_{r1} = \mu_{r2} = \epsilon_{r3} = \mu_{r3} = 1$, and $a_1/d = a_2/d = 0.45$; $\Delta m/m = 5\%$ with $m = k_0a_1$, ϵ_{r1}, μ_{r1}, k_0a_2, ϵ_{r2}, μ_{r2}, ϵ_{r3}, μ_{r3}, and k_0d.

Table 5.1 The parameter with 5% variation (while others have no variation) in each calculation of variability of effective constitutive parameters of a non-metallic metamaterial consisting of an array of identical spheres, Fig. 5.1.

Calculation	I	II	III	IV	V	VI
Parameter	k_0a	ϵ_{r1}	μ_{r1}	ϵ_{r3}	μ_{r3}	k_0d

the higher part of the DNG band studied ($k_0d \geq 0.4$); variations of ϵ_{r1} and μ_{r1} have similar effects on $\Delta\epsilon_r^{eff}$, giving rise to the third most significant effects on $\Delta\epsilon_r^{eff}$ over the lower part of the DNG band studied ($k_0d \leq 0.4$) and the second most significant effects over the higher part of the DNG band studied ($k_0d \geq 0.4$); whereas variations of ϵ_{r3} and μ_{r3} have the least effects on $\Delta\epsilon_r^{eff}$. Hence, it is noted that variation in the parameters of the sphere (sphere radius, permittivity, and permeability) perturb the predicted behavior of the DNG band more strongly than other parameters of the system. Note that effects of the variations in k_0a and k_0d on $\Delta\epsilon_r^{eff}$ are exactly the same as those on $\Delta\mu_r^{eff}$ since both negative ϵ_r^{eff} and negative μ_r^{eff} in the vicinity of the DNG band are provided by the same magnetodielectric sphere embedded in a simple cubic lattice, which has only one set of geometric parameters: k_0a and k_0d.

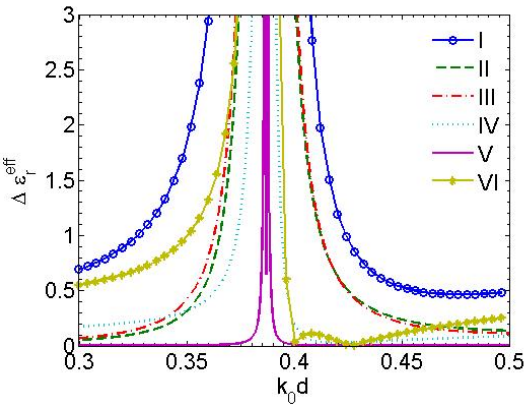

Figure 5.7 Variabilities of effective relative permittivity in the vicinity of the DNG band ($k_0 d = 0.4$) of a non-metallic metamaterial consisting of a cubic array of identical magnetodielectric spheres, Fig. 5.1, in each calculation, Table 5.1. Parameters of this array are as in Fig. 5.5. The equivalent plot for $\Delta\mu_{\rm r}^{\rm eff}$ is not shown here since the only difference is that the effects of variations in $\epsilon_{\rm r1}$, $\epsilon_{\rm r3}$ and those of variations in $\mu_{\rm r}$, $\mu_{\rm r3}$ are interchanged.

In practical fabrication, it is expected that a metamaterial consisting of an array of identical spheres would exhibit a combination of variations in its parameters, due to achievable fabrication tolerances. To analyze the effects of different combinations of parameter variations on effective constitutive parameters of the metamaterial in the vicinity of the DNG band, the following parameter variations are studied, $\Delta m/m = 0.78\%$, 3%, and 5% ($m = k_0 a$, $\epsilon_{\rm r1}$, $\mu_{\rm r1}$, $\epsilon_{\rm r3}$, $\mu_{\rm r3}$, and $k_0 d$), where variation of the six parameters are assumed to be equal to each other. For each of these combinations, $\Delta\epsilon_{\rm r}^{\rm eff}$ is calculated from Eq. (5.6). The ideal value of effective relative permittivity, $\epsilon_{\rm r}^{\rm eff,idl}$, is computed from Eq. (5.3). Based on these results, the variation range of $\epsilon_{\rm r}^{\rm eff}$,

$$\epsilon_{\rm r}^{\rm eff,idl} - \Delta\epsilon_{\rm r}^{\rm eff} < \epsilon_{\rm r}^{\rm eff} < \epsilon_{\rm r}^{\rm eff,idl} + \Delta\epsilon_{\rm r}^{\rm eff}, \tag{5.31}$$

is obtained for each of these combinations, giving the shaded areas in Fig. 5.8. Similarly, the variation range of $\mu_{\rm r}^{\rm eff}$ can be obtained. It can be seen that the variation ranges increase as the parameter variations increase. According to these results it is seen that the DNG behavior may be extinguished when $\Delta m/m \geq 0.78\%$ ($m = k_0 a$, $\epsilon_{\rm r1}$, $\mu_{\rm r1}$, $\epsilon_{\rm r3}$, $\mu_{\rm r3}$, and $k_0 d$).

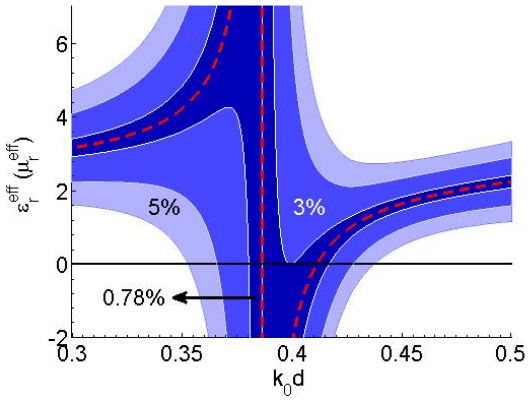

Figure 5.8 Ideal values and variation ranges of the effective relative permittivity and permeability for a non-metallic metamaterial consisting of a cubic array of identical magnetodielectric spheres, Fig. 5.1. Dashed line: ideal values of $\epsilon_{\rm r}^{\rm eff}$ and $\mu_{\rm r}^{\rm eff}$; dark, medium, and light shaded areas: variation ranges for $\Delta m/m = 0.78\%$, 3%, and 5% with $m = k_0a$, $\epsilon_{\rm r1}$, $\mu_{\rm r1}$, $\epsilon_{\rm r3}$, $\mu_{\rm r3}$, and k_0d. Other parameters are as in Fig. 5.5.

5.5.2 Cubic arrays of dielectric spheres with equal radius but two different permittivities

In this section, a similar analysis to that described in Sec. 5.5.1 is performed for an array of two types of dielectric spheres, with equal radius but different permittivity, arranged on the nodes of a simple-cubic lattice, Fig. 5.2. As before, the variability of effective constitutive parameters of the non-metallic metamaterial is computed by Eq. (5.6). In each computation, one of k_0a_1, $\epsilon_{\rm r1}$, $\mu_{\rm r1}$, k_0a_2, $\epsilon_{\rm r2}$, $\mu_{\rm r2}$, $\epsilon_{\rm r3}$, $\mu_{\rm r3}$, and k_0d is set to be 5% different from the nominal value while other parameters have no variation, Table 5.2. The calculated $\Delta\epsilon_{\rm r}^{\rm eff}$ and $\Delta\mu_{\rm r}^{\rm eff}$

Table 5.2 The parameter with 5% variation (while others have no variation) in each calculation of variabilities of effective constitutive parameters of a non-metallic metamaterial consisting of a two-sphere array, Fig. 5.2.

Calculation	I	II	III	IV	V	VI	VII	VIII	IX
Parameter	k_0a_1	$\epsilon_{\rm r1}$	$\mu_{\rm r1}$	k_0a_2	$\epsilon_{\rm r2}$	$\mu_{\rm r2}$	$\epsilon_{\rm r3}$	$\mu_{\rm r3}$	k_0d

are shown in Fig. 5.9. Since the negative $\epsilon_{\rm r}^{\rm eff}$ ($\mu_{\rm r}^{\rm eff}$) is provided by the first resonance of Mie electric (magnetic) dipole scattering coefficient of the 1-spheres (2-spheres), their parameter variations, Δk_0a_1, $\Delta\epsilon_{\rm r1}$, and $\Delta\mu_{\rm r1}$ (Δk_0a_2, $\Delta\epsilon_{\rm r2}$, and $\Delta\mu_{\rm r2}$), have the dominant effects on $\epsilon_{\rm r}^{\rm eff}$

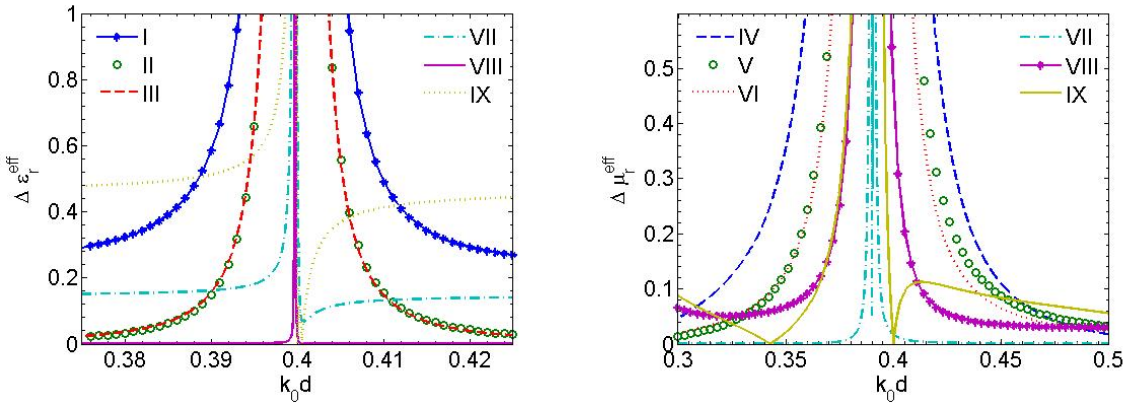

(a) (b)

Figure 5.9 Variabilities of effective relative permittivity (a), and permeability (b), in the vicinity of the DNG band ($k_0d = 0.4$) of a non-metallic metamaterial consisting of a cubic array of dielectric spheres with equal radius but two different permittivities, Fig. 5.2, in each calculation, Table 5.2. Parameters of this array are as in Fig. 5.6.

(μ_r^{eff}) in the vicinity of the DNG band. Hence, only the effects of parameter variations of 1-spheres (2-spheres) on ϵ_r^{eff} (μ_r^{eff}) are shown in Fig. 5.9 and are analyzed in detail. As shown in Fig. 5.9(a): variation of k_0a_1 has the most significant effect on $\Delta\epsilon_r^{eff}$; variations of ϵ_{r1} and μ_{r1} have similar effects on $\Delta\epsilon_r^{eff}$, which are less than that of k_0a_1; variation of k_0d has the fourth most significant effect on $\Delta\epsilon_r^{eff}$; and variations of ϵ_{r3} and μ_{r3} have the least effects on $\Delta\epsilon_r^{eff}$. As shown in Fig. 5.9(b): variation of k_0a_2 has the most significant effect on $\Delta\mu_r^{eff}$; variations of ϵ_{r2} and μ_{r2} have similar effects on $\Delta\mu_r^{eff}$, which are less than that of k_0a_2; variations of μ_{r3} and k_0d have similar effects on $\Delta\mu_r^{eff}$, which are less than those of ϵ_{r2} and μ_{r2}; and variation of ϵ_{r3} has the least effect on $\Delta\epsilon_r^{eff}$.

To analyze the effects of different combinations of parameter variations on ϵ_r^{eff} (μ_r^{eff}) in the vicinity of the DNG band, the following parameter variations are studied, $\Delta m/m = 0.016\%$, 0.03%, and 0.1% (1.2%, 3%, and 5%) with $m = k_0a_1$, ϵ_{r1}, μ_{r1}, k_0a_2, ϵ_{r2}, μ_{r2}, ϵ_{r3}, μ_{r3}, and k_0d, are taken into account. In each case, variations of the nine parameters are assumed equal to each other. For each of these combinations, the variation range of ϵ_r^{eff}, Eq. (5.31), is obtained, giving the shaded areas in Fig. 5.10. Similarly, the variation range of μ_r^{eff} can be obtained. It can be seen that the variation ranges increase as the parameter variations increase. The negative ϵ_r^{eff} (μ_r^{eff}) may be extinguished when $\Delta m/m \geq 0.016\%$ (1.2%) with $m = k_0a_1$, ϵ_{r1}, μ_{r1},

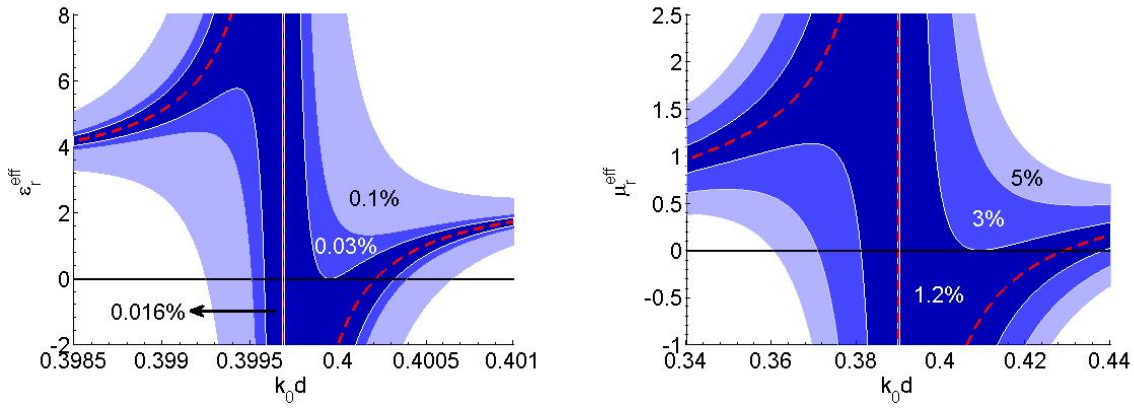

(a) (b)

Figure 5.10 Ideal values and variation ranges of the effective relative permittivity (a), and permeability (b), for a non-metallic metamaterial consisting of a cubic array of dielectric spheres with equal radius but two different permittivities, Fig. 5.2, with six combinations of parameter variations. Dashed line: ideal values of ϵ_r^{eff} (a), and μ_r^{eff} (b); dark, medium, and light shaded areas: variation ranges for $\Delta m/m = 0.016\%$, 0.03%, and 0.1% (a), 1.2%, 3%, and 5% (b) with $m = k_0a_1$, ϵ_{r1}, μ_{r1}, k_0a_2, ϵ_{r2}, μ_{r2}, ϵ_{r3}, μ_{r3}, and k_0d. Other parameters are as in Fig. 5.6.

k_0a_2, ϵ_{r2}, μ_{r2}, ϵ_{r3}, μ_{r3}, and k_0d. Consequently, the DNG behavior may be extinguished when $\Delta m/m \geq 0.016\%$. Note that the negative ϵ_r^{eff} of this metamaterial is much more sensitive to parameter variations than negative μ_r^{eff}. The reason for this is that the first resonance of the Mie electric dipole scattering coefficient of the set of 1-spheres for which, in this calculation, $\epsilon_{r1} = 621.1$ and which provides the negative ϵ_r^{eff}, is narrower than the first resonance of the Mie magnetic dipole scattering coefficient of the set of 2-spheres ($\epsilon_{r2} = 302.7$), which provides the negative μ_r^{eff}.

5.5.3 Cubic arrays of dielectric spheres with equal permittivity but two different radii

Following the design procedure presented in Ref. [34], a non-metallic metamaterial consisting of a cubic array of two types of dielectric spheres with equal permittivity but different radii is designed with parameters $\epsilon_{r1} = \epsilon_{r2} = 621.1$, $\mu_{r1} = \mu_{r2} = \epsilon_{r3} = \mu_{r3} = 1$, $a_1/d = 0.45$, and $a_2/d = 0.31$, to yield DNG behavior in the vicinity of $k_0d = 0.4$, similar to the behavior of the metamaterials analyed in Secs. 5.5.1 and 5.5.2.

Similar to the analysis in the first paragraph of Sec. 5.5.2, the effects of different parameters are compared for this metamaterial. As shown in Fig. 5.11(a): variation of k_0a_1 has the most

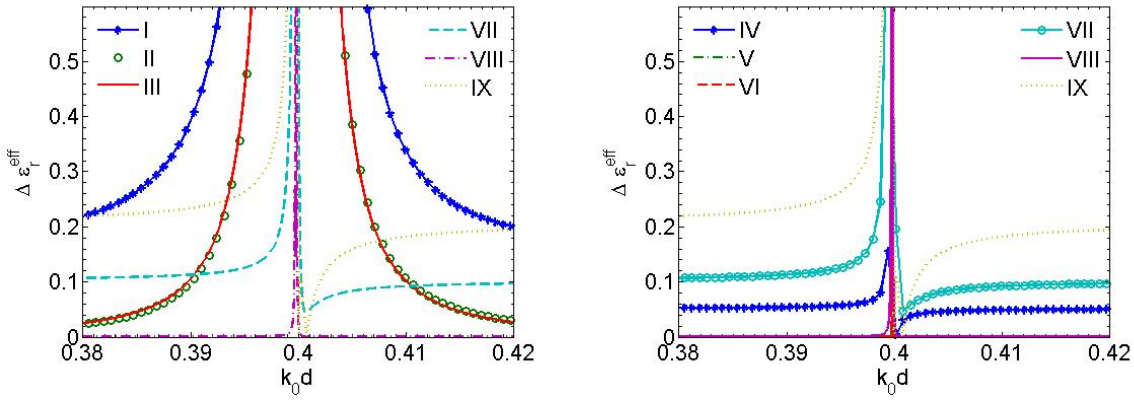

(a) (b)

Figure 5.11 Variabilities of effective relative permittivity (a), and permeability (b), in the vicinity of the DNG band ($k_0d = 0.4$) of a non-metallic metamaterial consisting of a cubic array of dielectric spheres with equal permittivity but two different radii, Fig. 5.2, in each calculation, Table 5.2. In these calculations, $\epsilon_{r1} = \epsilon_{r2} = 621.1$, X$\mu_{r1} = \mu_{r2} = \epsilon_{r3} = \mu_{r3} = 1$, $a_1/d = 0.45$, and $a_2/d = 0.31$.

significant effect on $\Delta\epsilon_r^{eff}$; variations of ϵ_{r1} and μ_{r1} have similar effects on $\Delta\epsilon_r^{eff}$, which are less than that of k_0a_1; variation of k_0d has the fourth most significant effect on $\Delta\epsilon_r^{eff}$; and variations of ϵ_{r3} and μ_{r3} have the least effects on $\Delta\epsilon_r^{eff}$. As shown in Fig. 5.11(b): variation of k_0a_2 has the most significant effect on $\Delta\mu_r^{eff}$; variations of ϵ_{r2} and μ_{r2} have similar effects on $\Delta\mu_r^{eff}$, which are less than that of k_0a_2; variation of μ_{r3} has the fourth most significant effect on $\Delta\mu_r^{eff}$; and variations of ϵ_{r3} and k_0d have the least effects on $\Delta\mu_r^{eff}$.

Similar to the analysis in the second paragraph of Sec. 5.5.2, the effects of different combinations of parameter variations on ϵ_r^{eff} and μ_r^{eff} in the vicinity of the DNG band are investigated for this metamaterial. As shown in Fig. 5.12, the variation ranges increase as the parameter variations increase. The negative ϵ_r^{eff} (μ_r^{eff}) may be extinguished when $\Delta m/m \geq 0.016\%$ (0.4%) with $m = k_0a_1$, ϵ_{r1}, μ_{r1}, k_0a_2, ϵ_{r2}, μ_{r2}, ϵ_{r3}, μ_{r3}, and k_0d. Hence, the DNG behavior may be extinguished when $\Delta m/m \geq 0.016\%$. Note that the negative ϵ_r^{eff} of this metamaterial is more sensitive to parameter variations than negative μ_r^{eff}. The reason is that the first resonance of Mie electric dipole scattering coefficient, which corresponds to 1-spheres ($a_1/d = 0.45$) and

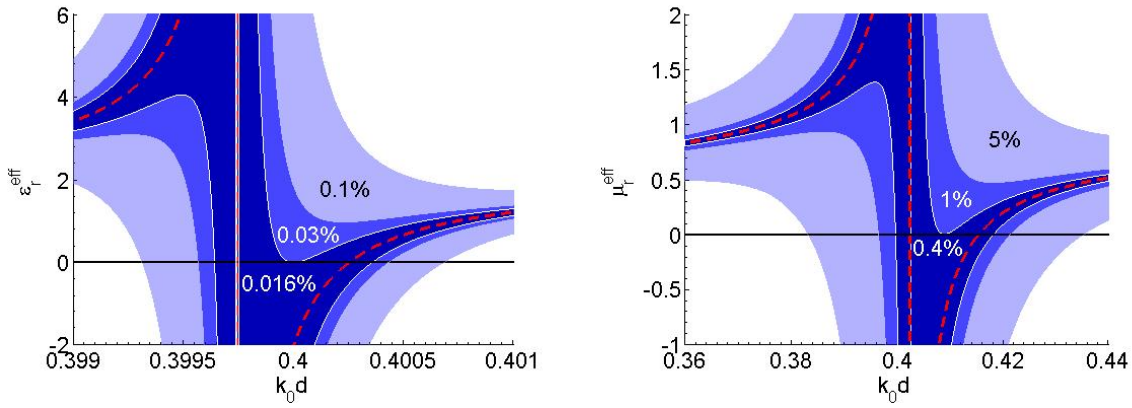

(a) (b)

Figure 5.12 Ideal values and variation ranges of the effective relative permittivity (a), and permeability (b), for a non-metallic metamaterial consisting of a cubic array of dielectric spheres with equal permittivity but two different radii, Fig. 5.2, with six combinations of parameter variations. Dashed line: ideal values of ϵ_r^{eff} (a), and μ_r^{eff} (b); dark, medium, and light shaded areas: variation ranges for $\Delta m/m = 0.016\%$, 0.03%, and 0.1% (a), 0.4%, 1%, and 5% (b) with $m = k_0a_1$, ϵ_{r1}, μ_{r1}, k_0a_2, ϵ_{r2}, μ_{r2}, ϵ_{r3}, μ_{r3}, and k_0d. Other parameters are as in Fig. 5.11.

provides negative ϵ_r^{eff}, is narrower than the first resonance of Mie magnetic dipole scattering coefficient, which corresponds to 2-spheres ($a_2/d = 0.31$) and provides negative μ_r^{eff}.

5.6 Conclusion

Considering constitutive parameters of the array medium, the Clausius-Mossotti relations have been developed for calculating the effective (bulk) constitutive parameters of two types of non-metallic metamaterials: a cubic array of identical magnetodielectric spheres and a cubic array of two different dielectric spheres. These relations have been tested by comparing their dispersion diagrams with those calculated by MPB. Analytical expressions describing the variability of effective constitutive parameters of non-metallic metamaterials, as a function of the constituent geometric and material parameters and their variations, have been developed from the total differential of the derived Clausius-Mossotti relations. These expressions have been verified by comparing their results with those calculated by analytical expressions developed by Mathematica. In practical fabrication, the presented analysis is important for predicting the performance of a metamaterial with particular variations in the parameters of

its constituents, which arise due to achievable tolerance in the fabrication process, and can be used to guard against extinction of desired DNG behavior. Based on this theory, the effects of different parameters and of different combinations of parameter variations on effective constitutive parameters have been analyzed for three types of metamaterials: i) cubic arrays of identical magnetodielectric spheres; ii) cubic arrays of dielectric spheres with equal radius but two different permittivities; and iii) cubic arrays of dielectric spheres with equal permittivity but two different radii. These effects are evaluated in terms of the computed variations in values of the effective constitutive parameters of the metamaterial in the vicinity of the DNG or SNG band for particular geometric and material parameters and their variations. Results show that variation in the following parameters impacts DNG bandwidth. In order from most to least: i) sphere radius; ii) sphere permittivity and permeability; iii) lattice constant of the array, and iv) the constitutive parameters of the array medium, all impact the width of the achievable DNG band. For particular cases studied here, results also show that the DNG behavior may be extinguished if there are 0.78%, 0.016%, and 0.016% variations in all parameters of metamaterial types i), ii), and iii), respectively, as defined above. For the design of non-metallic metamaterials with inclusions, having arbitrary shapes and material parameters, in either periodic or random arrangement, the presented results can give a qualitative guide on the level of fabrication tolerances that should be achieved in order to observe SNG or DNG behavior experimentally. The extinction of DNG behavior at variances above an extremely tight fabrication tolerance (0.016%) in all the geometric and material parameters of the particular cases considered here suggests that fabrication of metamaterial types ii) and iii) may not be realizable in practice.

5.7 Acknowledgments

This material is based upon work supported by the Air Force Research Laboratory under Contract FA8650-04-C-5228 at Iowa State University's Center for NDE. The authors wish to express their deep gratitude to Dr. Robert A. Shore (Air Force Research Laboratory, Hanscom AFB, MA) and Mr. Xing-Xiang Liu (The University of Texas at Austin) for very helpful discussions and communications.

5.8 References

[1] N. Engheta and R. W. Ziolkowski, *Electromagnetic Metamaterials: Physics and Engineering Explorations*. Wiley, New York, 2006.

[2] C. M. Soukoulis and M. Wegener, "Past achievements and future challenges in the development of three-dimensional photonic metamaterials," *Nat. Photonics*, vol. 5, no. 9, pp. 523–530, Sep. 2011.

[3] C. Holloway, E. Kuester, J. Baker-Jarvis, and P. Kabos, " A double negative (DNG) composite medium composed of magnetodielectric spherical particles embedded in a matrix," *IEEE Trans. Antennas Propag.*, vol. 51, no. 10, pp. 2596–2603, Oct. 2003.

[4] C.-W. Qiu and L. Gao, " Resonant light scattering by small coated nonmagnetic spheres: magnetic resonances, negative refraction, and prediction," *J. Opt. Soc. Am. B-Opt. Phys.*, vol. 25, no. 10, pp. 1728–1737, Oct. 2008.

[5] Q. Zhao, J. Zhou, F. Zhang, and D. Lippens, " Mie resonance-based dielectric metamaterials," *Mater. Today*, vol. 12, no. 12, pp. 60–69, Dec. 2009.

[6] W. Shu and J. Song, " Sommerfeld integral path for layered double negative metamaterials," *IEEE Trans. Antennas Propag.*, vol. 60, no. 3, pp. 1496–1504, Mar. 2012.

[7] A. Yaghjian, " Scattering-matrix analysis of linear periodic arrays," *IEEE Trans. Antennas Propag.*, vol. 50, no. 8, pp. 1050–1064, Aug. 2002.

[8] R. A. Shore and A. D. Yaghjian, " Travelling electromagnetic waves on linear periodic arrays of lossless spheres," *Electron. Lett.*, vol. 41, no. 10, pp. 578–580, May 2005.

[9] ——, "Traveling electromagnetic waves on linear periodic arrays of lossless penetrable spheres," *IEICE Trans. Commun.*, vol. E88B, no. 6, pp. 2346–2352, Jun. 2005.

[10] C. R. Simovski and S. A. Tretyakov, " Local constitutive parameters of metamaterials from an effective-medium perspective," *Phys. Rev. B*, vol. 75, no. 19, p. 195111, May 2007.

[11] R. A. Shore and A. D. Yaghjian, " Traveling waves on two- and three-dimensional periodic arrays of lossless scatterers," *Radio Sci.*, vol. 42, no. 6, p. RS6S21, Dec. 2007.

[12] ——, "Electromagnetic waves on partially finite periodic arrays of lossless or lossy penetrable spheres," *IEICE Trans. Commun.*, vol. E91B, no. 6, pp. 1819–1824, Jun. 2008.

[13] ——, " Traveling waves on three-dimensional periodic arrays of two different alternating magnetodielectric spheres," *IEEE Trans. Antennas Propag.*, vol. 57, no. 10, pp. 3077–3091, Oct. 2009.

[14] X.-X. Liu and A. Alù, " Limitations and potentials of metamaterial lenses," *J. Nanophotonics*, vol. 5, p. 053509, Jun. 2011.

[15] X.-X. Liu, D. A. Powell, and A. Alu, "Correcting the Fabry-Perot artifacts in metamaterial retrieval procedures," *Phys. Rev. B*, vol. 84, no. 23, Dec. 2011.

[16] X.-X. Liu and A. Alù, "Homogenization of quasi-isotropic metamaterials composed by dense arrays of magnetodielectric spheres," *Metamaterials*, vol. 5, no. 2-3, p. 56, Jun-Sep 2011.

[17] R. A. Shore and A. D. Yaghjian, " Complex waves on periodic arrays of lossy and lossless permeable spheres: 1. Theory," *Radio Sci.*, vol. 47, p. RS2014, Apr. 2012.

[18] ——, " Complex waves on periodic arrays of lossy and lossless permeable spheres: 2. Numerical results," *Radio Sci.*, vol. 47, p. RS2015, Apr. 2012.

[19] N. I. Landy, S. Sajuyigbe, J. J. Mock, D. R. Smith, and W. J. Padilla, " Perfect metamaterial absorber," *Phys. Rev. Lett.*, vol. 100, no. 20, May 2008.

[20] A. Alu and N. Engheta, " Robustness in design and background variations in metamaterial/plasmonic cloaking," *Radio Sci.*, vol. 43, no. 4, May 2008.

[21] N. Papasimakis, V. A. Fedotov, Y. H. Fu, D. P. Tsai, and N. I. Zheludev, " Coherent and incoherent metamaterials and order-disorder transitions," *Phys. Rev. B*, vol. 80, no. 4, Jul. 2009.

[22] S. Savo, N. Papasimakis, and N. I. Zheludev, " Localization of electromagnetic fields in disordered metamaterials," *Phys. Rev. B*, vol. 85, no. 12, Mar. 2012.

[23] I. Vendik, O. Vendik, and M. Odit, "Isotropic artificial media with simultaneously negative permittivity and permeability," *Microw. Opt. Technol. Lett.*, vol. 48, no. 12, pp. 2553–2556, Dec. 2006.

[24] I. B. Vendik, O. G. Vendik, and M. A. Odit, "An isotropic metamaterial formed with ferroelectric ceramic spherical inclusions," *Phys. Solid State*, vol. 51, no. 8, pp. 1590–1594, Aug. 2009.

[25] K. L. Kumley and E. F. Kuester, "Effect of scatterer size variations on the reflection and transmission properties of a metafilm," 2012, talk at National Radio Science Meeting, Boulder, CO.

[26] Y. Li and N. Bowler, "Traveling waves on three-dimensional periodic arrays of two different magnetodielectric spheres arbitrarily arranged on a simple tetragonal lattice," *IEEE Trans. Antennas Propag.*, vol. 60, no. 6, pp. 2727–2739, Jun. 2012.

[27] Y. Li and R. A. Shore, " Corrections to "traveling waves on three-dimensional periodic arrays of two different alternating magnetodielectric spheres (vol 57, pg 3077, 2009)"," *IEEE Trans. Antennas Propag.*, vol. 59, no. 7, pp. 2753–2754, Jul. 2011.

[28] A. Sihvola, *Electromagnetic Mixing Formulas and Applications*. The Institution of Engineering and Technology, London, 1999.

[29] S. I. Grossman, *Calculus*, 3rd ed. Academic Press, Orlando, 1984.

[30] Y. Li and N. Bowler, " Analysis of double-negative (DNG) bandwidths for metamaterials composed of three-dimensional periodic arrays of two different magnetodielectric spheres arbitrarily arranged on a simple tetragonal lattice," *IEEE Antennas Wirel. Propag. Lett.*, vol. 10, pp. 1484–1487, 2011.

[31] S. G. Johnson and J. D. Joannopoulos, "Block-iterative frequency-domain methods for maxwell's equations in a planewave basis," *Opt. Express*, vol. 8, no. 3, pp. 173–190, 2001.

[32] I. Vendik, O. Vendik, I. Kolmakov, and M. Odit, " Modelling of isotropic double negative media for microwave applications," *Opto-Electron. Rev.*, vol. 14, no. 3, pp. 179–186, 2006.

[33] J. D. Joannopoulos, S. G. Johnson, J. N. Winn, and R. D. Meade, *Photonic Crystals: Molding the Flow of Light*, 2nd ed. Princeton University Press, Princeton.

[34] Y. Li and N. Bowler, "Rational design of double-negative metamaterials consisting of 3D arrays of two different non-metallic spheres arranged on a simple tetragonal lattice," in *2011 IEEE International Symposium on Antennas and Propagation*, IEEE, 2011, pp. 1494–1497.

CHAPTER 6. GENERAL CONCLUSIONS

6.1 General Discussion

The work of this thesis is motivated by the need for low-loss, isotropic nonmetallic metamaterials. Based on the scattering matrix method and point-dipole approximations, Chapter 2 develops dispersion equations for metamaterials consisting of a tetragonal array of two different magnetodielectric spheres with arbitrary arrangements. These dispersion equations are tested by comparing their dispersion diagrams with those calculated by MPB. In MPB, fully-vectorial eigenmodes of Maxwell's equations with periodic boundary conditions are computed by preconditioned conjugate-gradient minimization of the block Rayleigh quotient in a planewave basis [1]. The backward wave and DNG bandwidths of 3D periodic arrays with different arrangements of spheres are analyzed for three combinations of sphere types. Based on this analysis, Chapter 3 presents a rational design procedure for DNG metamaterials consisting of two-sphere arrays. This procedure can give a design with widest possible DNG bandwidth and desired effective constitutive parameters at the operating frequency.

To calculate the total differential of variabilities of effective constitutive parameters of nonmetallic metamaterials, Chapter 4 develops analytical expressions for the derivatives of Mie scattering coefficients with respect to the sphere size, relative permittivity and permeability of both the sphere and medium. These expressions are verified by comparing their results with those calculated by analytical expressions developed by Mathematica. Considering the array medium constitutive parameters, Chapter 5 develops the Clausius-Mossotti relations for effective (bulk) constitutive parameters of two types of nonmetallic metamaterials: a cubic array of identical magnetodielectric spheres and a cubic array of two different dielectric spheres. Based on these relations, analytical expressions of variabilities of effective constitutive parameters

depending on geometric and material parameter variations are developed using total differential. The presented Clausius-Mossotti relations have been tested by comparing their dispersion diagrams with those calculated by MPB. Expressions for variabilities of effective constitutive parameters are verified by comparing their results with those computed by analytical expressions developed by Mathematica. Effects of different parameters and of different combinations of parameter variations have been analyzed for three types of metamaterials. These effects are evaluated in terms of the variabilities in effective constitutive parameters around the DNG or SNG frequency region for given geometric and material parameters and their variations.

Compared with metal-based metamaterials, non-metallic metamaterials show a much better performance in the pursuit of isotropy. A 3D array of identical dielectric cubes can achieve similar SNG behaviors in three different directions, [100], [110], and [111] [2]. On the other hand, most metal-based metamaterials can show DNG behavior only in some particular directions. An array of thin wires and SRRs show DNG behavior in the direction parallel to the sample surface [3]. For an array of metallic cut-wire pairs, the incident wave needs to be normal to the sample surface [4]-[6]. However, non-metallic metamaterials also have their own intrinsic disadvantages, such as narrow DNG/SNG bandwidth, which make their experimental implementation quite challenging. As shown in Table 6.1, the DNG/SNG bandwidths of non-metallic metamaterials are narrower than those of metal-based metamaterials in the same operation frequency range. In particular, transmission-line based metamaterials show a much wider DNG bandwidth than resonant-element based metamaterials since their DNG behavior does not rely on resonant unit-cells.

6.2 Recommendations for Future Work

In future work, non-metallic metamaterials can be fabricated and characterized based on the theoretical analysis presented in this thesis. In Table 6.2, magnetodielectric materials potentially useful for fabricating a metamaterial composed of an array of identical spheres in a frequency range less than 1 GHz are listed. On the other hand, dielectric materials available for the fabrication of two-sphere arrays are listed for microwave and THz frequencies. ROHACELL® 31HF with dielectric constant around 1.05 and loss tangent less than 0.01 in

Table 6.1 Measured DNG/SNG ranges and bandwidths of different metal-based and non-metallic metamaterials in X-band

Type	Resource	Structure	DNG/SNG range (GHz)	Bandwidth (%)
Metal-based	[3]	SRRs & wires	[10.2, 10.8]*	6
	[7]	SRRs & wires	[8.7, 9.9]*	13
	[8]	Transmission-line	[10, 12]*	18
Non-metallic	[2]	One-cube array	[8.53, 8.85]**	3.7
	[9]	Two-rod array	[10.6, 11]*	4
	[10]	Cubes & rods	[9.97, 10.4]*	4.2

*DNG.
**SNG.

Table 6.2 Potential materials for fabrication of inclusions of non-metallic metamaterials

Type	Resource	Chemical formula	ϵ_r	μ_r	Freq. (GHz)
I*	[17]	$Co_2Z(Ba_3Co_2Fe_{24}O_{41})$	$12 + 0.03i$	$12.5 + 4i$	1
	[17]	TT2-101	$10.2 + 0.05i$	$14.6 + 0.4i$	0.1
II**	[2]	$Ba_{0.5}Sr_{0.5}TiO_3$	$1600 + 4.8i$	-	3-18
	[14]	$SrTiO_3$	$323 + 10^{-4}i$	-	8-12
	[9]	$Ba_xSr_{1-x}Ti_{1-y}Mn_yO_3$	$575 + 3.45i$	-	8-12
	[18]	$La_{15/8}Sr_{1/8}NiO_4$	> 100***	-	$< 10^4$
	[10]	$Ba_{0.6}Sr_{0.4}TiO_3$-$La(Mg_{0.5}$-$Ti_{0.5})O_3$	$103 + 0.165i$	-	8-12

*Magnetodielectric.
**Dielectric.
***ϵ_r'' is unknown above 330 MHz at room temperature.

the frequency range 2.5 to 26.5 GHz can be used to fabricate the matrix [11]. For the characterization, there are two widely used measurement systems: free-space [12], [15] and waveguide measurement systems [2], [9], [10], [13], [14], [16]. The latter approach is preferable since it requires a smaller sample and simpler measurement configuration.

6.3 References

[1] S. G. Johnson and J. D. Joannopoulos, "Block-iterative frequency-domain methods for maxwell's equations in a planewave basis," *Opt. Express*, vol. 8, no. 3, pp. 173–190, 2001.

[2] Q. Zhao, L. Kang, B. Du, H. Zhao, Q. Xie, X. Huang, B. Li, J. Zhou, and L. Li, "Experimental demonstration of isotropic negative permeability in a three-dimensional dielectric composite," *Phys. Rev. Lett.*, vol. 101, no. 2, p. 027402, Jul. 2008.

[3] R. Shelby, D. Smith, and S. Schultz, "Experimental verification of a negative index of refraction," *Science*, vol. 292, no. 5514, pp. 77–79, Apr. 2001.

[4] V. Shalaev, W. Cai, U. Chettiar, H. Yuan, A. Sarychev, V. Drachev, and A. Kildishev, "Negative index of refraction in optical metamaterials," *Opt. Lett.*, vol. 30, no. 24, pp. 3356–3358, Dec. 2005.

[5] S. Zhang, W. Fan, N. Panoiu, K. Malloy, R. Osgood, and S. Brueck, "Experimental demonstration of near-infrared negative-index metamaterials," *Phys. Rev. Lett.*, vol. 95, no. 13, p. 137404, Sep. 2005.

[6] G. Dolling, C. Enkrich, M. Wegener, C. Soukoulis, and S. Linden, "Simultaneous negative phase and group velocity of light in a metamaterial," *Science*, vol. 312, no. 5775, pp. 892–894, May 2006.

[7] M. Bayindir, K. Aydin, E. Ozbay, P. Markos, and C. Soukoulis, "Transmission properties of composite metamaterials in free space," *Appl. Phys. Lett.*, vol. 81, no. 1, pp. 120–122, Jul. 2002.

[8] A. K. Iyer and G. V. Eleftheriades, "Multilayer negative-refractive-index transmission-line (NRI-TL) metamaterial free-space lens at X-band," *IEEE Trans. Antennas Propag.*, vol. 55, no. 10, pp. 2746–2753, Oct. 2007.

[9] T. Lepetit, E. Akmansoy, and J.-P. Ganne, "Experimental measurement of negative index in an all-dielectric metamaterial," *Appl. Phys. Lett.*, vol. 95, no. 12, p. 121101, Sep. 2009.

[10] J. Wang, Z. Xu, Z. Yu, X. Wei, Y. Yang, J. Wang, and S. Qu, "Experimental realization of all-dielectric composite cubes/rods left-handed metamaterial," *J. Appl. Phys.*, vol. 109, no. 8, p. 084918, Apr. 2011.

[11] [Online]. Available: http://www.rohacell.com

[12] L. Peng, L. Ran, H. Chen, H. Zhang, J. A. Kong, and T. M. Grzegorczyk, "Experimental observation of left-handed behavior in an array of standard dielectric resonators," *Phys. Rev. Lett.*, vol. 98, no. 15, p. 157403, Apr. 2007.

[13] X. Cai, R. Zhu, and G. Hu, "Experimental study for metamaterials based on dielectric resonators and wire frame," *Metamaterials*, vol. 2, no. 4, pp. 220–226, 2008.

[14] Y. G. Ma, L. Zhao, P. Wang, and C. K. Ong, "Fabrication of negative index materials using dielectric and metallic composite route," *Appl. Phys. Lett.*, vol. 93, no. 18, p. 184103, Nov. 2008.

[15] J. F. Carroll III, J. H. Loui, P. G. Clem, and M. B. Sinclair, "Magnetodielectric sphere composites: an all dielectric route for low loss DNG metamaterials," in *Fourth International Congress on Advanced Electromagnetic Materials in Microwaves and Optics*, 2010.

[16] T. Lepetit, E. Akmansoy, and J. P. Ganne, "Experimental evidence of resonant effective permittivity in a dielectric metamaterial," *J. Appl. Phys.*, vol. 109, no. 2, p. 023115, Jan. 2011.

[17] [Online]. Available: http://www.trans-techinc.com

[18] S. Krohns, P. Lunkenheimer, C. Kant, A. V. Pronin, H. B. Brom, A. A. Nugroho, M. Diantoro, and A. Loidl, "Colossal dielectric constant up to gigahertz at room temperature," *Appl. Phys. Lett.*, vol. 94, no. 12, p. 122903, Mar. 2009.